Influence of Frequency-Directional Wave Spectra on Wave-Induced Fatigue Loads on Offshore Wind Turbines

Comparative Analysis of Wave Characteristics on Fatigue Load Differences between 2D and JONSWAP Wave Spectra

by

Julia Mattenklott

in partial fulfillment of the requirements for the degree of

Master of Science

in Offshore and Dredging Engineering
at the Delft University of Technology

Student number: 5695163
Siemens Gamesa Renewable Energy Supervisors: Dr. D. P. Rijnsdorp, Ir. M. van der Meulen
Delft University of Technology Supervisors: Dr. G. Lavidas, Dr. M. F. S. Tissier
Project Duration: February, 2024 - November, 2024
Faculty: Faculty of Mechanical Engineering, TU Delft

TU Delft SIEMENS Gamesa RENEWABLE ENERGY

Abstract

The current trend in the offshore renewable energy industry is to install ever larger offshore wind turbines (OWT) in ever deeper waters. This results in an increased capacity requirement of the substructure which results in increased dimensions and thus higher hydrodynamic loads.

For the design of OWT the fatigue limit state is next to the ultimate limit state a crucial design loading condition to consider. In the current engineering practice, wave spectra are mostly reconstructed with the JONSWAP spectral parametrization which gives a simplified representation of the actual sea surface based on bulk wave parameters for wave components, such as wind-sea and swell. By using realistic frequency-directional (2D)-wave spectra instead of the JONSWAP spectral model, the wave spectral density distribution can be showed in its most authentic form.

This study investigates the influence of 2D-wave spectra on the wave-induced fatigue loads on OWT's, as a comparison to the commonly used JONSWAP spectral parametrization. Therefore the relation of different wind and wave parameter as well as of the wave spectral characteristics on the wave-induced loads and the load differences between both spectra are investigated. Wave spectral data as well as bulk wave parameters for a wind-sea and swell wave component were obtained from the DHI MetOcean database for the Dutch North Sea. Based on those the fatigue loads were calculated in the frequency domain using Dirlik's method.

Results show that the JONSWAP spectral parametrization leads to an overall overestimation in the range of $\sim$ 12 - 15 % of the total wave-induced fatigue loads compared to those obtained from 2D-wave spectra. The highest fatigue load differences and DEL overestimation between the JONSWAP and 2D-wave spectra were observed for significant wave heights between 2 and 3.8 m (14.70 % overestimation), peak periods between 8 and 15 s (13.63 % overestimation) and wind speeds between 10 and 20 m/s (15.04 % overestimation).

Furthermore, it was observed that narrow frequency and directional width, between 0.1 - 0.3 Hz and 20 and 30 deg, lead to the highest discrepancies for the calculated fatigue loads between the JONSWAP and 2D-wave spectra ($\sim$ 13 % overestimation). For extreme sea states, that correspond to the upper 5 % of the observed data it appears that the JONSWAP spectral parametrization leads mostly to an underestimation of the calculated fatigue loads.

With the distance correlation calculation the dependencies between the wave characteristics, such as the frequency width, directional width and the peakedness parameter, and the fatigue load differences was quantified. But this analysis did not result in additional research insights since the obtained correlation coefficients were almost identical and only exhibiting weak dependencies.

Still, it can be concluded that using 2D-wave spectra in the engineering practice and for the fatigue load calculation on OWT's with monopiles as substructures, physically more representative loads can be obtained compared to those computed with the simplified JONSWAP spectral model. This more realistic load estimation could finally lead to an improved design of OWT's.

Julia Mattenklott
Delft, November 2024

Acknowledgements

Writing this master's thesis and contributing to the research in the field of ocean waves has been my vision since the beginning of my master's programme in Offshore and Dredging Engineering, when I discovered my passion for this field.

I am very much aware of the fact that I would not have reached what I have reached without my friends, my family and my supervisors that were supporting me throughout the past months in all kind of challenging situations. First of all, I would like to express my deepest gratitude to my Siemens Gamesa Renewable Energy (SGRE) supervisors, Dr. D. P. Rijnsdorp and Ir. M. van der Meulen, who were always taking their time to discuss research issues with me and who were trying their best to give answers to my questions. Next to that, they were guiding me through the whole process of my research, making sure that I keep my focus on the most important research issues and often reminding me to take one step back to look careful and critical on what investigations I did and what contribution these have in answering my research questions. The whole process of how to start with the research with thinking about what do I want to reach and what do I want to show, as well as what methods are useful and necessary to get there, is something that I learned from them.

Furthermore, I am sincerely appreciative of my supervisors, Dr. G. Lavidas and Dr. M. F. S. Tissier, from the Delft University of Technology, for their invaluable guidance throughout my master's thesis. Their insightful evaluation of my research progress, as well as their contributions in helping me identifying areas for further investigation and those not essential to exclude from my thesis, have been crucial to me.

Next to my supervisors, I am grateful for my dear friends who were always there for me, who always listened to me and helped wherever they could. This is why I want to express my deepest gratitude for them. Through my studies and within the team of students at SGRE I have got to know so many great people with which I got through difficult times together and from who I learned a lot. And even if I did not see my family often in the past 9 months, they provided so much mental support and tried to support me every time. Everybody in its own way.

With the encouragement I got from my supervisors, my friends and my family, I got the energy and perseverance to complete this research. Many thanks to all of them.

Julia Mattenklott
Delft, November 2024

Contents

List of Figures

List of Tables

Nomenclature

Abbreviations

Abbreviation	Definition
DEL	Damage Equivalent Loads
DHI	Dansk Hydraulisk Institut
DLC	Design Loading Condition
FE	Finite Element
FLS	Fatigue Limit State
FUEL	Frequency Domain Utility for the Estimation of Loads
IJV	Ijmuiden Ver
IJVWFZ	Ijmuiden Ver Wind Farm Zone
JONSWAP	Joint North Sea Wave Project
MWD	Mean Wave Direction
OWT	Offshore Wind Turbine
PWD	Peak Wave Direction
RVO	Rijksdienst voor Ondernemend Nederland
SW	Spectral Wave model
SWAG	Siemens Wellen Analyse Gerät
ULS	Ultimate Limit State
WRF	Weather Research and Forecasting
2D	Two-Dimensional
1D	One-Dimensional

Symbols

Symbol	Definition	Unit
A	Cross sectional area of the monopile	[m^2]
a_1	Fourier moment	[-]
b_1	Fourier moment	[-]
d	Water depth	[m]
C_d	Drag coefficient	[-]
c_d	Hydrodynamic damping coefficient	[-]
C_m	Inertia coefficient	[-]
D	Monopile diameter	[m]
d_{Cor}	Distance correlation coefficient	[-]
D_{fat}	Cumulative fatigue damage	[-]
D_θ	Directional distribution	[m]
DEL	Damage equivalent load	[Nm]
f	Wave frequency	[Hz]
f_{peak}	Peak wave frequency	[Hz]
f_d	Drag force	[N]
f_i	Inertia force	[N]
g	Gravitational acceleration	[m/s^2]
H	Combined transfer function	[m]
H_a	Hydrodynamic transfer function	[N]
H_n	Structural transfer function	[m/N]
H_s	Significant wave height	[m]

Symbol	Definition	Unit
K	Stiffness	[N/m]
k	Wave number	[1/m]
M	Bending moment	[Nm]
m	Wohler's slope	[-]
m_0	Zeroth order spectral moment	[m^2]
m_1	First order spectral moment	[m^2/s deg]
m_2	Second order spectral moment	[m^2/s^2 deg^2]
N	Number of reference cycles	[-]
Q_p	Peakedness parameter	[-]
R_d	Design resistance	[N]
S	Wave spectral density	[m^2/Hz]
S_d	Design load	[N]
S_{PM}	Pierson-Moskowitz wave spectral density	[m^2/Hz]
$S_{JONSWAP}$	JONSWAP wave spectral density	[m^2/Hz]
s	Spreading parameter	[-]
T_m	Spectral mean wave period	[s]
T_m	Peak wave period	[s]
T_z	Mean zero up-crossing wave period	[s]
U	Velocity of the flow resolved normal to the monopile	[m/s]
U_{10}	Wind velocity at 10 m height	[m/s]
$\dot{U}$	Acceleration of the flow resolved normal to the monopile	[m/s^2]
s_{10}	Wind velocity at 10 m height	[m/s]
α	Energy scale parameter	[-]
η	Wave kinematic distribution function	[m/s]
γ	Peak enhancement factor	[-]
γ_f	Partial safety factor	[-]
λ	Wave length	[m]
ω	Angular wave frequency	[rad/s]
ω_0	Angular natural wave frequency	[rad/s]
Φ	Mode shape function	[-]
ρ	Density of water	[kg/m^3]
σ	Peak width parameter	[-]
σ_θ	Directional width	[deg]
σ_f	Frequency width	[Hz]
θ	Direction	[deg]
θ_0	Mean wave direction	[deg]

1. Introduction

1.1. Research context

A rapidly developing climate change is caused by the exorbitant use of fossil fuels, which did lead on the one hand to a serious energy crisis and on the other hand to an excessive environmental pollution which threatens the security and development of all humans and life in general on earth. Through this issue, the need for alternative, clean and sustainable energy sources has emerged with wind energy as one of them [1].

Due to limited available land and challenges such as noise pollution and visual impact on the natural environment, onshore wind farm development often faces resistance, especially from residents who oppose the construction of wind turbines near their homes.

In contrast, offshore wind turbines (OWT's) offer several advantages despite functioning similarly to onshore turbines. Offshore locations provide more space, and concerns about visual intrusion and noise impact are significantly reduced. Additionally, wind over the open sea is generally more consistent, smoother, and stronger, making offshore wind power more efficient. Thus exploiting offshore wind energy helps to reduce the greenhouse gas emissions and to ease the pressure on the power supply [1]. But still, the installation of OWT comes with higher costs and difficulties due to the rough environmental conditions at sea.

Within the offshore wind industry the current development trend is to install ever larger offshore wind turbines in ever deeper waters for which harsher wave impacts can be expected, which also result from intensifying climatic conditions [2, 3, 4]. As the size of the offshore wind turbines increases, also the aerodynamic loads increases which results on the other hand in an increased capacity requirement of its substructure. By increasing the structural capacity of the substructures, their dimensions needs to be increased as well which leads to higher hydrodynamic loads [5].

Offshore wind turbines are continuously subjected to environmental loads from wind, waves, and currents, with wind-generated waves often being the dominant force causing dynamic excitation in their structures [6]. An increased wave action on the substructure of OWT's is the predominant cause of fatigue damage which is the design loading condition that determines the final dimensions of support structures such as monopile foundations [5, 7].

In this research, a monopile is considered as the substructure for the OWT. This choice is practical, as monopiles are the most widely used substructures in the offshore wind industry and, depending on their diameter, they can be installed in water depths of up to 60 m [8, 9, 10]. Furthermore, the wave load impact on a monopile substructure is larger compared to other fixed offshore structures, like jacket structures and therefore crucial to consider during the design process. Therefore all parameters describing the distribution of the wave spectral density within a wave spectrum must be carefully analyzed. Small changes in the structural dimensions of the monopile, such as wall thickness, can lead to significant variations in the experienced loads, which is not as pronounced for jacket structures [10].

Additionally, due to its compact shape, the monopile is less sensitive to marine growth compared to substructures such as tripods or lattice structures. Its simpler construction process also results in lower costs compared to jacket substructures [11].

Costs in the offshore wind sector can be reduced by using advanced technologies to optimize the manufacturing, installation, maintaining and decommissioning processes. Therefore, a correct and realistic estimation of the wave loads on the OWT can make a valuable contribution to the improvement of the design and especially the selection of the dimensions of the structure [1].

The goal of this research is to improve OWT design standards, to contribute to more reliable fatigue life estimates, and to support the development of a safer, more efficient renewable energy infrastructure.

1.2. Problem statement

Frequency-directional wave spectra, also known as 2D-wave spectra, provide a detailed representation of the wave spectral density distribution across different frequencies and directions of the sea surface. However, this realistic representation is often simplified using the JONSWAP spectral model, which reconstructs wave spectra across frequencies, based on bulk wave parameters derived from the actual 2D-wave spectra. While a directional spreading function can be applied to these reconstructed wave spectra to account for the directional variability, the approach of using the JONSWAP spectral model does not take into account much of the detailed wave energy information, leading to uncertainties in wave load predictions [12].

The JONSWAP spectral parametrization, relying on bulk wave parameters, cannot fully capture the complexity of wind-generated ocean waves, often resulting in inaccuracies in load predictions. This limitation arises because bulk wave parameters fail to represent the detailed interactions within the wave field [12]. However, detailed considerations of the ocean wave environment are critical for accurate load estimation, as they are essential for many engineering applications [13].

Therefore, this study aims to address these uncertainties by investigating the influence of 2D-wave spectra on the wave-induced fatigue loads, providing a more realistic approach to the design of OWT's.

1.3. Research objective

This study aims to enhance the accuracy of wave-induced fatigue load predictions for OWT's by analyzing how wave characteristics and environmental parameters influence fatigue loads. It focuses on comparing wave-induced fatigue loads obtained with the commonly used JONSWAP spectral parametrization and with actual 2D-wave spectra to provide a better understanding of their influence on fatigue load estimation.

To achieve this, the study aims to answer the following questions:

1. **How do the bi-modal JONSWAP wave spectra, based on bulk wave parameters, and the 2D-wave spectra, based on wave spectral densities distributed across frequency and directional values, influence the wave-induced fatigue load predictions on offshore structures?**

   This question examines how the choice of the wave spectrum affects the structural response and fatigue damage estimation. With the JONSWAP and 2D-wave spectra the wave energy distribution can be represented in distinct. Understanding how each model impacts fatigue damage is essential for improving the accuracy of fatigue life predictions of OWT.

2. **What ranges of the investigated environmental parameters, significant wave height, peak period, wind speed as well as wind and wave direction, lead to the highest wave-induced fatigue loads and differences between the JONSWAP and 2D-wave spectra?**

   This question aims to determine the specific ranges of environmental conditions, such as the significant wave height, peak period, wind speed as well as wind and wave direction, that cause the highest fatigue loads and fatigue load differences in load predictions between the wave spectra. Identifying these ranges is crucial for risk assessment and design optimization.

3. **Which wave characteristics, such as frequency width, directional width or peakedness, contribute most to the discrepancies between the JONSWAP and 2D-wave spectra in predicting fatigue damage?**

   With this question it is aimed to identify which of the wave characteristic has the strongest correlation and thus highest dependence on the fatigue load differences between JONSWAP and 2D-wave spectra.

To narrow the scope of this research, the focus will be set on the hydrodynamic loads, specifically on the wave impact on the substructure. The research is limited to fixed OWT's located in the Dutch North Sea. Data from 1979 to 2023 will be used to assess the long-term wave patterns. This selected time frame provides a long-term dataset, allowing for a robust analysis of wave patterns and their impact on fatigue loads.

1.4. Methodology

This section outlines the approaches used to address the research questions defined earlier, detailing the methods for data analysis and wave-induced fatigue-load calculations.

For the fatigue-load calculation, wave spectral data will be used to represent actual 2D-wave spectra, alongside with bulk wave parameters for a wind-sea and swell wave component. The actual 2D-wave spectra will provide a comprehensive representation of the sea surface, while the bulk wave parameters will be employed to reconstruct a frequency-dependent wave spectra using the JONSWAP spectral model.

No directional spreading function will be applied to the reconstructed JONSWAP wave spectra. Both the wind-sea and swell components are assumed to propagate in a single, distinct direction. Wave spectral data and bulk wave parameters will be sourced from the DHI MetOcean database.

Based on the obtained JONSWAP and 2D-wave spectra, wave loads will be calculated in the frequency domain using the Morison's equation. A structural and hydrodynamic transfer function will be combined and applied to the obtained wave load spectrum to derive the structural response spectrum. Subsequently, the Dirlik's stress range counting method will be used to estimate the cumulative fatigue damage, which can be set in relation to the Damage Equivalent Loads (DEL) that represent the wave-induced loads for the design of OWT. These calculations will be performed using Siemens Gamesa Renewable Energy's internal MATLAB-based Frequency Domain tool.

An initial analysis of the MetOcean data will investigate the relationships between wave characteristics, such as the directional width, frequency width, and peakedness, and wind and wave parameters, including the significant wave height, peak period, wave and wind directions, and the wind speed. Additionally, the relation between the wave characteristics as well as between the wind and wave parameters and the calculated absolute DEL and the relative damage will be assessed with scatter density plots and box plots.

Distance correlation analysis was applied to quantify the dependencies of wave characteristics on the DEL differences between the JONSWAP and 2D-wave spectra. While initially included to explore potential correlations between the directional width, frequency width, peakedness and the fatigue load differences, the distance correlation analysis did not reveal further insights beyond those provided by other methods in this study.

It is hypothesized that 2D-wave spectra will provide more realistic predictions of wave-induced fatigue loads than could be gained with the JONSWAP spectral parametrization, as 2D-wave spectra offer a more authentic representation of the sea surface. This hypothesis will be tested through the analysis methods outlined, aiming to validate the improved accuracy of 2D-wave spectra.

1.5. Report structure

The meaning of frequency-directional wave spectra as well as of wave spectral parametrizations and how from these wave characteristics can be derived will be explained in chapter 2. It will be shown how these differ in its wave spectral shape, compared to the JONSWAP spectral parametrization, considering the distribution of the wave spectral density over the frequencies and directions.

Furthermore, an overview of the calculation and meaning of wave-induced fatigue loads will be given in chapter 3. The process of calculating the wave-induced fatigue damage and the corresponding DEL's based on different input wave spectral data will be explained as well as which internal tool at Siemens Gamesa Renewable Energy therefore is used. Next to that, the structural and environmental design considerations that need to be taken into account will be mentioned.

Based on the explanation of the theoretical background, first the obtained MetOcean data will be analyzed in chapter 4. Therefore, an overview of the site conditions of the chosen location in the Dutch North Sea and the corresponding wave and wind climate are given. Furthermore, it will be investigated how the bulk wave parameters, such as significant wave height, peak period or wave direction as well as wind parameters such as the wind speed and wind direction can be set into relation to the wave spectral characteristics, such as directional width, frequency width and the peakedness parameter.

After analyzing the obtained MetOcean data, their dependence on the calculated absolute and relative

values of the wave-induced fatigue loads and the wave-induced fatigue load differences will be analyzed in chapter 5. Ranges of the wave and wind parameters and the wave spectral characteristics will be determined for which both spectra result in mostly equal loads and for which the highest load differences occur. Based on these determined ranges the dependence of the directional width, frequency width and the peakedness on the DEL differences will be quantified with a distance correlation calculation in section 5.4.

The limitations of the research as well as research recommendations will be addressed in chapter 6 to critically assess the findings of this research. Finally, the conclusion in chapter 7 brings together the key insights of this research, revisits the research objectives, and provides a concise summary of the results.

2. Literature review

2.1. Wave spectra characteristics

This chapter explores the characteristics of wave spectra, focusing on both the JONSWAP spectral model and 2D-wave spectra. Theoretical background is given on how wave parameters can be derived from wave spectra and explains how a frequency-dependent wave spectrum can be constructed using the JONSWAP wave spectral model. Additionally, the chapter discusses the role of a directional spreading function, which can be applied to distribute the wave spectral density across different directions to reconstruct a 2D-wave spectrum from an initially frequency-dependent calculated JONSWAP wave spectrum.

Furthermore, methods for calculating key wave characteristics such as directional width, frequency width, and the peakedness parameter will be outlined. Understanding how these wave parameters and characteristics are derived is essential for the analysis presented in later sections, as they directly impact wave-induced load predictions.

2.1.1. Frequency-directional wave spectral data

Frequency-directional wave spectra, also known as '2D-wave spectra', represents the wave spectral density across both frequency and directional distribution [14, p. 163]. Long-term wave conditions can be derived using simulated historical MetOcean data, which is based on reconstructed or archived wind fields, by making use of numerical modeling. Even for offshore locations without measured data, wave conditions can be obtained by interpolating data from similar conditions [15, p. 13], [14, p. 146]. To convert time series records of the sea surface data into 2D-wave spectral data, signal processing and wave spectral analysis techniques can be employed [16]. This approach enables the analysis of multiple time records of the sea surface, rather than a single observation, ensuring a more comprehensive representation of all possible sea conditions at the time of observation [14, p. 31].

By integrating the spectral density matrix $S(f, \theta)$ of the wave spectrum over the directional vector, the spectral densities over the frequencies $S(f)$ can be obtained.

$$S(f) = \int_{0deg}^{360deg} S(f, \theta) d\theta \tag{2.1}$$

On the other hand, by integrating the spectral density matrix from the minimum to the maximum frequency, a spectral density is obtained that only depends on the directions anymore.

$$S(\theta) = \int_{f_{min}}^{f_{max}} S(f, \theta) df \tag{2.2}$$

Directional wave spectra that occur at the open sea can have many spectral forms. Indeed a situation in which one locally generated wind-sea system occurs simultaneously with one or more swell systems can happen very often [13]. Locally generated waves are short in wave length and show a more irregular behavior. These are referred to as wind-sea waves which originated in the North Sea mostly from south-west directions [17]. Swell waves that are often generated in a distant storm are associated with longer wave periods and a smoother shape. These waves are referred to in regions were they left their area of generation [14]. In the Dutch North sea, swell mainly propagates from the Norwegian and Greenland Seas, which corresponds to north and northwest directions. Moreover, swell waves can also result from moving storms in the northern part of the sea [18].

As many different wave systems can occur in one investigated wave field, multi-modal directional distributions can be visible within a considered wave spectrum. This leads to a distribution of the wave energy within the wave spectrum in several directions as can be seen in figure 2.1.

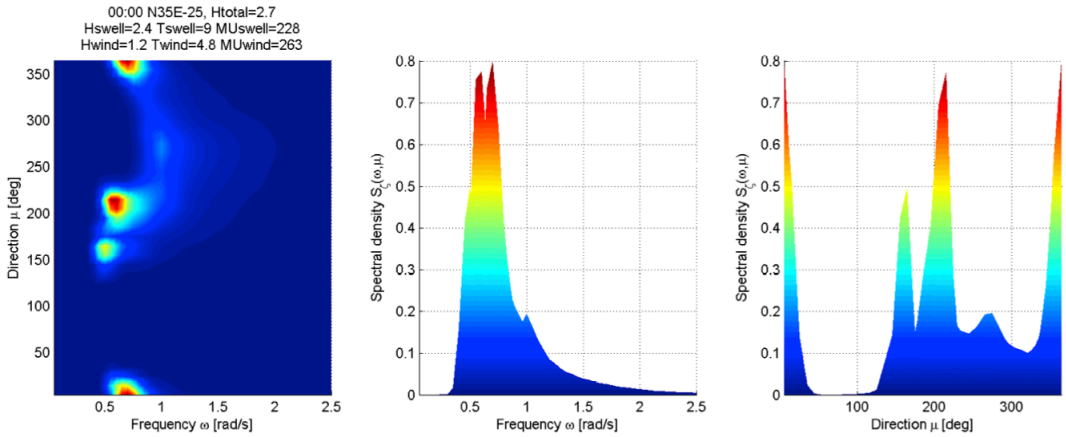

Figure 2.1: Multi-modal wave spectrum, [19]

The wave loads, that are acting on the monopile, can be influenced immensely by the multi-directionality of the waves. Within some design loading cases only the worst case direction is considered for the load calculations instead of assuming a spreading in the direction of the waves that are approaching the structure [20, p. 90].

While characterizing ocean waves by means of a directional wave spectrum, the sea surface can be described as a stochastic process in which a lot more important information about the versatility of the sea states is captured than can be gained by using bulk parameters such as the significant wave height, peak period or the wave direction [12]. The difference of the wave energy distribution of actual 2D-wave spectra from hindcast data and from the derived spectral shape parametrization, from bulk wave parameters, by using the JONSWAP spectral model is illustrated in figure 2.2.

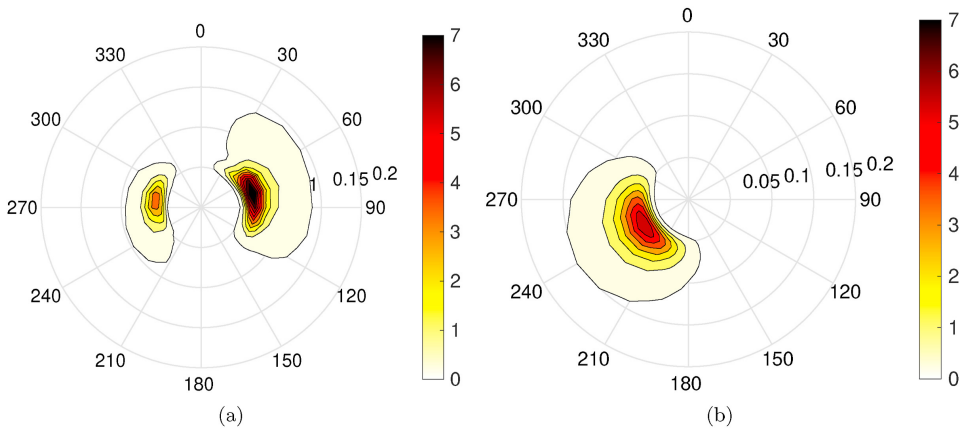

Figure 2.2: Comparison of actual 2D-wave spectra from actual hindcast data (a) and a derived spectral shape parametrization from that hindcast data by applying the JONSWAP spectral model (b), [21]

From figure 2.2 it can be seen that the wave spectra that is reconstructed with the JONSWAP spectral model (right plot), shows a very evenly spread wave spectral shape with only one spectral peak, which leads to a more simplified representation of the actual 2D-wave spectra that can be seen in the left plot of the figure.

2.1.2. Wave spectral moments

One of the most important measures of the wave spectrum is the zero spectral moment m_0 which also represents the variance of the wave surface and the total contained energy. The wave spectral moment for the 2D-wave spectrum is calculated with equation 2.3.

$$m_0 = \int_0^{\infty} \int_0^{360} S(f,\theta) df d\theta = \int_0^{\infty} \int_0^{2\pi} S(\omega,\theta) d\omega d\theta \tag{2.3}$$

Greater uncertainty and larger errors are expected for spectral moments higher than the 3rd order, due to larger discrepancies in both directional spread and magnitude compared to spectral moments below 3rd order [22, 23]. Higher order spectral moments can be obtained by integrating the spectrum numerically through applying equation 2.4 [14, 22].

$$m_n = \int_0^{\infty} \int_0^{360} f^n S(f,\theta)\, df d\theta = \int_0^{\infty} \int_0^{2\pi} \omega^n S(\omega,\theta)\, d\omega d\theta \quad \text{for n= ..., -3, -2, -1, 0, 1 ,2, 3,...} \tag{2.4}$$

From the wave spectral moments wave spectral parameters can be calculated, such as the significant wave height and peak period. The spectral moments can be calculated for a 2D-wave spectrum based on the frequency f in [hertz] and the direction θ or based on the angular frequency ω in [rad/s]. The frequency can be replaced with the angular frequency by applying equation 2.5 [12].

$$f = \omega / 2\pi \tag{2.5}$$

Since several wave components, such as wind-sea and swell wave components can be observed in one sea state as described in paragraph 2.1.1, different spectral moments, such as a wind-sea spectral moment $m_{n,windsea}$ and a swell spectral moment $m_{n,swell}$, can be assigned to these wave components. The total spectral moment, based on different wave components that occur within one sea state, can be calculated by combining both components.

$$m_n = m_{n,windsea} + m_{n,swell} \tag{2.6}$$

Wave spectral data for several wave components per sea state can be read from the bulk wave parameters which are obtained from the MetOcean database. To calculate wave spectral data for different wave components it must be made use of spectral partitioning which will not be part of this research. Still, for the sake of completeness this approach is mentioned.

2.1.3. Bulk wave parameters

Significant wave height

The significant wave height is a statistical measure of the wave heights in a sea state. It was originally determined as the mean height of the highest one-third of the zero up-crossing waves. This measure is calculated with equation 2.7 [24, p. 10].

$$H_s = 4\sqrt{m_0(f,\theta)} = 2\pi\sqrt{m_0(\omega,\theta)} \tag{2.7}$$

As an example for applied spectral partitioning, the total significant wave height from different wave component, such as wind-sea and swell wave components, is obtained with equation 2.8. $H_{s,windsea}$ refers to the significant wave height of the calculated wind-sea component and $H_{s,swell}$ refers accordingly to the significant wave height of the calculated swell component [25, p. 64], [26].

$$H_{s,total} = \sqrt{H_{s,windsea}^2 + H_{s,swell}^2} \tag{2.8}$$

Spectral mean wave period

From the zeroth and the first order wave spectral moment the mean wave period can be calculated with equation 2.9 [19].

$$T_m = T_{01} = m_0/m_1 = 2\pi(m_0/m_1) \tag{2.9}$$

Mean zero-up-crossing period

The mean zero-up-crossing period of a sea state is equal to the average period of the zero-up-crossing waves that can be measured during one record of the sea surface. A zero up-crossing wave is defined as the part of the wave elevation time history that can be measured between two zero up-crossing. The rising of the sea surface through the still water level describes such a zero up-crossing [15, p. 19]. This measure is in the practice often calculated based on the zeroth and second order wave spectral moments, as defined with equation 2.10 [19],[24, p. 7].

$$T_z = T_{02} = \sqrt{m_0(f,\theta)/m_2(f,\theta)} = 2\pi\sqrt{m_0(\omega,\theta)/m_2(\omega,\theta)} \tag{2.10}$$

Peak wave period

The periods of the largest waves of the obtained wave record are best described with the peak period or the significant period than with average wave periods [22].

The peak wave period is equal to the reciprocal of the peak wave frequency and is defined for the total sea state at the frequency at which the maximum value of the wave energy is measured [25, 27]. The corresponding equation 2.11 denotes the peak frequency f_p within the wave spectrum. The peak frequency of the wave spectrum corresponds to the frequency at which the wave spectral energy reaches its maximum value.

$$T_p = 1/f_p \tag{2.11}$$

Peak wave direction

The wave direction within the wave spectrum at which the energy density has its maximum value can be seen as the peak wave direction.

$$PWD = \theta(S(f,\theta), max) \tag{2.12}$$

2.1.4. JONSWAP wave spectral parametrization

In the common practice an idealized spectral shape parametrization is typically used, to represent the sea surface [19, 28]. This kind of spectra are analytically reconstructed based on bulk wave parameters from hindcast data using mostly the Pierson-Moskowitz (PM) or the JONSWAP spectral model [16, 21]. With the PM and the JONSWAP spectral model, the wave spectral density gets without the application of a directional spreading function expressed in terms of its frequency distribution.

The Pierson-Moskowitz wave spectrum is used for fully developed sea states in which waves do not grow further anymore as the wind speed is equal to the wave speed. But this condition is rather unrealistic as very long fetches would be required. The Pierson-Moskowitz spectral shape can be derived with the following equation with α_{PM} as the energy scale and f_{PM} as the peak frequency [14, p. 151-158].

$$S_{PM}(f) = \alpha_{PM} g^2 (2\pi)^{-4} f^{-5} \exp\left[-\frac{5}{4}\left(\frac{f}{f_{PM}}\right)^{-4}\right] \tag{2.13}$$

In the context of the Joint North Sea Wave Project (JONSWAP) which laid the scientific foundation for the modern wave predictions and which is based on measurements in the North Sea, a wave spectrum was observed that is different compared to the Pierson-Moskowitz wave spectrum [14]. The JONSWAP spectral shape takes the dependence on the fetch and wind speed into account [29]. These initially one-dimensional JONSWAP spectrum is characterized by its evolution from high frequencies towards lower frequencies while it keeps its shape along the fetch. The JONSWAP wave spectrum is usually applied for young sea states based on short fetches in which the waves grow fast in the beginning, but with a decreasing pace the larger the fetch growth and the further the spectrum develops [14, p. 151-155]. As an extension of the PM spectral parametrization, the original expression of the idealized JONSWAP spectral model, according to Hasselmann [30], is shown with equation 2.14.

$$S_{\text{JONSWAP}}(f) = \alpha g^2 (2\pi)^{-4} f^{-5} \exp\left[-\frac{5}{4}\left(\frac{f}{f_p}\right)^{-4}\right] \gamma^{\exp\left[-\frac{1}{2}\left(\frac{f/f_p^{-1}}{\sigma}\right)^2\right]} \tag{2.14}$$

with

$$\begin{aligned} \alpha &= \text{energy scale parameter} \\ \gamma &= \text{peak enhancement factor} \\ \sigma &= \text{peak width parameter} \end{aligned} \tag{2.15}$$

The energy scale parameter can be expressed by means of the dimensionless peak frequency [14, p. 162].

$$\alpha = 0.0317 \tilde{f}_{\text{peak}}^{0.67} \tag{2.16}$$

The dimensionless peak frequency considers the gravitational acceleration g and the wind speed at 10 m height U_{10}.

$$\tilde{f}_{\text{peak}} = f_{\text{peak}} \frac{U_{10}}{g} \tag{2.17}$$

One significant characteristic of the JONSWAP spectrum is its sharper peak. While parameterising the observations, this enhancement of the peak of the wave spectrum could be considered while implementing a peak-enhancement function consisting of a peak-width parameter σ and a peak enhancement factor γ. According to the DNV GL, the non-dimensional peak enhancement factor γ is in the range between 1 and 5 and can be calculated based on the Tp/Hs-ratio [25, p. 63].

$$\gamma = \begin{cases} 5 & \text{for } \frac{T_p}{\sqrt{H_s}} \leq 3.6 \\ \exp\left(5.75 - 1.15 \frac{T_p}{\sqrt{H_s}}\right) & \text{for } 3.6 < \frac{T_p}{\sqrt{H_s}} < 5 \\ 1 & \text{for } 5 \leq \frac{T_p}{\sqrt{H_s}} \end{cases} \tag{2.18}$$

with

$$\gamma \in [1, 7] \tag{2.19}$$

How the peakedness parameter γ influences the sharpness of the peak of the JONSWAP spectrum can be seen in figure 2.3. Higher values of the peakedness parameter correspond to wave spectra with a sharper peak whereas lower values of the peakedness parameter correspond to a less sharp wave spectrum.

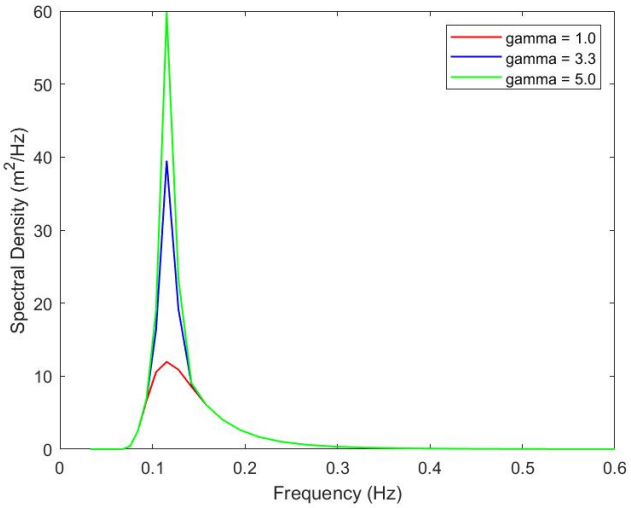

Figure 2.3: Dependence of the peakedness parameter on the JONSWAP wave spectral shape

By just assuming the peak enhancement factor to be 1, the peak-width parameter would become irrelevant and the PM-wave spectrum would be regained [14, p. 159-162]. In order to account for the widths on the left and right side of the of the spectral peak, the peak-width parameter σ is introduced which is calculated per frequency bin of the wave spectrum [25].

$$\sigma = \begin{cases} \sigma_a = 0.07, & \text{if } f \leq f_p \\ \sigma_b = 0.09, & \text{if } f > f_p \end{cases} \tag{2.20}$$

Mazzaretto et al., [12], investigated the JONSWAP spectra suitability in the coastal regions of Europe and Oceania by comparing the Scatter Index (SI) from spectra obtained from hindcast data with those obtained from measurements with buoys. They found that the JONSWAP spectrum is not suitable at all investigated regions. Moreover, they investigated that for the peak enhancement factor a value of $\gamma \sim 1.54$ seems to be a better global estimation than the standard value of $\gamma = 3.3$. As the peak enhancement factor defines how narrow or widely banded the spectral shape looks like it can be concluded that a value of $\gamma \sim 1.54$ represents a broader JONSWAP spectrum [12]. In general it can be said that this factor depends on the considered sea state.

Furthermore, they stated that for locations where many different wave systems in one wave field occur such as wind-sea states combined with multiple swell systems and where high energetic swell systems occur in general, the JONSWAP spectral model is not a very accurate representation anymore. Both the PM and the JONSWAP wave spectra describe occurring wind-sea and swell spectra usually individually, so that each is represented in a uni-modal form [28]. Still, uni-modal wave spectra for two different wave components can be combined to obtain a bi-modal wave spectrum. They concluded that the JONSWAP spectral shape is a good approximation in many regions of Europe, such as in the Mediterranean Sea, Northern Spain, Portugal, Island, Baltic Sea and West-Ireland. Compared to that they found that the performance of the JONSWAP spectral model is worse in Oceania.

To find out about more realistic directional wave spectra the focus must be laid on the understanding, identifying and finally combining of different wave systems in an observed wave field [12]. Björnsson, [19], investigated how large the arising errors from the use of such a one-dimensional spectral shape parametrization are compared to actual 2D-wave spectra for ship response predictions and concluded that 2D-wave spectra must be used to prevent large errors and in order to obtain correct performance predictions of the ships motions.

2.1.5. Idealized directional spreading

The one-dimensional wave spectral representation do not provide enough information about its directional energy characteristics, which is necessary for many scientific and engineering applications [31,

13]. To account for the spreading of the wave energy over different directions, the JONSWAP spectral function can be multiplied with an idealized spreading function. One often used cosine spreading function is the parametric model, as indicated in equation 2.21, which was set up by Mitsuyasu et al. to consider for the mean wave direction θ_0, a spreading parameter s, as well as a normalization factor A, as defined in equation 2.24 [14, p. 160], [32].

$$D(\theta)_{idealized} = A\cos^{2s}\left(\frac{1}{2}(\theta-\theta_0)\right) \quad \text{for} -180^\circ < \theta \leq 180^\circ \tag{2.21}$$

The spreading parameter s can be assumed with $2n+1$, with values of n usually ranging between 2 and 10, for wind generated sea states. Low values of n refer to low wind sea states and high values of n can be assigned to higher wind sea states. A relative larger value of the n (> 10), should be applied for long-crested swell sea states. For the fatigue loading case, n should be chosen as the most unfavourable value which would lay in the range between 2 and 6, corresponding to a broader spread of the wave spectral density over the directions. With this assumption it can be accounted for a more damaging effect of the wave loads on the OWT for the fatigue loading case, which considers repeated but more moderate loading cycles over time represented by a broader wave energy distribution, leading to a more continuous wave action and lower individual wave heights. For the extreme wave loading case, n should be assumed to be larger than 10 which corresponds to a narrower spread of the wave spectral densities of the JONSWAP wave spectrum over the directions [25, p. 65].

The normalization condition of the spreading function must be satisfied in order to make sure that the energy is distributed accurately. Therefore, the integral of $D(\theta)$ over all directions is equal to 1 as it is stated in equation 2.22 [33]. The directional distribution $D(\theta; f)$ may vary with frequency, but this frequency dependence is often neglected which means that $D(\theta; f)$ can be written as $D(\theta)$ [14, p. 163].

$$\int_0^{360} D(\theta; f)\, d\theta = \int_0^{360} D(\theta)\, d\theta = \int_0^{360} \frac{E(f,\theta)}{E(f)}\, d\theta = \frac{\int_0^{360} E(f,\theta)\, d\theta}{E(f)} = \frac{E(f)}{E(f)} = 1 \tag{2.22}$$

The spreading function must be multiplied with a normalization factor A which considers the spreading parameter s as well as the gamma function Γ and in order to obtain a normalized spreading function, the spreading function D_θ must be divided by its integral [32].

$$A = \left(\frac{2^{(2s-1)}}{\pi}\right)\left(\frac{\Gamma^2(s+1)}{\Gamma(2s+1)}\right) \tag{2.23}$$

The reconstructed 2D-wave spectrum can be obtained by multiplying the frequency-dependent JONSWAP spectrum with the idealized directional spreading function [25, p. 35].

$$S(f,\theta) = S(f)D(\theta,f) = S(f)D(\theta) \tag{2.24}$$

Correspondingly, a double-peaked wave spectrum, consisting of one swell and one wind-sea component is obtained by applying the following equation within each wave spectrum is multiplied by the corresponding idealized directional spreading function [25, p. 35].

$$S(\omega,\theta) = S_{\text{wind sea}}(\omega)D_{\text{wind sea}}(\theta)_{idealized} + S_{\text{swell}}(\omega)D_{\text{swell}}(\theta)_{idealized} \tag{2.25}$$

Figure 2.4 shows how the result of such a uni-modal 2D-wave spectral parametrization by considering one wave component, indicated with one spectral peak, with applied directional spreading function could look like.

The top-left plot represents the 2D-distribution of the wave spectrum over the direction and frequency. The top-right plot illustrates how the obtained spectrum does look like from a top view. The bottom left

plot shows the wave spectral density distribution over its frequency distribution and the bottom-right plot over the direction distribution.

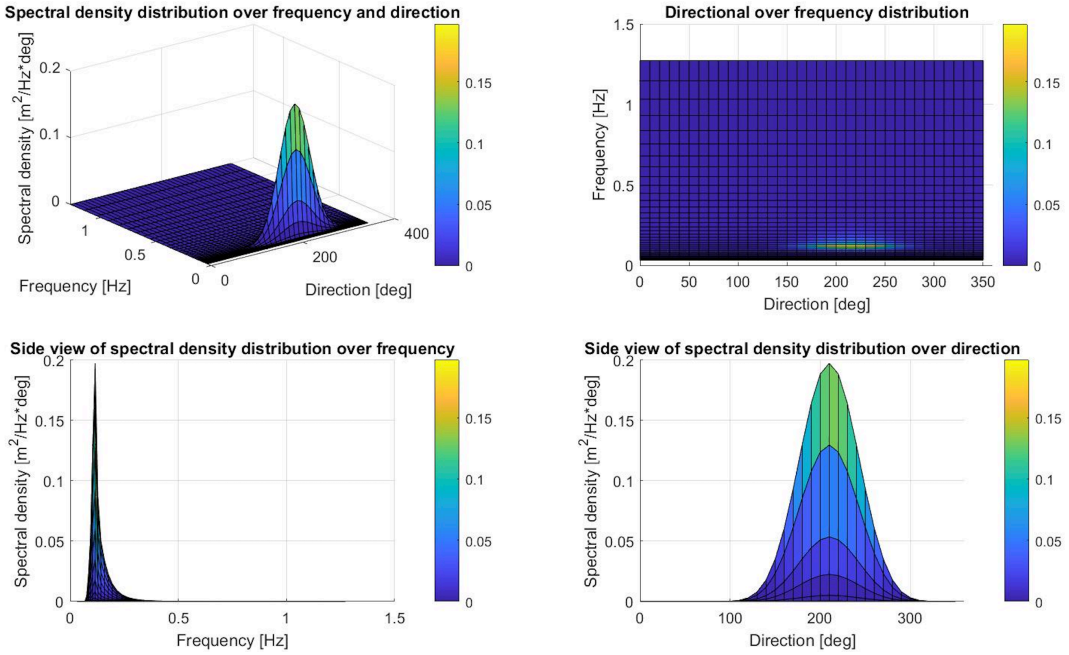

Figure 2.4: Uni-modal 2D-wave spectral parametrization from different views

Since only one spectral peak in this uni-modal directional shape is visible, it can be concluded that all the energy, that is captured within the wave spectrum, is evenly spread along the directional ranges. The highest amount of wave energy is distributed in the direction of the spectral peak of the wave spectrum. This can indeed be the case for a simplified situation, but for more complex situations this it is not a good approximation anymore [13].

In fact at the peak frequency of the two-dimensional reconstructed wave spectra, that is based on the JONSWAP spectral model, the directional distribution seems to be rather sharp and uni-modal but towards higher frequencies this is not a realistic representation [14, p. 166]. As most of the wind energy is travelling downwind, the idealized directional distribution can be assumed to have its maximum value in the direction of the wind. Correspondingly, it can be assumed that the idealized directional width takes on decreasing values for the off-wind directions [14, p. 163-164].

By making use of spectral partitioning, total spectral measures, such as of the significant wave height H_s or the peak period T_p, can be split into measures of several wave systems. Each wave system would assumed to be oriented in a different direction θ. This could be applicable for one wind-sea and one swell wave component or instead of the swell component another newly developed wave component within the observed wave field could occur, which can have its energy distribution in another direction [29].

Bi-modal wave spectra describe double-peaked spectra to represent two simultaneously occurring wave systems. Based on numerical experiments and field measurements, it was observed that most of the wave energy towards the higher frequencies, for short waves with high wave numbers, is propagating oblique to the wind in the two side lobes of the main wind direction which results in a symmetrical bi-modal directional distribution that differs in its shape to the simplified uni-modal directional distribution [14, 34, 35]. Soares [29], concluded in his research that the application of double-peaked sea wave spectra leads to an improvement of the calculation of more realistic motions or design loads of marine structures.

2.1.6. Wave spectral shape characterizations

Directional width distribution

The 2D-wave spectrum $S(\theta, f)$ shows the non-normalized distribution of the the wave spectral density over both direction and frequency. The directional distribution $D(\theta)$ gives per frequency the normalized distribution of the wave spectral density over the directions as it was shown in equation 2.22. The directional distribution function $D(\theta)$ of the 2D-wave spectrum can be expressed with equation 2.26 [14, p. 162].

$$D(\theta) = \frac{S(f,\theta)}{S(f)} \tag{2.26}$$

The one-sided directional width σ_θ of the directional distribution function can be approached with the following equation in which θ refers to the direction that is relative to the mean wave direction [14, p. 163].

$$\sigma_\theta^2 = \int_{0deg}^{360deg} \left[2\sin\left(\frac{1}{2}(\theta - \theta_{mean})\right)\right]^2 D(\theta)\, d\theta \tag{2.27}$$

The mean wave direction θ_{mean} can be calculated from the lowest two Fourier moments a_1 and b_1 of the directional distribution $D(\theta, f)$ of the wave spectral density [36].

$$\theta_{mean} = \arctan\frac{b_1(f)}{a_1(f)} \tag{2.28}$$

with

$$a_1(f) = \int_{0deg}^{360deg} d\theta \cos\theta D(\theta; f) \tag{2.29}$$

$$b_1(f) = \int_{0deg}^{360deg} d\theta \sin\theta D(\theta; f) \tag{2.30}$$

Frequency width distribution

To characterize the frequency distribution of a wave spectrum, one can use the spectral bandwidth σ_f of the frequency which is formulated by Blackman and Tukey, [37, 38].

$$\sigma_f = \frac{\left[\sum_{f_{\min}}^{f_{\max}} S(f)df\right]^2}{\sum_{f_{\min}}^{f_{\max}} S^2(f)df} \tag{2.31}$$

Peakedness distribution

Goda [39], introduced the parameter Q_p to characterize the spectral peakedness which indicates how sharp the peak of the wave spectrum is. A sharp spectrum around the dominant energy peak is indicated by large values of Q_p [38]. The peakedness parameter can be related to the frequency width distribution since it considers the squared one-dimensional spectral density over the frequencies.

$$Q_p = \frac{2\sum_{f_{\min}}^{f_{\max}} fS^2(f)df}{\left[\sum_{f_{\min}}^{f_{\max}} S(f)df\right]^2} \tag{2.32}$$

2.2. Wave-induced fatigue load calculation

The theoretical approach of the wave-induced fatigue load calculation in the frequency domain is described in this section. The process for the wave-induced fatigue loading case is visualized with the figure 2.5.

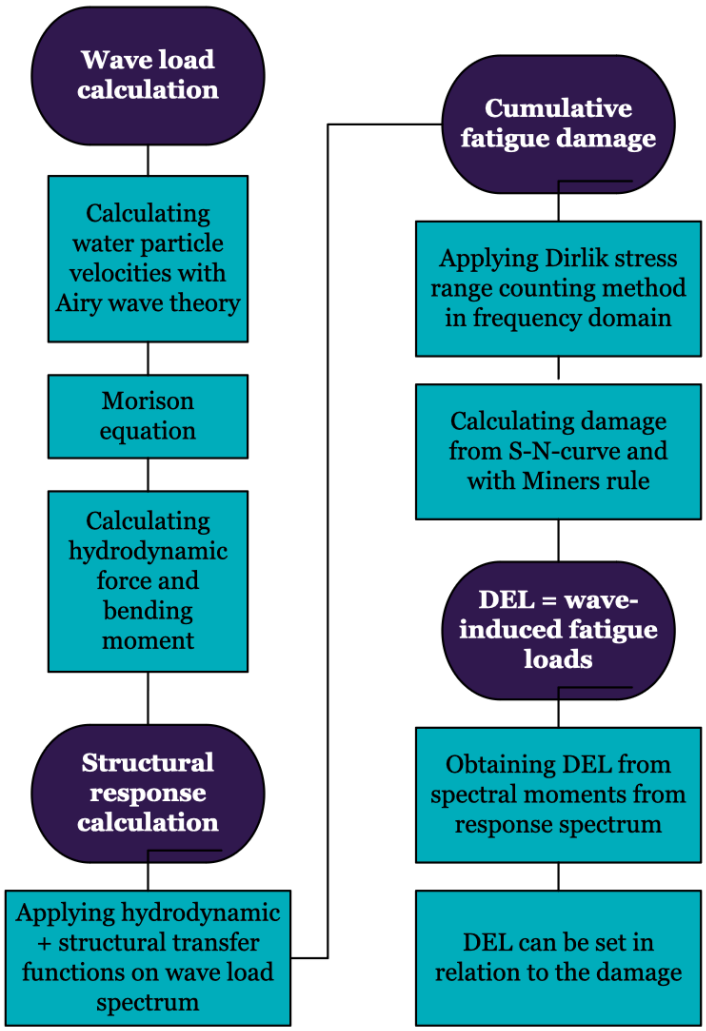

Figure 2.5: Procedure of the wave-induced fatigue load calculation

In the following sections the process, including the necessary equations for the fatigue load calculation will be described in detail.

2.2.1. Wave load calculation

To calculate the water particle velocities due to waves it can be made use of the straightforward and mostly widely used approach of the Airy linear wave theory. Within this theory water particles are assumed to move in closed orbits in an elliptical orbit for intermediate, and in a circular orbit for deep water depths. With increasing water depth below the free surface, the axes of the ellipse (short axis vertical, long axis horizontal) and the radius of the circle are decreasing as can be seen in figure 2.6 [40].

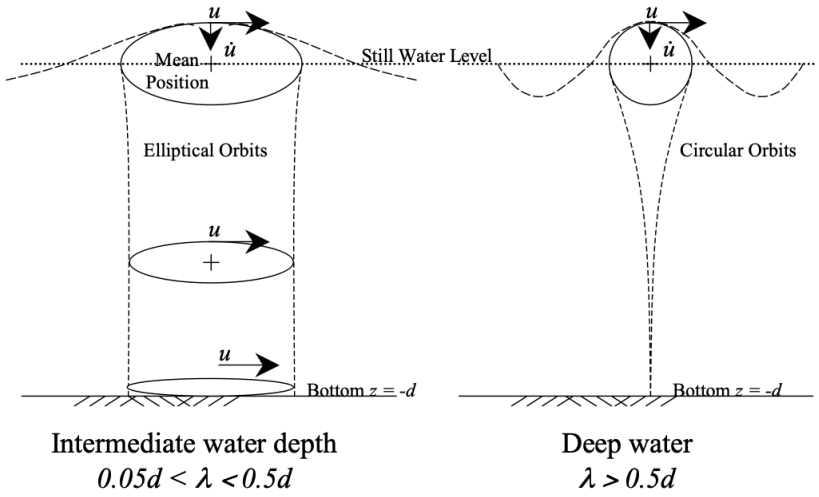

Figure 2.6: Particle orbits behaviour in deep an intermediate water according to Airy theory

The horizontal water particle kinematics, wave velocity u and acceleration $\dot{u}$ according to Airy theory can be calculated with equation 2.33 and 2.34 while considering the z-axis to point upwards from the free sea surface and the position s to point horizontal as it can be seen in figure 2.7 [40].

$$u = \xi \cdot \omega \frac{\cosh k(z+d)}{\sinh kd} \cos(ks) \tag{2.33}$$

$$\dot{u} = \xi \cdot \omega^2 \frac{\cosh k(z+d)}{\sinh kd} \sin(ks) \tag{2.34}$$

with

$$\begin{aligned} \xi &= \text{wave amplitude} \\ k &= \text{wave number} \\ \omega &= \text{wave frequency} \end{aligned} \tag{2.35}$$

The wave number k is calculated based on the wave length λ.

$$k = \frac{2\pi}{\lambda} \tag{2.36}$$

A slender member under the influence of hydrodynamic loading is shown in the following figure [40].

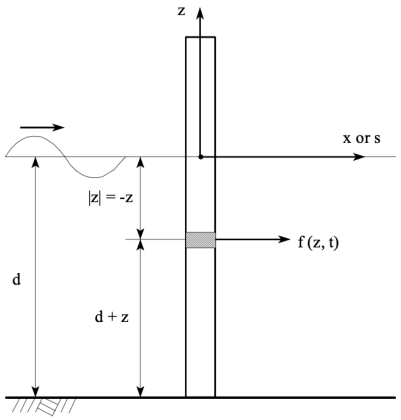

Figure 2.7: Axes definition of substructure with hydrodynamic loading

For each sea state that is defined by wave spectral parameters or with bulk wave parameters, respectively, wave kinematics and wave force spectra are calculated. The hydrodynamic force can be calculated with the Morison's equation for each fluid point that is defined in the structural model [40].

$$f = f_d + f_i \tag{2.37}$$

$$f_d = C_d \cdot \frac{1}{2}\rho D \cdot |u|u \tag{2.38}$$

$$f_i = C_m \cdot \frac{\rho \pi D^2}{4} \cdot \dot{u} \tag{2.39}$$

with

$$\begin{aligned} D &= \text{Diameter of the support structure} \\ C_d &= \text{Drag coefficient} \\ C_m &= \text{Inertia coefficient} \\ \rho &= \text{Water density} \\ f_d &= \text{Drag force} \\ f_i &= \text{Inertia force} \end{aligned} \tag{2.40}$$

The Morison's equation is partly nonlinear because it consists of the nonlinear drag term and the linear inertia term. By applying Borgmann's method, the nonlinear drag term can be linearized. For this research the impact of currents in the Morison equation is neglected at all.

In the frequency domain the flow conditions do not provide that much details to calculate the Morison coefficients. Assumptions and simplifications for the computation of the Morison coefficients must be made. Therefore e. g. marine growth and appurtenances which influence the roughness of the structure can be investigated. Furthermore, generic wave conditions are assumed that often occur for the fatigue loading case. The Morison coefficients C_d and C_m of the fluid flow must be calculated for each fluid point that is defined in the structural model to obtain the corresponding wave loads.

By integrating the inertia force f_i from the seabed $z = -d$ to the instantaneous water surface elevation ξ the hydrodynamic force F and bending Moment M can be obtained [40].

$$F = \int_{-d}^{\zeta} \{f_d\}\, dz \tag{2.41}$$

$$M = \int_{-d}^{\zeta} \{f_d\} \cdot (d + z)\, dz \tag{2.42}$$

The load that experiences the support structure is impacted by the hydrodynamic force which results from the interaction between the structural elements of the OWT and the waves. Stress fluctuations in the structure can be caused by the varying wave-induced bending moment which contributes to the fatigue damage.

2.2.2. Structural response calculation

From the calculated wave loads, the internal loads described as shear load and overturning moment in the monopile can be obtained. These internal loads are a function of frequency and height and describe thus a spectrum in the frequency domain. By making use of transfer functions the loads on the structure can be gained based on the calculated wave loads at the fluid points.

The hydrodynamic transfer function consists of a drag related term $\bar{F}_{D,n}(\omega)$ and an inertia related term $\bar{F}_{M,n}(\omega)$ and can be expressed for each mode n with the following formula [6]:

$$H_{a,n}(\omega) = \bar{F}_{D,n}(\omega) + i \cdot \bar{F}_{M,n}(\omega) \tag{2.43}$$

$$\bar{F}_{D,n}(\omega)+i\cdot\bar{F}_{M,n}(\omega)=\omega\cdot\rho\int_0^d c_d(z)\cdot\eta(\xi,\omega)\cdot\Phi_n(\xi)\,dz+i\cdot\omega^2\cdot\rho\cdot\int_0^d C_M(z)\left[\frac{\pi\cdot D(z)^2}{4}\right]\eta(\xi,\omega)\cdot\Phi_n(\xi)\,dz \tag{2.44}$$

with:

d : Water depth measured from seabed to still water level
$c_d(z)$: Hydrodynamic damping coefficient
$C_M(z)$: Inertia coefficient
ρ : Density of sea water
$D(z)$: Diameter of the structure at elevation z
$\eta(z,\omega)$: Distribution function for wave kinematics

Since only the inertia term is considered for monopiles with large diameters, the hydrodynamic transfer function can be reduced as shown below [6].

$$H_{a,0}=\rho\cdot\omega_0^2\cdot\int_0^d C_M(z)\cdot\left[\pi\cdot\frac{D(z)^2}{4}\right]\cdot\eta_0(z)\cdot\Phi_0(z)\,dz=\text{const} \tag{2.45}$$

The structural transfer function for mode n is defined as [6]:

$$H_n(\omega)=\frac{1}{1-\left(\frac{\omega}{\omega_n}\right)^2+2\cdot i\cdot\xi_n\cdot\frac{\omega}{\omega_n}}\cdot\frac{1}{K_n} \tag{2.46}$$

with:

ξ_n : Modal damping ratio for mode n
K_n : Generalized stiffness for mode n

The structural response spectrum can be obtained from the square of the combined structural and hydrodynamic transfer functions and the wave spectrum $S_{\zeta\zeta}(\omega)$ which results from the input wave field [6].

$$\begin{aligned}S_{uu}(z,\omega)&=|H(z,\omega)|^2\cdot S_{\zeta\zeta}(\omega)\\&=\left|\sum_{n=1}^{\infty}\Phi_n(z)\cdot H_n(\omega)\cdot H_{a,n}(\omega)\right|^2\cdot S_{\zeta\zeta}(\omega)\end{aligned} \tag{2.47}$$

The equation for the combined transfer function $|H(z,\omega)|$ that considers the mode shapes $\Phi_n(z)$ is stated below [6].

$$H(z,\omega)=\sum_{n=1}^{\infty}\Phi_n(z)\cdot H_n(\omega)\cdot H_{a,n}(\omega) \tag{2.48}$$

The process of the structural response calculation can be described in a matrix considering the input force and obtaining the response force as an output. Through interpolation, the response load spectra per element, which is considered as a node, can be found. By doing so it is made sure there is a relation to the load which is applied on the fluid points to the element loads of the structural model. The process of calculating the bending stress spectrum with the Morison's equation and the overturning moment based on the calculated wave particle kinematics with Airy linear wave theory is shown in figure 2.8.

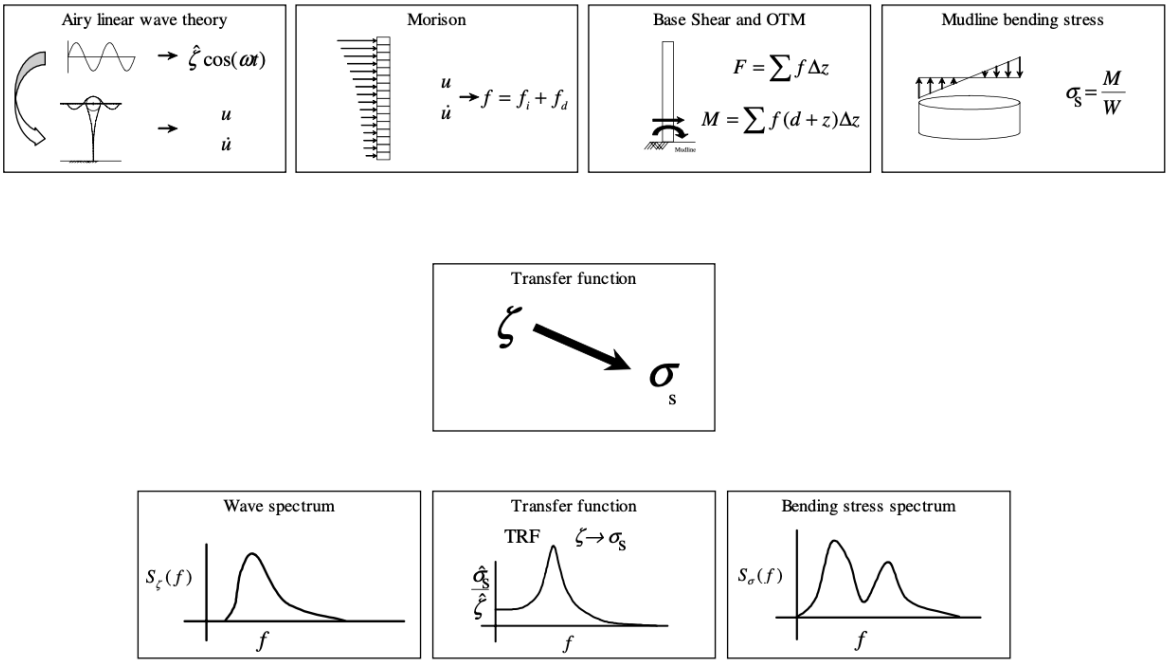

Figure 2.8: Process of obtaining the bending stress spectrum [41]

2.2.3. Cumulative fatigue damage and DEL

The irregular ocean waves result in dynamic loads that cause fatigue damage to the OWT substructure. The stress response spectrum describes how stresses vary as a function of frequency. To evaluate fatigue, the stress range experienced by the structure is needed. To obtain fatigue data of a structure the number of cycles until failure occurs, N_f, can be recorded at different stress-level amplitudes S. By doing so, fatigue data can be made visual in the mostly sinusoidal occurring S/N-curve [42]. The fatigue life prediction is a crucial part of the design process of OWT.

With the standard approach of the Palmgren-Miners [43] rule the damage on the OWT can be estimated based on the number of stress variations N_i and the binned number of variations n_i that can be identified per stress range class S_i based on the S-N-curve [41]. The cumulative fatigue damage is calculated with equation 2.49.

$$D_{\text{fat}} = \sum_i \frac{n_i}{N_i} \tag{2.49}$$

To check whether no failure to fatigue occurs based on the Miner rule, the cumulative fatigue damage needs to be smaller than 1.

$$D_{\text{fat}} < 1.0 \tag{2.50}$$

The process of the fatigue calculation due to different stress ranges and while making use of the S-N-curve and the Miners sum is shown in figure 2.9.

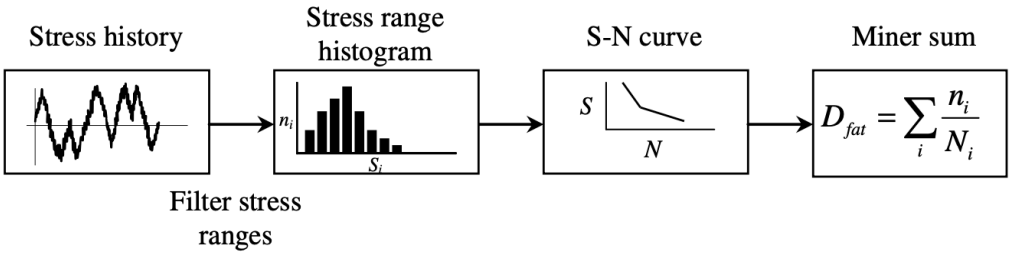

Figure 2.9: Fatigue damage calculation flow chart [41]

To identify the stress ranges and corresponding cycles one standard approach for time-domain calculations in the wind industry is the rainflow counting. One accurate approach that can be applied in the frequency domain and which delivers similar results to the rainflow counting is the empirical Dirlik method [41].

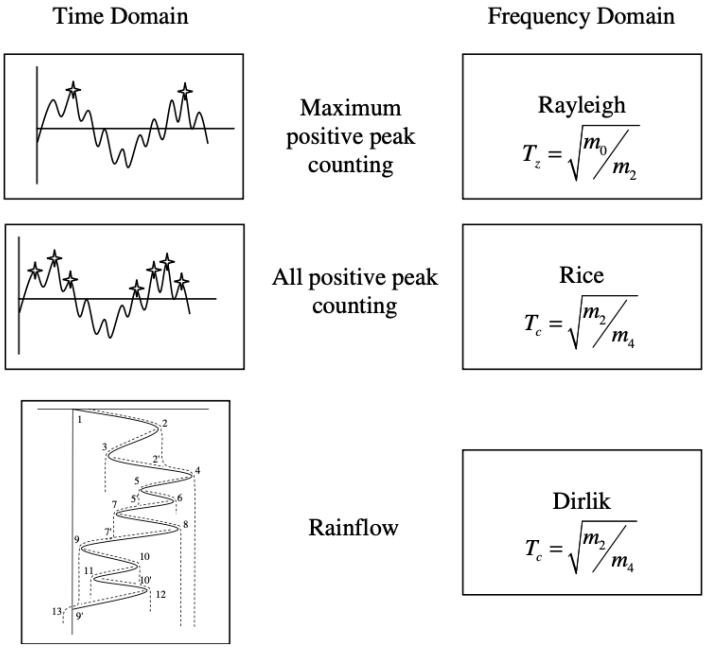

Figure 2.10: Overview of the time and frequency domain approaches of determining stress ranges [41]

The Dirlik probability density function is obtained with the following formula.

$$P_{\text{Dirlik}}(S_i) = \frac{\frac{D_1}{Q_D} e^{\frac{-z_D}{Q_D}} + \frac{D_2 Z_D}{R_D^2} e^{\frac{-z_D^2}{2R_D^2}} + D_3 Z_D e^{\frac{-z_D^2}{2}}}{2\sqrt{m_0}} \tag{2.51}$$

with the following Dirlik parameter:

$$Z_D = \frac{S_i}{2\sqrt{m_0}} \tag{2.52}$$

$$x_m = \frac{m_1}{m_0}\sqrt{\frac{m_2}{m_4}} = \frac{T_c}{T_m} \tag{2.53}$$

$$\gamma_D = \frac{m_2}{\sqrt{m_0 \cdot m_4}} = \sqrt{1-\epsilon^2} = \frac{T_c}{T_z} \tag{2.54}$$

$$D_1 = \frac{2(x_m - \gamma_D^2)}{1+\gamma_D^2} \tag{2.55}$$

$$D_2 = \frac{1 - \gamma_D - D_1 + D_1^2}{1 - R_D} \tag{2.56}$$

$$D_3 = 1 - D_1 - D_2 \tag{2.57}$$

$$Q_D = \frac{1.25(\gamma_D - D_3 - D_2 \cdot R_D)}{D_1} \tag{2.58}$$

$$R_D = \frac{\gamma_D - x_m - D_1^2}{1 - \gamma_D - D_1 + D_1^2} \tag{2.59}$$

The damage can be assumed to be proportional to the square root of the spectral wave energy at its first natural frequency. But this variable is an abstract quantity that is not physically measurable which is why a substitute for the damage, the Damage equivalent load (DEL) is introduced. The relation between Damage and DEL can be described with the following equation which considers the Wohler Slope m which is the inverse of the S-N-curve with values between usually 3 and 5 for steel as well as the number of reference cycles N [6].

$$Damage = (DEL)^m * N \tag{2.60}$$

With DEL, the load level for a specific number of cycles can be expressed that leads to the same damage as could have been obtained from the original summation of a number of different load cycles considering different amplitudes [44].

2.2.4. Design loads

On the obtained characteristic wave loads on the structure a partial safety factor can be applied to obtain the design wave loads on the structure. This would especially be relevant for the extreme wave loading case. The design criterion within the partial safety format considers that the design load effect S_d must not exceed the design resistance of the structure R_d.

$$S_d \leq R_d \tag{2.61}$$

This partial safety factor can be determined for normal or abnormal conditions. For wind turbine loads the partial safety factor is usually γ_f = 1,35 for normal and γ_f= 1.1 for abnormal events. Compared to that the partial safety factor for fatigue loads is usually γ_f = 1,0 for normal and abnormal design situations [45].

$$S_{d,i} = \gamma_{f,i} \cdot S_{k,i} \tag{2.62}$$

3. Methods

This section outlines the MetOcean data used for this research, specifying the source database and the location from which the data was collected. Additionally, it explains the process used to calculate wave-induced fatigue loads using the frequency domain tool FUEL.

3.1. Method of MetOcean data analysis

3.1.1. MetOcean data source

DHI (Dansk Hydraulisk Institut), an international water software development and engineering consultancy firm, was awarded in September 2018 by the Netherlands Enterprise Agency (Rijksdienst voor Ondernemend Nederland, RVO) to carry out a feasibility level study of the MetOcean conditions and to provide a MetOcean database consisting of detailed MetOcean data for the potential offshore wind farm zones Ijmuiden-Ver, Ten Noorden van de Waddeneilanden and Hollandse Kust (west) which are all part of the Dutch North Sea. This strategic water and wind site assessment is available for free for end-users of future offshore wind energy projects.

Initially, wave spectral data close to the Ijmuiden Ver Wind Farm Zone (IJVWFZ, Longitude [°E]: 3.29, Latitude [°N]: 52.48), recorded from 1979 until 2023 was obtained from the web interface of the DHI Metocean Data Portal, called MOOD. This is a web-based digital database that allows users to access the analysis results and the modelling data at a chosen location.

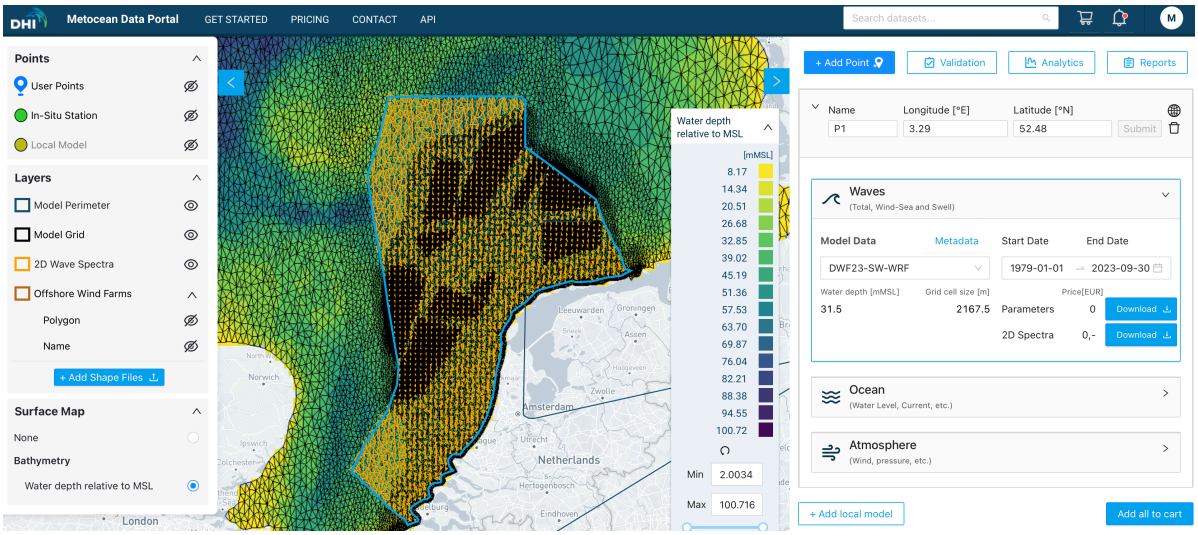

Figure 3.1: DHI's MOOD web interface, [46]

The following table summarizes data of the considered wave and wind data models.

Dependent variables	**Values**
Spectral wave data model	DWF23-SW-WRF
Start data record	01.01.1979
End data record	30.09.2023
Duration sea state [sec]	3600
Atmospheric wind data model	DWF23-AT-WRF
Start data record	01.01.1979
End data record	01.10.2023
Duration sea state [sec]	600

Table 3.1: Main data of the considered MetOcean wave spectral and atmospheric wind data models for the Dutch North Sea

For the 2D-wave spectra as well as for the bulk wave parameters the same data model is considered. This ensures consistency and provides the same framework for further calculations during this research. The duration of the sea states for the spectral wave data model is equal to 1 h which is a reasonable choice in order to assume the sea surface elevation as a stationary process. This 1-hour representation of the wave data corresponds to one wave data observation per hour [15, p. 135].

The basis for the wind data is given by an atmospheric data model, DWF23-AT-WRF which contains data of the wind speed at 10 m height, measured every 10 minutes. This data is resampled from 10-minute to hourly intervals to ensure consistency with the spectral wave data model.

The DWF23-SW-WRF is a hydrodynamic (HD) and spectral wave numerical model (SW) which was developed for the purpose of the construction of Dutch offshore wind farms (DWF) for the North Sea. With this dataset a large area of the Dutch North Sea sector is covered. It provides a high-resolution (down to $\sim$ 400 m) and is based on DHI's MIKE 21 software package. Using the MIKE 21 HD model, a local hindcast 2D hydrodynamic model was set up for the simulation of currents and water levels. Most of the Dutch offshore wind farm areas, and not only the IJV Offshore Wind Farm Zone, are covered with this data model, within Dutch maritime boundaries. With the MIKE 21 SW spectral wave model, which covers the same domain as the hydrodynamic model, the waves were simulated. Based on wave, wind, current and water level measurement data an extensive validation of the models was carried out. From that validation, a high quality model performance resulted [47].

The measured significant wave heights that were obtained from this spectral wave model were from the DHI MetOcean database validated against values of the significant wave height that were measured by a satellite altimeter.

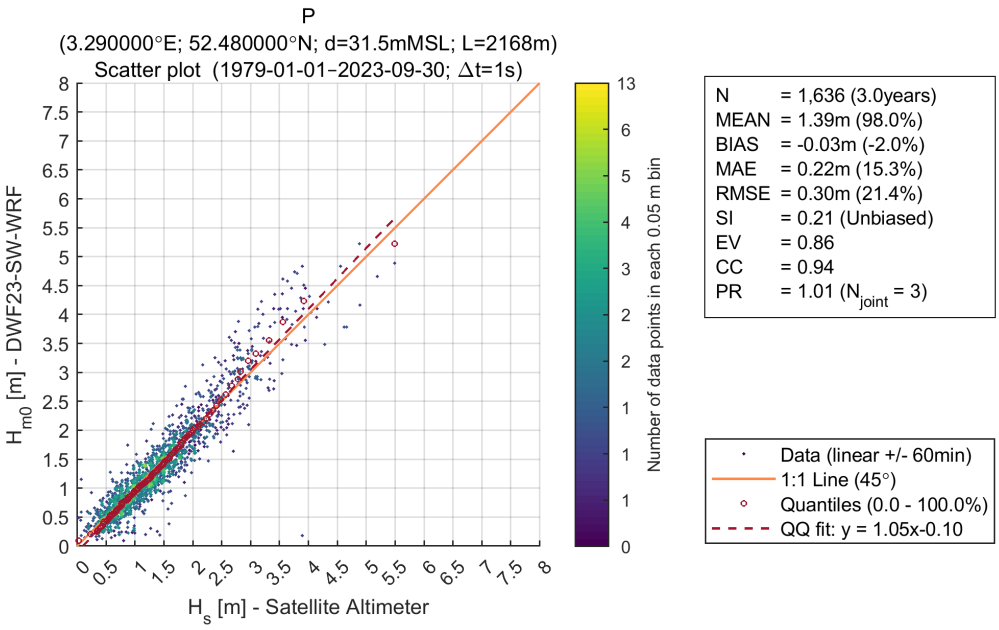

Figure 3.2: Validation of the significant wave height of the data model DWF23-SW-WRF with a satellite altimeter, [46]

The measured wind speeds at 10 m height that were obtained from the atmospheric Weather Research and Forecasting (WRF) model were from the DHI MetOcean database validated against wind speed data at 10 m height obtained from a satellite altimeter.

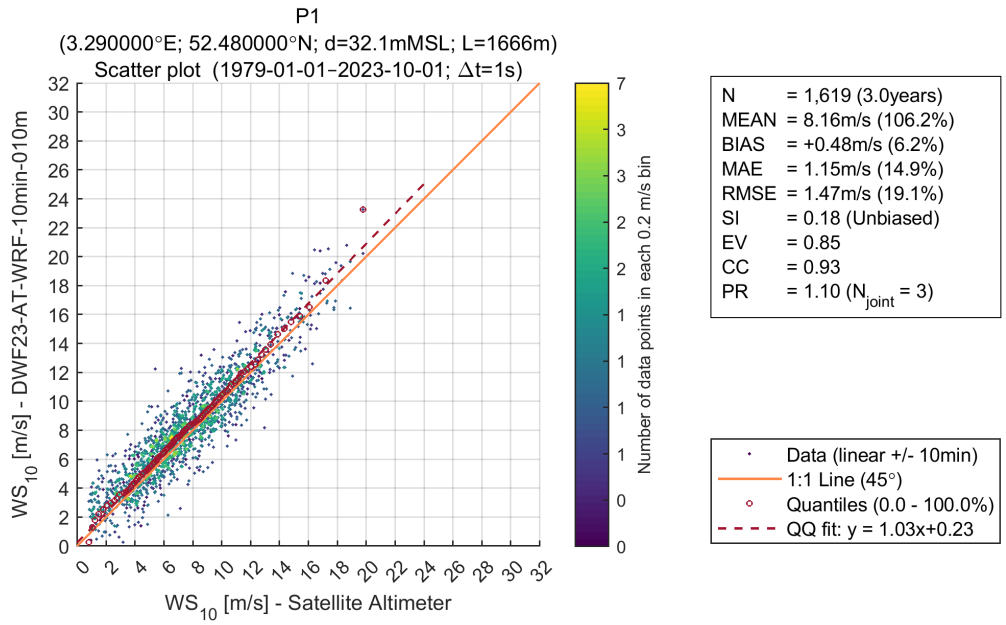

Figure 3.3: Validation of the wind speed of the atmospheric model DWF23-AT-WRF against satellite altimeter, [46]

From the figures it can be concluded, that the investigated parameters, significant wave height and wind speed show a good alignment with the obtained values from the satellite altimeter.

3.1.2. Location and geographic description

The IJmuiden Ver Wind Farm Zone (IJVWFZ) is situated 62 km (33.4 nautical miles) in the Dutch North Sea off the west coast of the Netherlands. It comprises three designated sites: Alpha (formerly IJVWFS I - II), Beta (formerly IJVWFS III - IV), and Gamma (formerly IJVWFS V - VI). The upcoming permit tenders will focus on the Alpha and Beta sites [48].

Figure 3.4: Location of Ijmuiden Ver wind farm zone, [48]

Table 3.2 summarizes the site parameters for the Ijmuiden Ver study area.

Dependent variables	Values
Longitude [°E]	3.29
Latitude [°N]	52.48
Water Density [kg/m^3]	1025
Water Depth [m]	31.5

Table 3.2: Site parameters for the Ijmuiden Ver study area

The combined surface area of IJVWFS Alpha and IJVWFS Beta, including the designated maintenance and safety zones, covers approximately 650 km². However, this area includes safety and maintenance zones around existing infrastructure, such as active cable crossings, which reduces the effective space available for new wind farm construction [48].

3.2. Method of fatigue load analysis

3.2.1. Frequency Domain Tool

Wave loads are applied in the frequency domain and as by doing so simplifications can be made and compact equations can be used to determine the wave loads efficiently [4]. The wave-induced fatigue loads can also be calculated with time domain simulations but this approach is rather time consuming and seems therefore to be less practical than using the frequency domain approach with which still very accurate fatigue loads can be calculated [49].

At Siemens Gamesa Renewable Energy a frequency domain tool called ”Frequency domain Utility for the Estimation of Loads” (FUEL) was developed for internal studies to calculate the wave-induced loads

and the corresponding structural response of primary structures such as monopiles. It is used together with another internal, hybrid tool called the ”Siemens WAve Generator” (SWAG), which operates in the time-domain as well as in the frequency domain.

The fatigue load calculations will be carried out with this frequency domain tool. So far, wave induced fatigue loads were calculated based on bulk wave parameters that were obtained from a MetOcean database and by applying the JONSWAP spectral model, the frequency-dependent spectral density distribution was calculated from which the wave loads, the structural response and finally the wave-induced fatigue loads were computed.

To account for frequency-directional wave spectral data instead of bulk wave parameters as input for the wave-induced fatigue load calculation, adjustments in the MATLAB-based frequency domain tool needed to be done. For the approach of using frequency-directional wave spectral data, the input data for the frequency domain tool included the wave spectral densities and the corresponding directional and frequency values instead of bulk wave parameters as it was the case for using the JONSWAP spectral parametrization. To implement the wave spectral data, the obtained MetOcean data first needed to be analyzed and processed as a preparation and to make sure that the implementation of the data is done correctly. The implementation considers the accessing of the processed wave spectral data which is distributed over a number of directions.

Wave spectral data input

For the calculation of wave-induced fatigue loads, frequency-directional wave spectral data and obtained bulk wave parameters are used. The frequency bins of the frequency-directional wave spectral data that was obtained from the DHI MetOcean database needed to be interpolated to achieve a better resolution of the wave spectral density distribution.

From the DHI MetOcean database bulk wave parameters, such as the significant wave height, peak period and wave direction were obtained for the same data model and the same location as the 2D wave spectral is based on. Within this obtained dataset it will be distinguished between parameters for the wind-sea and swell as well as for the combined (total) wave system. All necessary bulk wave parameters that were obtained, were stored in a simulation list which also contains the obtained wind data that was downloaded for the data model as it will be described in more detail in section 3.1.

To calculate a spectral shape parametrization, different spectral models can be used. The most widely applied and also during this research used spectral parametrization is the JONSWAP spectral model but also the Pierson-Moskowitz model could be used for the calculation of the distribution of the wave spectral density across frequencies. For these spectral types necessary parameters such as the peak frequency, the peakedness parameter and the spectral densities are calculated. The peakedness parameter γ can be calculated based on the Tp/Hs-ratio if it is not specified for the JONSWAP spectral shape. For each new sea state with different Tp/Hs-ratio combinations a different corresponding wave spectrum is calculated.

An overview of the processing of the used MetOcean data is given in figure 3.5.

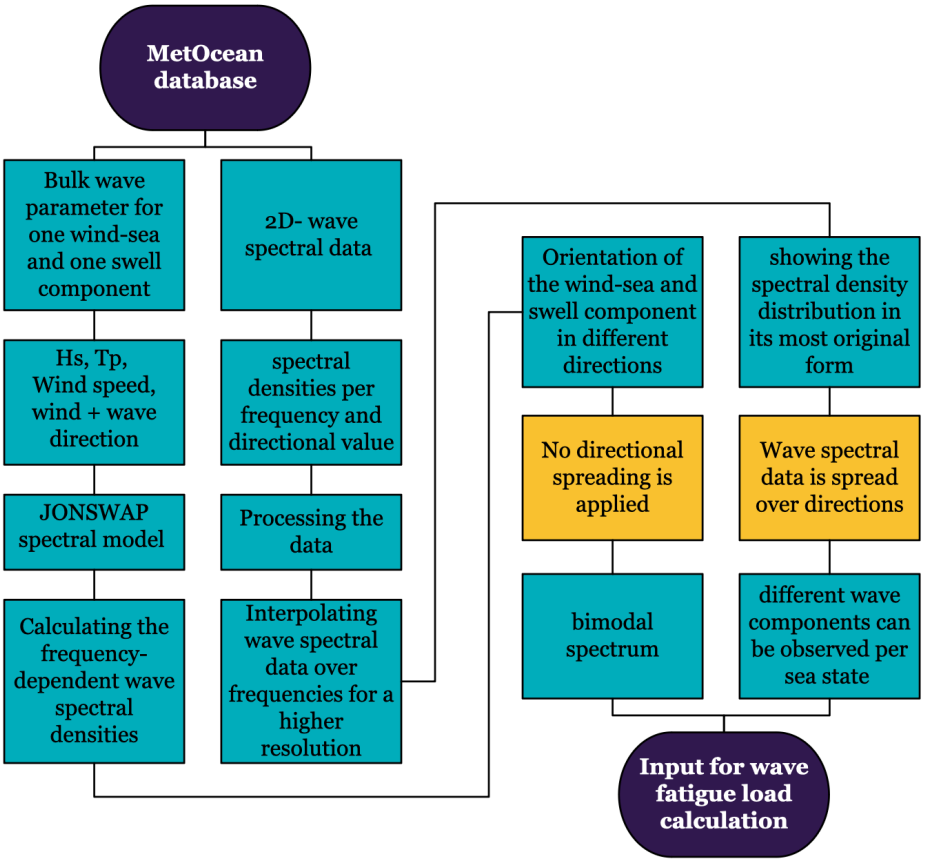

Figure 3.5: Procedure of calculating the wave-induced fatigue loads

3.2.2. Structural and environmental design considerations

The selection of an appropriate method to analyze the structural response to wave loading depends on understanding key influencing factors. These factors include the dynamic interaction between the structure and wave loading, which can be modeled using deterministic or stochastic design methods, depending on the specific design requirements [25, 50].

Fatigue limit state

For the design of substructures of OWT, the fatigue limit state (FLS) is an important design loading case (DLC) to consider to guarantee reliability and to cover the most significant load conditions. Fatigue of the substructure of OWT which can lead to its mechanical failure can occur due to the repetitive application of environmental loads such as wave loads. Structural failure due to fatigue loads differs from the mechanical failure due to extreme loads which results from the application of one single extreme component [42]. For the fatigue loading case all sea states, that are obtained from the Metocean database are considered.

In many cases the FLS drives the design but as weather conditions seem to become more extreme and as turbines must be constructed to withstand these increasingly harsher environmental conditions the Ultimate Limit State (ULS) becomes of higher relevance [51]. However, investigating the ULS is beyond the scope of this research.

Dynamic response of structures

A dynamic response of the structure can be caused if the natural period of the substructure would be close to the period of the wave-loading whereas a quasi-static response can be expected if the period of the wave-loading is a lot longer than the natural period of the substructure. As the resonant dynamic response from fatigue wave loading for substructures, such as a monopile, is of importance to make

sure that resonance is avoided, a spectral random wave analyses is required for which wave spectra will be analyzed [50].

Design load situations

Wave loads can be considered for different design situations such as production and idling [15]. The total lifetime of the OWT which is assumed to be 25 years, is divided into 23 years for the design loading situation of production and 2 years for the case of idling. During the power production design situation, the OWT is operating and is actively generating electricity while being connected to the electrical grid.

The idling design situation refers to the case that the OWT does not generate electricity. The rotor is in this situation rotating very slow which results in less aerodynamic effects. OWT are idling for the case of system malfunction, maintenance or if the wind speed would be out of the range of the operational wind speed, e. g. too low [15, 52]. Though, during idling the highest loads for the support structure occur and to ensure the technical availability of the OWT this design situation is considered during the design process [49].

The fatigue load calculatios are thus done for each sea state considering the idling design load situation.

Structural model for analysis

The considered structural model is based on the SG 14-222 DD Siemens Gamesa Renewable Energy offshore wind turbine which provides a capacity of up to 15 MW. The diameter of the monopile is approximately 9.00 m and varies slightly over the height of the structure. The OWT has an eigenfrequency of 153 mHz.

For the load calculation a finite element (FE) structural model of the axisymmetric fixed-bottom OWT is set up consisting of a mass which represents the rotor-nacelle assembly and a spring-damper system to account for the aerodynamic damping in fore-aft and side-side direction. These two directions represent the two degrees of freedom of the finite-element (FE) model. Structural damping occurs in the structure itself, but it does not account for the aerodynamic damping. That is considered in the FE model. The soil into which the monopile is embedded is assumed to be linear elastic.

Figure 3.6 shows the structural model of the OWT with the definition of the geometry, as well as load, axes and the fore-aft and side-side directions.

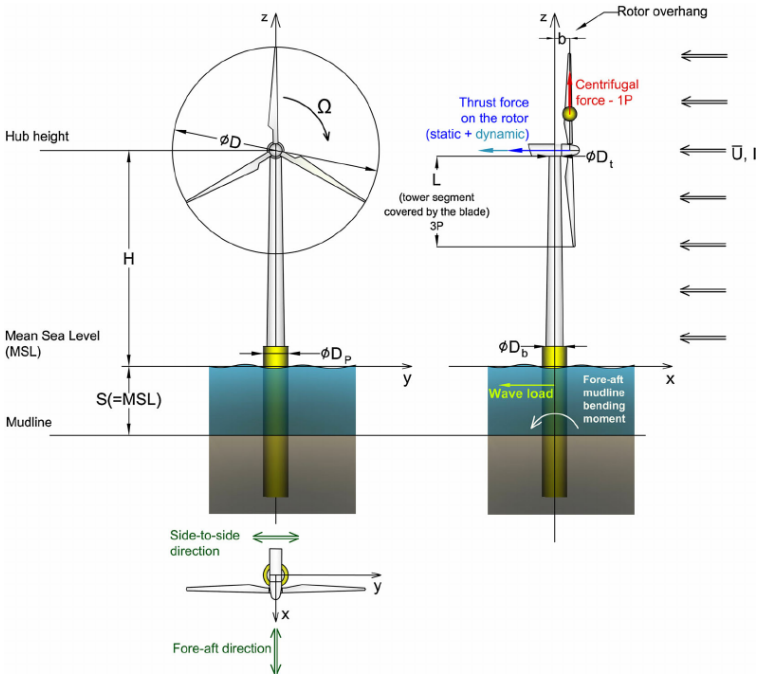

Figure 3.6: Structural model of the OWT with definition of the geometry, axes, loads and directions [53]

Wind-wave misalignment

For fixed-bottom founded offshore structures it was often seen as conservative to assume that the spectral density of wind and waves are coinciding in one direction, meaning they are co-directional. This resulted from the fact that the loading in fore-aft direction is the highest when the hydrodynamic and aerodynamic loading is assumed to originate from the same direction [54, 5].

To consider the correlation of normal wave and wind conditions for the DEL calculation in the frequency domain, wind-wave misalignment from the mean wave and wind conditions must be taken into account as the loads on the support structure are influenced by the multi-directional distributions of wave and wind directions [15].

From the response load spectra for each sea-state the fore-aft (longitudinal) and side-side (lateral) components for the description of the forces and moments acting on the OWT as indicated in figure 3.6, are investigated which are associated with spring-damper systems. Fore-aft loads are aligned with the wind direction and are acting along the plane of the rotor. From these fore-aft loads bending moments at the base of the tower are resulting whereas the side-to-side loads are acting perpendicular to the rotor plane. This means that the resulting wave spectrum for each sea-state is projected onto the fore-aft and the side-side component which results in two considerable spectra from which the spectral moments can be derived. Thus the occurring loads are mapped regarding these components of the OWT.

Moreover, these orthogonal wave directions are decomposed into three different bins per quadrant, each 30 deg in width, to account for the wind-wave misalignment. Thus a response spectrum to calculate the fatigue damage will be obtained for each considered misalignment angle (0,30,60,90 deg). The definition of this misalignment angles helps reducing the computational costs [55].

Since wave loading and structural response can be symmetrical with respect to wind and wave directions, mirroring the sectors would be a reasonable approach to extend the analysis from 0 to 360 deg. In practice, this means that the differences in the wave-induced fatigue load values between the JONSWAP and the actual 2D-wave spectra that were calculated for the 0–180-degree sectors can be applied to their mirrored counterparts in the 180–360-degree range which is shown in figure 3.7.

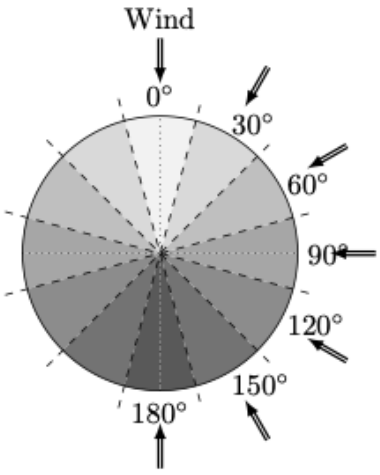

Figure 3.7: Structural model [5]

Sector (0°–180°)	Mirrored Sector (180°–360°)
0°–30°	330°–360°
30°–60°	300°–330°
60°–90°	270°–300°
90°–120°	240°–270°
120°–150°	210°–240°
150°–180°	180°–210°

Table 3.3: Mirrored sectors from 0°–180° to 180°–360° for DEL analysis.

Though, if no misalignment angle is available at all, an equivalent misalignment angle of 30 deg, established by Seidel, can be used to account for wind-wave misalignment [56].

3.2.3. Fatigue load differences

The fatigue load differences from the JONSWAP and the frequency-directional wave spectra will be investigated in the fatigue load analysis in chapter 5. Therefore, the DEL differences and the damage differences will be investigated.

Since the DEL are calculated with the frequency domain tool per sector, per sea state the sector with the largest DEL is considered. Next to the investigation of the absolute wave induced fatigue loads, the relative damage ratio and the damage difference ratio are considered for the analysis between the fatigue loads and the environmental parameter and wave characteristics in chapter 5. The damage ratio and damage difference ratio are calculated with the equations 3.1 and 3.2.

$$\text{Damage ratio} = \frac{\text{Damage per sea state}}{\sum \text{Total damage}} \tag{3.1}$$

$$\text{Damage difference ratio} = \frac{\text{Damage difference per sea state}}{\sum \text{Total damage difference}} \tag{3.2}$$

To show the overall fatigue potential that results from various sea states, the average cumulative fatigue damage will be used in chapter 5 since it is directly proportional to the number of load cycles and their intensity as it was shown in chapter 2.2.

Showing the averaged damage is a better approach than using averaged DEL for the overall load representation. This results from the fact that DEL are calculated load amplitudes, that cause the same fatigue damage as the varying loads the structure actually experiences. But DEL are no direct measures of the cumulative fatigue loads. To obtain this equivalent single value, DEL's are obtained from the stress history by applying Miner's rule and S-N-curves. But DEL's do not add linearly which is why using averaged DEL's is not the most accurate approach to gain insights in the overall wave-induced fatigue distribution since with the calculation of DEL's the direct link to load cycles or real stress range variations is not retained.

Instead of summing up the DEL's for further calculations, the damages can be summed up for a number of sea states and converted back into DEL's by considering the Wohler's slope and the the number of reference cycles.

3.3. Method of distance correlation analysis

3.3.1. Overview

With correlation coefficients which are usually expressed in numbers within the range of [0,1] or [-1,1], the strength of the dependence between random observations can be measured to analyse the MetOcean data statistically [57].

A simple linear correlation indicates a relationship between two variables or phenomena, where a change in one variable results in a corresponding change in the other, either increasing or decreasing. When both variables increase or decrease together, their relationship is positive. Conversely, if one variable decreases as the other increases, the relationship is negative.

Table 3.4 indicates the meaning of the values of correlation coefficients [58].

Value of correlation coefficient	The meaning
+1	Completely positive correlation
From 0.70 - 0.99	Strong positive association
From 0.50 - 0.69	Average positive correlation
From 0.01 - 0.49	Weak positive correlation
0	Not a positive relationship

Table 3.4: Interpretation of correlation coefficients

A distance correlation value close to 1 indicates a strong dependence between X and Y, whether linear or nonlinear. A value close to 0 indicates that X and Y are independent. It is particularly powerful for detecting more complex, nonlinear suspected relationships between the wave or wind characteristics and the DEL differences, that other correlation coefficients such as Pearson or Spearman coefficient might miss. It does not assume normality, linearity, or monotonicity, which makes it more flexible [57].

A key advantage of distance correlation is that it is zero if and only if the variables are independent, making it useful for independence testing. One disadvantage of the distance correlation is that for the calculation of the distance covariance, pairwise distances must be computed, for all points in the dataset, which can become computationally expensive for large datasets. For very small sample sizes, the distance correlation may be less stable, so it's more appropriate for larger datasets which is the case for the investigated MetOcean dataset [57].

3.3.2. Aim

The aim of this correlation analysis is to identify how the wave spectral characteristics such as frequency width, directional width and peakedness parameter depend on defined ranges of the DEL differences, which were determined in the previous chapter based on the analysis of the wave and wind parameters. The results of the distance correlation analysis which are shown in section 5.4 are based on the equations indicated in this section.

3.3.3. Calculation

The distance correlation coefficient is a standardized coefficient that can be used to detect linear as well as nonlinear relationships between variables as it measures the correlation based on the distance between the points in a dataset, rather than the raw values [57].

$$\mathrm{dCor}(X,Y) := \frac{\mathrm{dCov}(X,Y)}{\sqrt{\mathrm{dCov}(X,X)\cdot \mathrm{dCov}(Y,Y)}}. \tag{3.3}$$

with

$$\begin{aligned} X &= \text{random variable - investigated wave characteristic} \\ Y &= \text{random variable - DEL differences} \\ \mathrm{dCov} &= \text{Distance covariance} \end{aligned} \tag{3.4}$$

The distance covariance can be calculated with the following equation where $\mathbb{E}$ refers to the expectation (or average) of the quantity inside the brackets, meaning the average of the pairwise distances over all possible combinations of samples from the distribution of the X and Y variables.

$$\mathrm{dCov}^2(X,Y) := \mathbb{E}\left(|X-X'|\cdot|Y-Y'|\right) + \mathbb{E}\left(|X-X'|\right)\mathbb{E}\left(|Y-Y'|\right) - 2\mathbb{E}\left(|X-X'|\cdot|Y-Y''|\right) \tag{3.5}$$

The following term as part of the distance covariance equation captures the joint variability between the variables X and Y since it measures how distances between observations in X correlate with distances between observations in Y.

$$\mathbb{E}\left(|X-X'|\cdot|Y-Y'|\right) \tag{3.6}$$

The marginal variability's are measured separately for X and Y with the following term.

$$\mathbb{E}\left(|X-X'|\right)\mathbb{E}\left(|Y-Y'|\right) \tag{3.7}$$

To account for the correction of the marginal dependence between the two random variables X and Y, the following term is considered as well in the distance covariance equation. This term helps to remove the part of the covariance that is due to the variability of X and Y independently. The idea is that if X and Y were totally independent of each other, then their distance covariance would only reflect their separate variances, not their relationship. This term adjusts for that by isolating the variability that is specifically due to the interaction between the two variables.

In simpler terms, this adjustment helps to make sure that the distance covariance measures how X and Y are related to each other.

$$2\mathbb{E}(|X-X'|\cdot|Y-Y''|) \tag{3.8}$$

4. Results of MetOcean data analysis

4.1. Wave and wind climate

Within this section an overview of the statistics on the wave and wind characteristics will be given.

Table 4.1 summarized crucial statistical measures for the bulk wave parameters such as significant wave height, peak period and the wind speed, based on the combined wind-sea and swell component as they can be calculated with equation 2.8 as shown in section 2. The mean value indicated the average value of the MetOcean data and the median value the middle value that is found by ordering all values. The standard deviation shows in relation to the mean, how dispersed the data is. A large value of the standard deviation indicated a broader spread of the data around the mean value, whereas a smaller value indicates a tighter clustering of the data around the mean. The range shows the difference between the maximum and minimum value. Below the value of the 10th percentile fall 10 % of the shown MetOcean data, whereas the 90th percentile indicates above which value still 10 % of the data can be observed.

Dependent variables	**Values**
Hs mean [m]	1.38
Hs median [m]	1.16
Hs max [m]	7.19
Hs standard deviation [m]	0.91
Hs range [m]	7.19
Hs 10 % range [m]	0.44
Hs 90 % range [m]	2.62
Hs 95 % range [m]	3.22
Tp mean [s]	9.62
Tp median [s]	9.26
Tp max [s]	27.54
Tp standard deviation [s]	2.93
Tp range [s]	26.13
Tp 10 % range [s]	6.24
Tp 90 % range [s]	13.43
Tp 95 % range [s]	15.12
Wind speed mean [m/s]	10.19
Wind speed median [m/s]	9.65
Wind speed max [m/s]	38.36
Wind speed standard deviation [m/s]	5.18
Wind speed range [m/s]	38.3
Wind speed 10 % range [m/s]	3.85
Wind speed 90 % range [m/s]	17.22
Wind speed 95 % range [m/s]	19.68

Table 4.1: Statistical overview of key MetOcean parameter

The mean and median values for the significant wave height are relatively low, indicating that most sea states have moderate wave heights. However, the maximum value of 7.19 m indicates the presence of extreme wave conditions that can drive higher fatigue loads. The 90 % range indicates that most sea states have significant wave height values below 2.62 m, which correlates with the higher density of points clustered in the lower significant wave height range as can be seen in figure 4.1.

Extreme events will be associated within this research with those data points occurring in the upper 5 % of the datasets of the significant wave height, the peak period and the wind speed. Sea states with significant wave heights above 3.22 m can thus be counted to the extreme events.

The peak period is important because longer periods are typically associated with more powerful waves that can drive greater structural responses. The higher 90 % range for peak periods (13.43 s) and the maximum value (27.54 s) suggest the occurrence of long-period waves. Peak periods with values above $\sim$ 15 s can be associated with extreme events. The relationship between the significant wave height and the peak period, as visualized in figure 4.1, indicates a clustering of points in the lower peak period range for lower significant wave height values, but with longer periods for higher wave heights (above 4 m).

The mean and median wind speeds (around 10 m/s) align with moderate sea states, but the maximum wind speed of 38.36 m/s shows that there are occasional extreme wind events that may drive large wave heights and contribute to outliers in the fatigue damage results. The plot of the significant wave height against the wind speed in figure 4.1 shows a general correlation between higher wind speeds and higher significant wave heights, which can be expected. Sea states with associated wind speeds of more than $\sim$ 20 m/s can be referred to as extreme sea states. The mean and median values for all parameters are indicative of more typical, moderate conditions.

The relationships between the combined significant wave heights of the wind-sea and swell components and the peak period as well as the wind speed are shown in figure 4.1, with a color density indication for the number of sea states at different points. The histogram of the significant wave height shows its probability distribution.

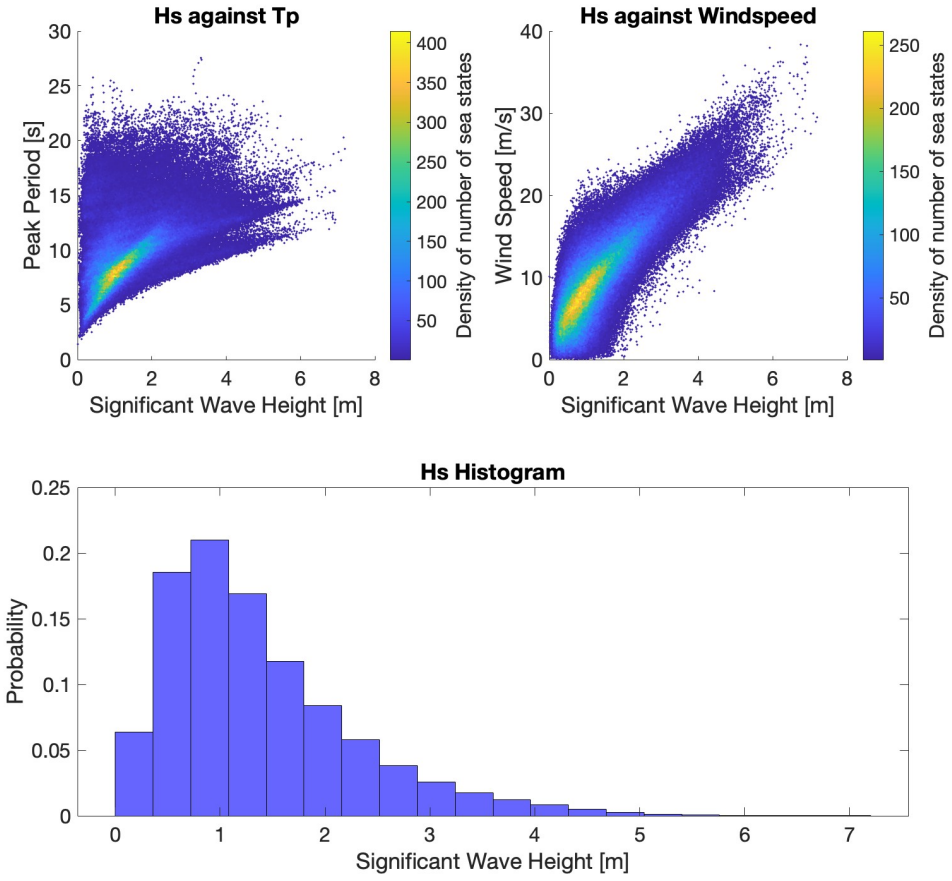

Figure 4.1: Significant wave height characteristics

The top left plot shows a positive correlation between the significant wave height and the peak period indicating that higher waves tend to have longer periods. The density of the number of sea states (represented by the color bar) is highest at wave heights around 2–4 meters and periods of around 5–15

seconds. As the wave height increases, the peak period also increases, which is typical for more developed sea states.

In the top right plot a clear positive correlation is visible between the significant wave height and the wind speed. As the wind speed increases, so does the wave height. Most sea states occur at lower wind speeds around 5–15 m/s and moderate wave heights around 2–4 m. It can be concluded that the wind speed plays a major role in wave development, as stronger winds are typically associated with larger waves. As waves grow taller, their periods grow longer, and stronger winds tend to generate larger waves. Clear positive correlations are visible between the significant wave height against the peak period and the wind speed.

The histogram, as shown in the bottom plot, shows the probability distribution of the significant wave height, which is binned within 20 bins. It shows that the most common and frequently observed wave heights are around 1 meter, with a probability peak around this value. As the wave height increases, the probability of occurrence decreases, indicating that higher waves are less common than lower ones.

The peak period characteristics such as its relation to the wind speed and wind-sea wave direction (considering the wind-sea component) as well as a histogram, showing the probability distribution of the in 20 bins binned peak period is shown in figure 4.2. The data of the peak period, shown in this figure corresponds to the combined peak period values of the wind-sea and swell wave component.

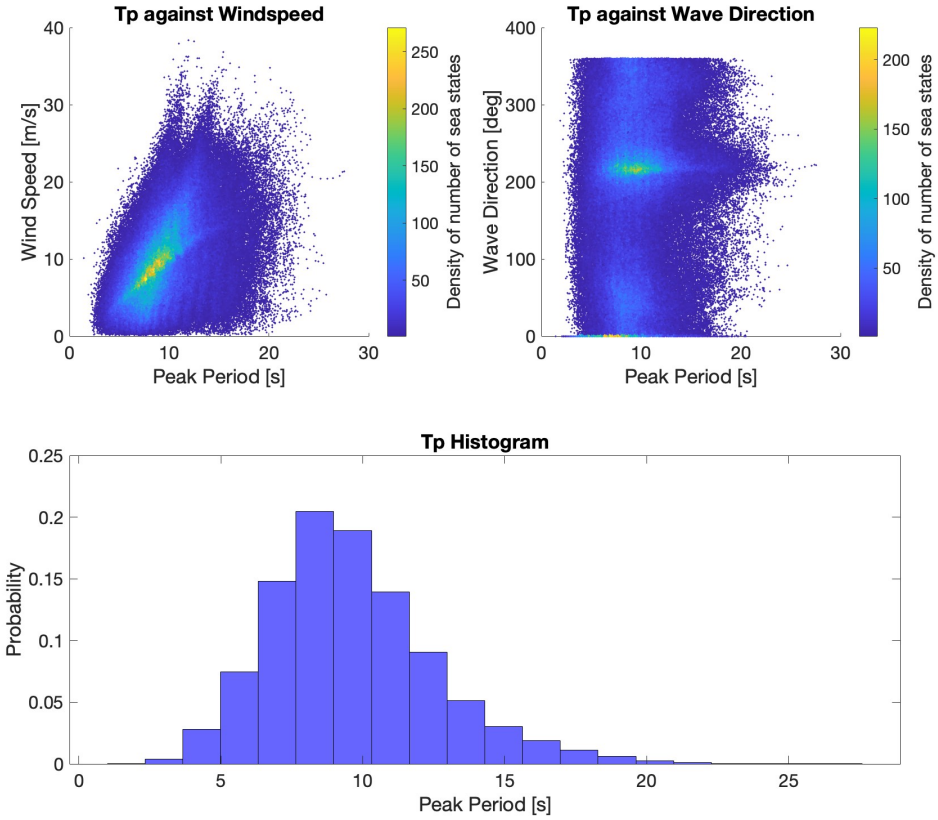

Figure 4.2: Peak period characteristics

In the top left plot there is a positive correlation between the peak period and the wind speed visible. As the wind speed increases, the peak period also increases. The highest density of sea states is observed in wind speeds ranging from 5–15 m/s and peak periods between 5–15 s. This correlation suggests that stronger winds are typically associated with longer wave periods. It aligns with the general understanding that the wind speed is one of the primary drivers of wave period development. Wave periods are

spread across different wave and wind directions, with no strong trend visible. The highest density of sea states is observed around wind-sea wave directions of approximately 210°–250°, across all peak periods.

The histogram, shown in the bottom plot, shows the probability density distribution of the peak period, binned in 20 bins. The calculated mean and median values of the peak period corresponding to the considered dataset, as shown in table 4.1, can also be identified within probability distribution which shows peak values, for peak period between 8 and 10 s.

Figure 4.3 indicates the wind characteristics by showing the wind speed scatter plot against the wind direction, a wind direction rose plot as well as a wind speed histogram.

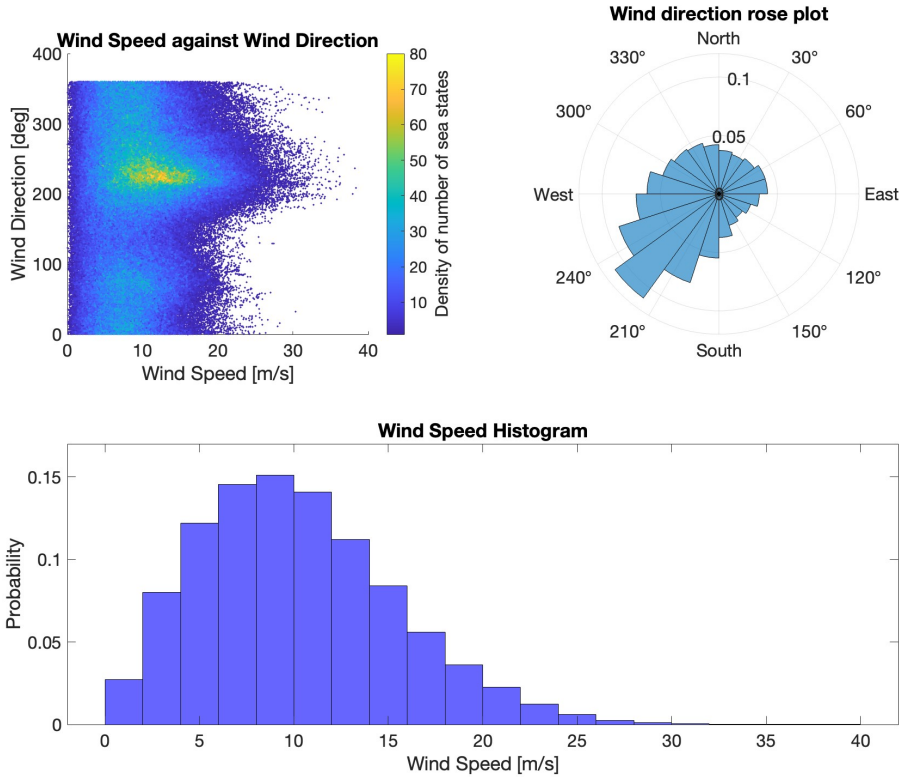

Figure 4.3: Wind speed characteristics

The top left plot shows the relationship between the wind speed and the wind direction. The density of the data points indicates that the majority of the wind speeds cluster between 5 to 20 m/s with the highest wind speeds resulting from wind directions between approximately 210°–270°.

The wind direction rose plot shows that most of the wind is coming from wind directions between 200° and 270° which aligns with the wind-sea direction rose plot. Most of the wind originates from South-West directions which aligns with the prevailing wind generation area for the North Sea. The histogram of the wind speed indicates that the highest number of sea states corresponds with wind speeds between $\sim$ 5 to 15 m/s. Peak values of the probability distribution occur within $\sim$ 7 to 12 m/s.

Figure 4.4 shows the wind-sea and swell wave distributions, binned per 30 deg directional width, for the observed sea states.

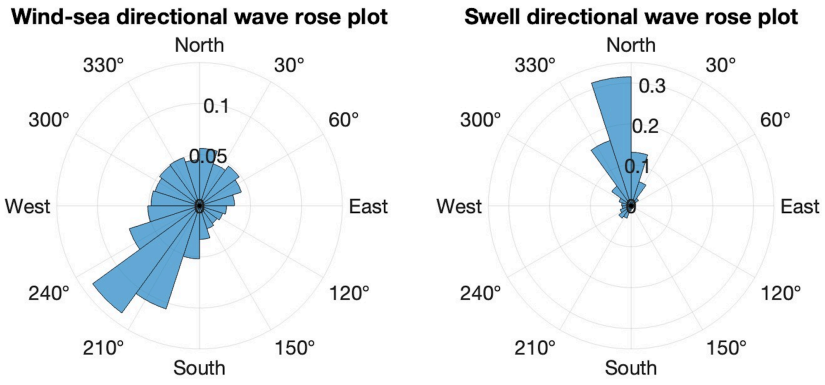

Figure 4.4: Wave rose for the wind-sea and swell wave component

It can be seen that most of the wind-sea components of the considered dataset are coming from south-west (∼ 200° - 270°) and the swell components mostly from north and northwest directions (∼ 320° - 360°). For the North Sea this is are reasonable observations since the propagation pattern agrees with the typical generation area for swell and wind-sea waves as stated in section 2.1.1.

4.2. Directional width dependence

The dependence of the directional width of the 2D-wave spectral data against the significant wave height, peak period and wind speed is shown in figure 4.5. The colorbar gives an indication of the highest density of the sea states, meaning a higher number of sea states have its directional width in the brighter indicated part of the scatter plot and less sea states have its directional width located in the darker part of the scatter plot.

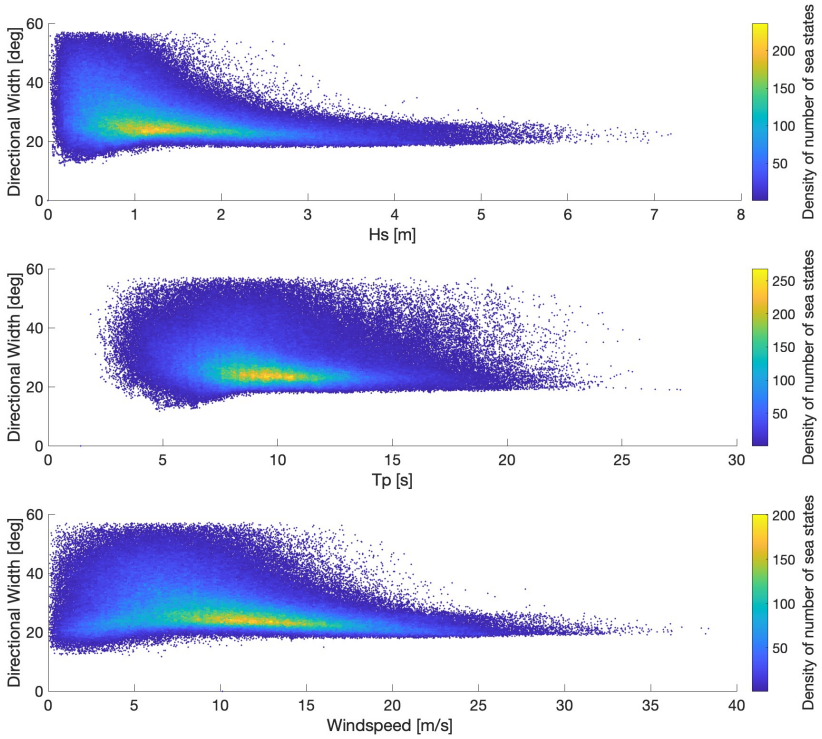

Figure 4.5: Directional width dependence on significant wave height, peak period and wind speed

From the scatter plot it can be seen that the directional width of the considered sea states is not smaller than approximately 15 deg and that it shows maximum values reaching up to approximately 58 deg. The dependence of the directional width on the wave spectral shape is shown in the figure 4.6. For this representation two sea states were chosen out of the whole dataset, that have corresponding directional width values of 50 deg (left plot) and 20 deg (right plot).

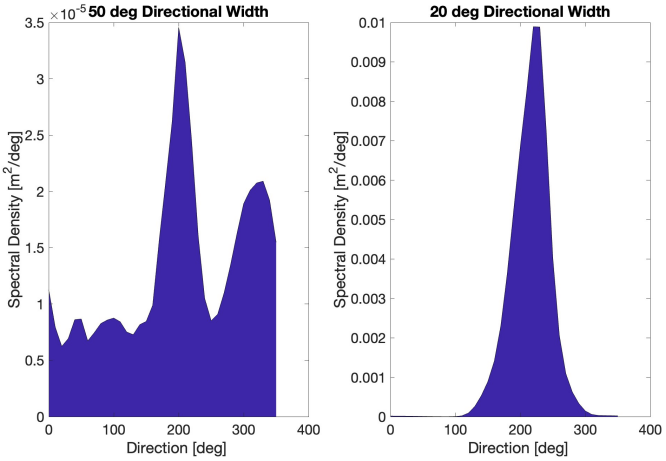

Figure 4.6: Dependence of the directional width on the wave spectral shape

A high value of the directional width, such as 50 deg, indicates a wide spreading of the spectral density over the directions, whereas a small value of the directional width, such as 20 deg indicates a more narrow spread of the spectral density over the directional distribution. The observed pattern for a narrow and wide directional width is representative for other sea states with small or large values of the directional width. Though, the number of observed peaks in the wave spectrum can differ per sea state. Still for wave spectra with a broad directional width it could be expected to detect more peaks referring to a higher number of occurring wave systems than for wave spectra with small directional width values.

4.3. Frequency width dependence

Figure 4.7 shows the frequency width distribution of the 2D-wave spectral data as well as of the JONSWAP spectral parametrizations with different gamma values against the significant wave height, peak period and wind speed. The 2D-wave spectral data, referred to as IJV Data is indicated with the scatter data points, showing different colors that correspond to the density of the number of sea states. JONSWAP wave spectra, calculated with a gamma value of 5.0 is indicated with a red solid line and with a value of 3.3 is indicated with a blue solid line. The dashed green line represents frequency width, calculated with a JONSWAP value of 1.0 and since those frequency width, calculated based on the Tp/Hs-ratio are that close aligned to the ones based on gamma values of 1.0, they are shown with pink scatter data points.

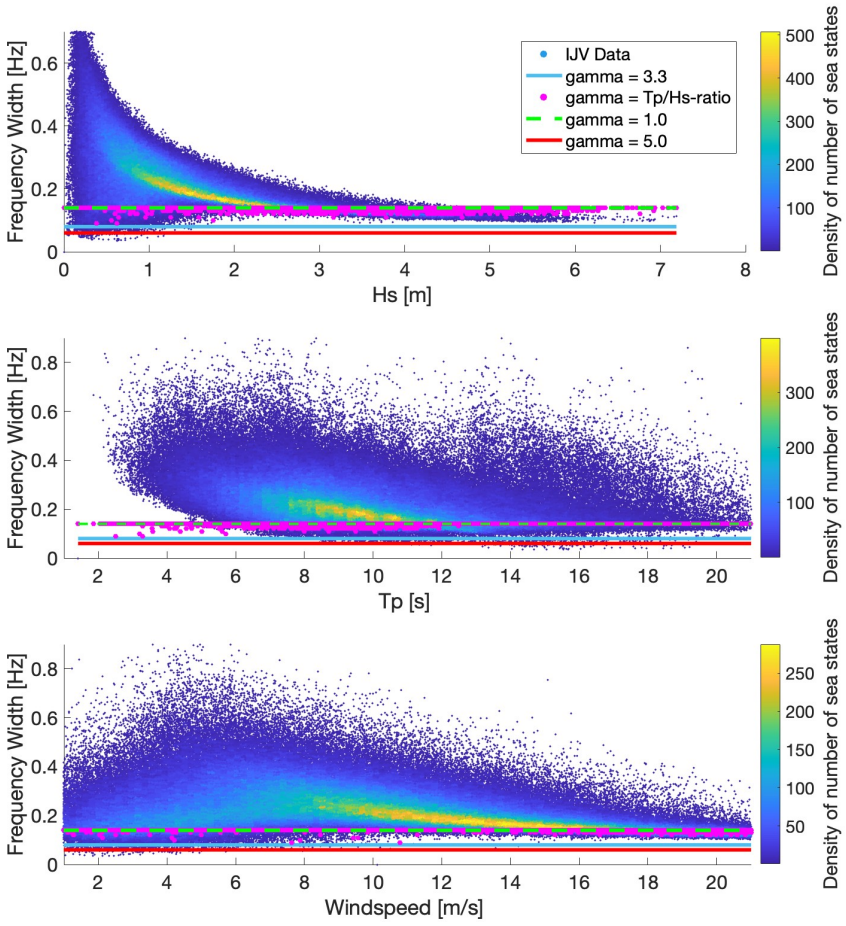

Figure 4.7: Frequency width dependence on significant wave height, peak period and wind speed

From figure 4.7 it can be seen that those JONSWAP spectral parametrizations with gamma values, that are calculated based on the Tp-Hs-ratio as well as those with a gamma value of 1.0 are laying within the lowest range of the frequency width of the 2D-wave spectral scatter plot. Compared to that, those JONSWAP spectral parametrizations, that were calculated with a standard gamma value of 3.3 or with the upper-limit that is considered for the Tp-Hs-ratio calculation which is equal to 5 are varying significantly from the frequency width of the 2D-wave spectra data scatter plot. It can thus be concluded that smaller gamma values lead to JONSWAP wave spectra that represent the 2D-wave spectra more accurate than gamma values of 3.3 or 5.0 which correspond to wave spectra with a sharp spectral peak.

Figure 4.8 gives an indication of the dependence of the frequency width on the wave spectral shape. For this representation two sea states out of the dataset were chosen, which correspond to frequency width values of 0.5 (left plot) and 0.2 Hz (right plot).

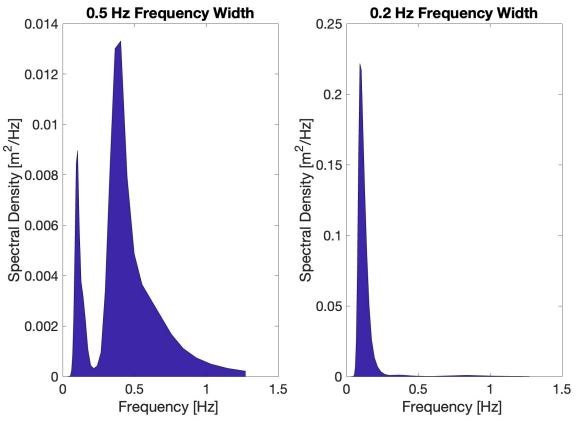

Figure 4.8: Dependence of the frequency width on the wave spectral shape

Larger values of the frequency width, such as 0.5 Hz correspond to a wave spectrum with a spectral density that is spread over a broader range of directions. Smaller values of the frequency width, such as 0.2 Hz, correspond to wave spectra with a spectral density that is spread over a more narrow range of frequencies.

4.4. Peakedness parameter dependence

The peakedness distribution as a function of the significant wave height, the peak period and the wind speed of the 2D-wave spectral data and JONSWAP parametrizations with different gamma values is shown in figure 4.9. The different datasets are indicated in the same way as it was done for the frequency width dependence in figure 4.7.

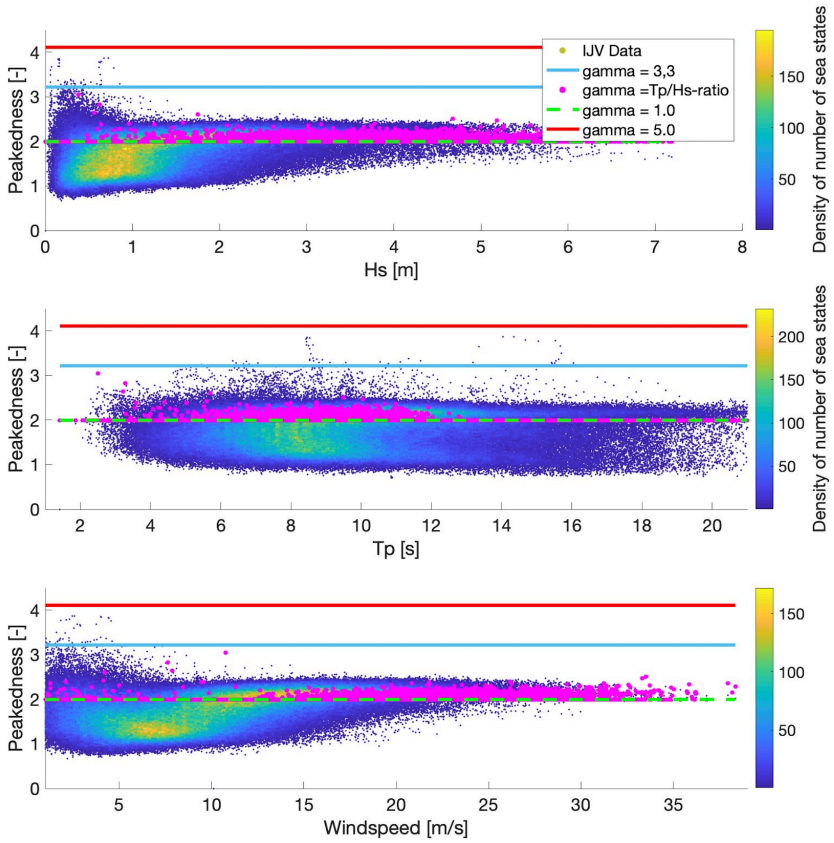

Figure 4.9: Relation between the wind and wave characteristics and the peakedness parameter

JONSWAP wave spectra, that was calculated with gamma values based on the Tp/Hs-ratio or with gamma values equal to 1.0 are laying in the upper range of the peakedness parameter distribution, whereas JONSWAP wave spectra that were calculated with higher values are laying more far out of the range of the peakedness parameter range.

Figure 4.10 shows the dependence of the peakedness on the wave spectral shape. For the representation, sea states out of the total data set were chosen which correspond to a peakedness parameter of 1.3 (right plot) and 2.3 (left plot), describing the shape of sea states with small and large peakedness parameter.

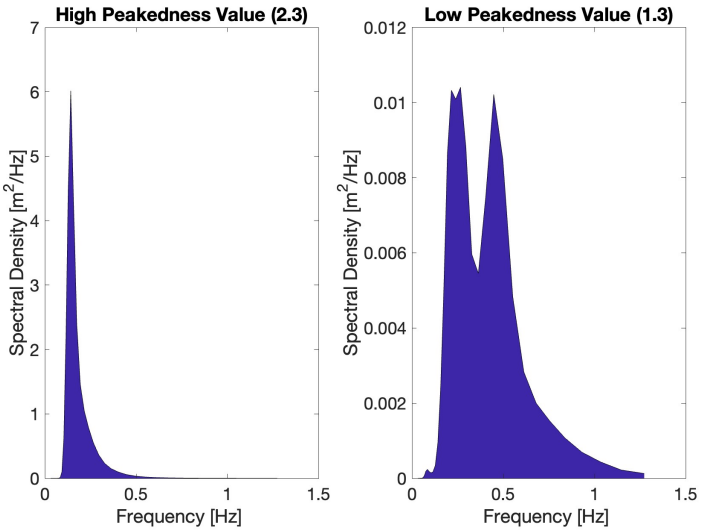

Figure 4.10: Dependence of the peakedness parameter on the wave spectral shape

Larger values of the peakedness, such as 2.3, correspond to higher sea states regions with higher spectral densities and a more narrow spectral shape, whereas lower values of the peakedness, such as 1.3, are corresponding to lower sea states regions with lower spectral densities and a broader spectral shape. Similar wave spectral shapes can be expected for peakedness parameter close to those indicated.

It can be concluded that those JONSWAP wave spectra, that are calculated based on a gamma value of 1 and on the Tp/Hs-ratio are fitting better in the range of the peakedness distribution of the realistic 2D-wave spectral data. Compared to that, JONSWAP wave spectra which is based on gamma values of 3.3 or 5, gives peakedness parameters that are laying far more out of the range of the actual 2D-wave spectral data. This leads to the interpretation that with smaller gamma values, JONSWAP wave spectra can be reconstructed that represents the realistic 2D-wave spectra more accurate than JONSWAP wave spectra which is based on gamma values of 3.3 or 5.0.

5. Results of fatigue load analysis

5.1. Overview

The obtained fatigue loads from the JONSWAP and 2D-wave spectra and the DEL differences between them will be analyzed in this section. Therefore, relations between the fatigue loads and the wave and wind parameters, including significant wave height, peak period, wave and wind direction as well as wind speed and the wave characteristics, such as directional width, frequency width and peakedness, will be investigated. Furthermore, it will be quantified for which ranges of this environmental parameters and wave characteristics the highest fatigue load differences are occurring, based on the JONSWAP spectral model and the actual 2D-wave spectral data.

Figure 5.1 shows the calculated DEL from JONSWAP and 2D-wave spectra plotted against each other. The color scale provides insights into the frequency of the occurrence of the sea states. The warmer colors (yellow, orange) represent a higher concentrations of sea states.

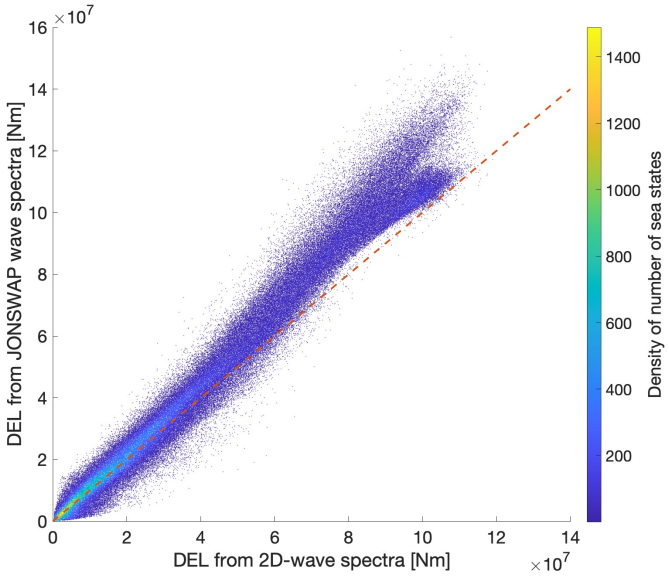

Figure 5.1: Scatter plot of the fatigue loads from 2D-wave spectra against JONSWAP wave spectra

For DEL values below approximately 4 to 5 MNm, the data points from the JONSWAP and 2D-wave spectra follow a nearly 1:1 relationship, indicating that both spectra produce very similar DEL predictions for lower sea states or less severe wave conditions. Beyond DEL values of approximately 4 to 5 MNm, a noticeable divergence begins to occur. The JONSWAP wave spectra produce higher DEL values compared to the 2D-wave spectra for the same conditions.

This observation suggests that wave-induced fatigue loads tend to be overestimated based on the JONSWAP wave spectra, compared to those calculated with the more realistic 2D-wave spectra. A better agreement of the wave-induced fatigue loads below values of $\sim$ 4 - 5 MNm between JONSWAP and 2D-wave spectra can be observed.

How the total DEL vary per defined sector, as it was described in section 3.2.2, is shown in figure 5.2 The total DEL values were obtained by summing up the damage per sector and converting it based on the Wohler slope m and the number of reference cycles N to DEL's.

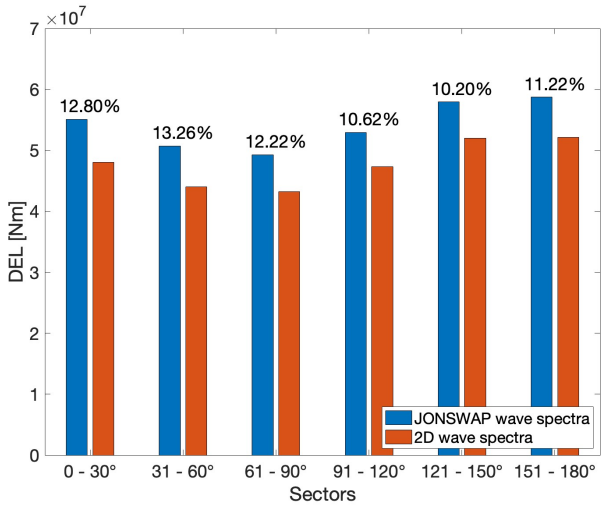

Figure 5.2: Differences in the total DEL per sector of the OWT

From figure 5.2 it can be seen that per defined sector, the fatigue loads between the JONSWAP and 2D-wave spectra are varying with the JONSWAP wave spectra leading consistently to higher fatigue loads, compared to the 2D-wave spectra. This overestimation ranges between values of approximately 10.20 % and 13.30 % as indicated in the figure.

5.2. Dependence on MetOcean parameter

Within this section the relation between the wave and wind parameter and the DEL, the DEL differences as well as the damage ratios and the damage ratio differences will be investigated. Considered wave and wind parameter are the significant wave height, peak period, wind speed as well as the wind and wave direction.

5.2.1. Significant wave height

Figure 5.3 shows the relation between the absolute values of the DEL against the significant wave height for the JONSWAP and 2D-wave spectra.

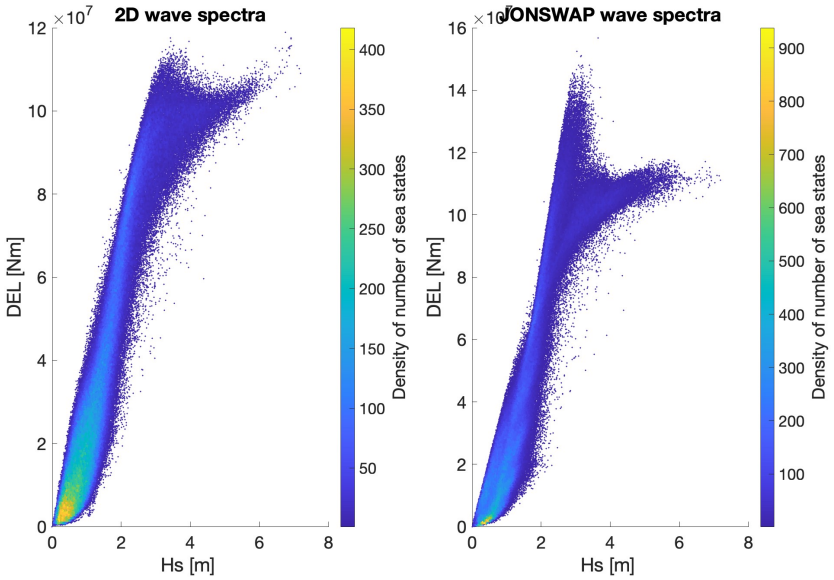

Figure 5.3: DEL of frequency-directional and JONSWAP wave spectra against significant wave height

For wave heights below 2 m, the DEL increases steadily, without sudden jumps or major variations, especially for DEL resulting from the 2D-wave spectra, which exhibits a nearly linear behavior in this range. DEL's resulting from JONSWAP-wave spectra, however, show more outliers.

For significant wave heights above 3.5 m, JONSWAP wave spectra show a broader spread of DEL values with a higher number of outliers, indicating more severe fatigue loads in these higher sea states. The 2D-wave spectra on the other hand demonstrates a more contained spread, leading to more consistent predictions for fatigue damage in this significant wave height range. Wave heights above 3.5 m can be related to extreme sea states since they are occurring within the upper 5 % of the considered dataset.

Figure 5.4 shows the calculated absolute DEL values against the significant wave height as well as the DEL differences between the JONSWAP and 2D-wave spectra.

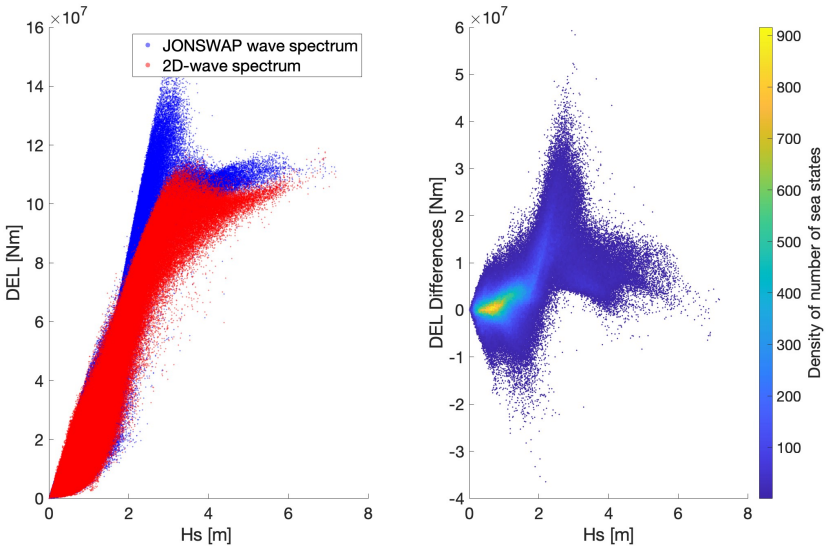

Figure 5.4: DEL and DEL differences between JONSWAP and 2D-wave spectra against Hs

For wave heights below 2 m, the DEL from both wave spectra are closely aligned, suggesting that for lower wave heights, both models provide similar results in terms of fatigue loading. The right-hand plot reinforces this, by showing minimal variance in DEL differences in this range.

As the wave height increases between $\sim$ 2 m and 3.8 m, the DEL between the wave spectra begin to diverge, as shown by the clear separation of red (2D) and blue (JONSWAP) points in the left-hand plot. This large discrepancies in the predicted DEL values, suggest that DEL's calculated with JONSWAP wave spectra are overestimated (with $\sim$ 14.7 %) by using JONSWAP wave spectra compared to realistic 2D-wave spectra. About 18 % of all considered sea states fall within this range.

For wave height values above 3.8 m, the DEL differences between both wave spectra are decreasing. Still, differences remain visible, but the overestimation trend between JONSWAP and 2D-wave spectra is less evident than in the investigated wave height range between 2 m and 3.8 m. To get more comprehensive insights into the relation between fatigue loads and the significant wave height, the damage ratios and damage difference ratios will be analyzed.

The left box plot in figure 5.5 shows the distribution of significant wave height data, binned per meter of the wave height, against the relative damage ratios for JONSWAP and 2D-wave spectra. The right box plot considers the damage difference ratios instead.

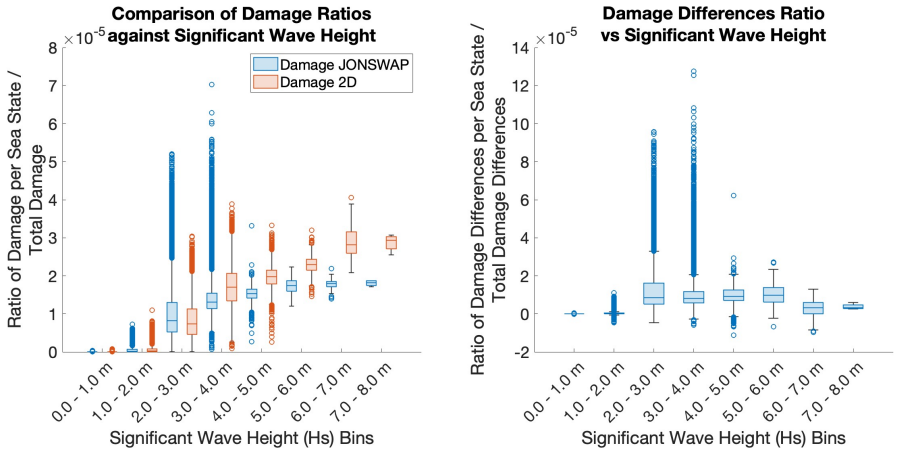

Figure 5.5: Damage and Damage Differences Ratio for JONSWAP and 2D Wave Spectra

For wave heights between 2 m and 3.8 m, the damage ratios based on JONSWAP wave spectra show greater variability than those obtained for the 2D-wave spectra. This sensitivity could result in less reliable and less consistent fatigue damage predictions, as shown by the wider interquartile ranges (IQR) and long whiskers and several extreme outliers in the damage difference ratio plots, highlighting a greater spread and more variability in the data. The presence of high outliers suggests that some sea states in this range cause large discrepancies between the two spectra. This analysis supports the interpretation which was done based on the previous figure 5.4 leading to the conclusion that DEL calculated with the JONSWAP wave-spectra are overestimated for a wave height range between 2 m and 3.8 m.

For wave heights above 3 m, the variability in damage ratios becomes more pronounced for the 2D-wave spectra, For an even increasing wave height the 2D-wave spectra leads to higher damage ratios and a consistent and slightly increasing damage ratio difference can becomes noticeable.

With the analysis of the damage and damage difference ratios, an additional insight in the behaviour of the wave-induced fatigue loads was gained, that was not visible by only looking at the scatter density plots of the DEL and the DEL differences.

Table 5.1 summarizes the defined significant wave height ranges for which the DEL differences can be observed.

Range	Description
Below 2 m	Close alignment of DEL values for both types of wave spectra.
2 m to 3.8 m	Range of the highest overestimation of DEL between JONSWAP and 2D-wave spectra. Also the highest DEL are observed within this range.
Above 3.8 m	DEL differences are still visible for this extreme wave height range but with JONSWAP wave spectra underestimating the DEL's compared to those obtained with 2D-wave spectra.

Table 5.1: Defined significant wave ranges based on DEL differences

5.2.2. Peak period

Figure 5.6 shows how the absolute values of the DEL, that were calculated from bulk wave parameters as well as the DEL's that were obtained from realistic 2D-wave spectra depend on the peak period.

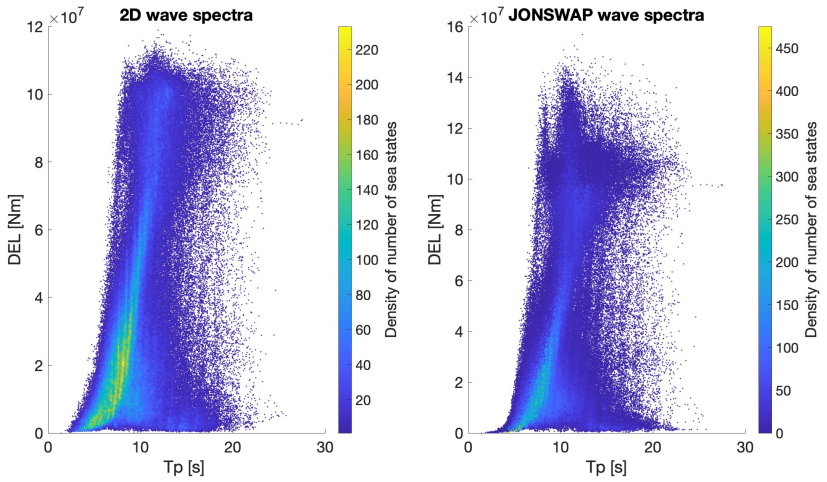

Figure 5.6: DEL of JONSWAP and 2D-wave spectra against peak period

DEL's calculated from 2D-wave spectra show a more concentrated distribution, with a relatively smooth increase. This becomes especially clear in the range below 8 seconds, where the majority of sea states for both wave spectra is observed, as indicated by the higher density of data points in the color scale. In general a slightly broader spread of DEL values can be concluded from the JONSWAP wave spectra, suggesting a more variable distribution of fatigue loads.

Figure 5.7 shows the dependence of the absolute DEL and DEL differences against the peak period for the JONSWAP and 2D-wave spectra.

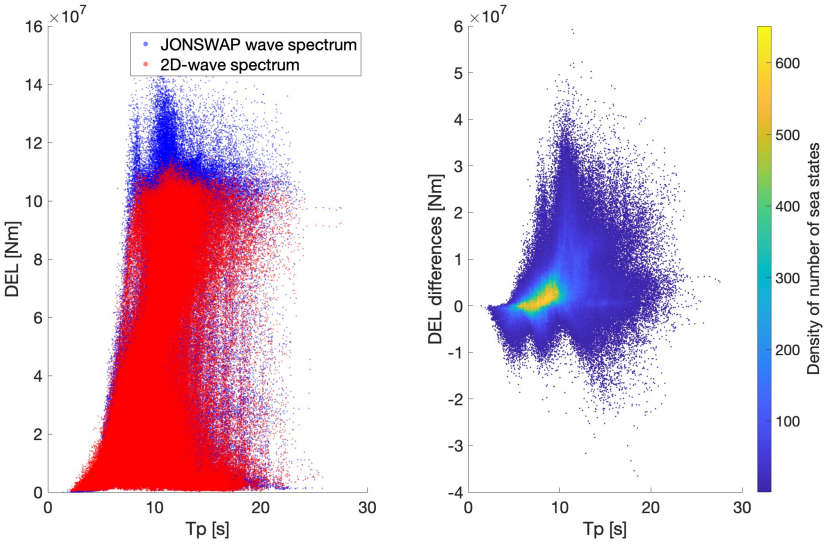

Figure 5.7: DEL and DEL differences of 2D and JONSWAP wave spectra against peak period

For peak periods below 8 seconds, the two spectra closely match, leading to minimal DEL differences. The differences begin to arise around 8 s, where the overlap between the two spectra diminishes, and the DEL differences start to appear sharply at or just after this point.

The plot on the right shows that the DEL differences exhibit peak values between 8 and 15 s, which is where the spectra diverge most significantly, as indicated by the higher density of sea states. Peak periods of more than 15 s can be associated with extreme sea states as it was shown in section 4.1. DEL's based on JONSWAP wave spectra are $\sim$ 13.6 % overestimated in this range, corresponding to $\sim$ 64 %

of all considered sea states, compared to those calculated with the 2D-wave spectra. To get a more in-depth insight in the relations between the wave-induced fatigue loads and the peak period, the damage ratios and damage difference ratios are investigated.

Figure 5.8 shows the relative damage and damage difference ratios against the peak period, which is binned per two seconds.

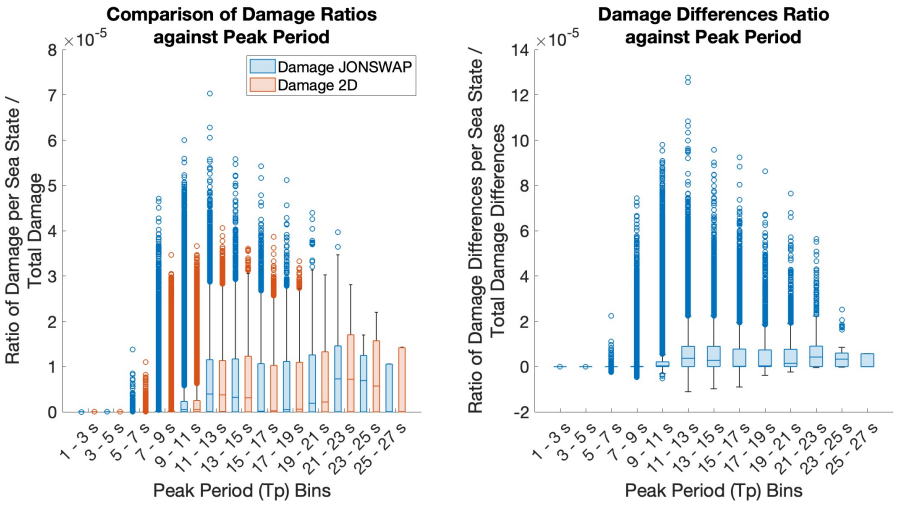

Figure 5.8: Damage and damage difference ratios against the peak period for JONSWAP and 2D wave spectra

The JONSWAP spectral model consistently results in higher damage ratios with higher outliers compared to those obtained with the 2D-wave spectrum for peak periods up to 23 s. Beyond this range, for the most extreme observed peak periods, the 2D-wave spectra seems to capture slightly higher damages.

The highest damage ratio differences are observed for the same range ($\sim$ 8 s - 15 s) as it was concluded from figure 5.7. Beyond this range the damage difference ratios between both spectra decrease slightly but differences remain. A shift in the median value of the damage ratio differences indicates, that the 2D-wave spectra leads for extreme peak periods to higher fatigue loads than it is estimated with the JONSWAP wave spectra.

Table 5.2 summarizes the ranges of the peak period for which the wave-induced fatigue load differences occur.

Range	**Description**
Below 8 s	Minimal DEL differences. The overlap between both wave spectra is significant.
Around 8 s	DEL differences begin to emerge. The overlap between the two spectra diminishes, and the DEL differences start to appear sharply.
8 to 15 s	The DEL and DEL differences between the two spectra reach peak values.
Beyond 15 s	Corresponding to extreme sea states. Differences between both spectra remain.

Table 5.2: Defined peak period ranges based on DEL differences

5.2.3. Wave direction

The wave direction has a significant impact on the loads experienced by offshore structures. Waves approaching from different directions can cause varying levels of fatigue loads on the structure, especially when combined with wind directions and currents. The DEL may vary with wave direction due to the way different directional waves interact with the structure. Comparing wave directions against wave-induced fatigue loads gives insights into how different wave directions influence the structural response under both spectra which helps identifying critical or less impactful directions.

Wind-sea wave component

Figure 5.9 shows the distribution of DEL for the JONSWAP and 2D-wave spectra over the wind-sea wave directions.

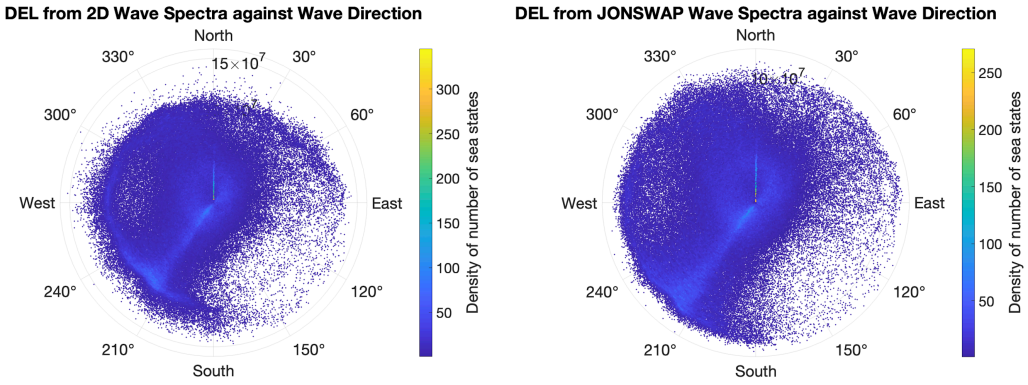

Figure 5.9: Dependence of the DEL from JONSWAP and 2D-wave spectra on the wind-sea wave directions

Both polar plots are densely populated, indicating that the DEL's are widely distributed across various wave directions, with a concentration of higher DELs, indicating a higher impact on the structure, in southwest direction between 200° and 240°. The DEL distribution for the JONSWAP wave spectra follows a pattern similar to the 2D-wave spectrum but it can be seen from figure 5.9 that the DEL calculated with the JONSWAP model are a little less sharply concentrated than those obtained with the 2D-wave spectral data. A fewer number of sea states is contributing to the wave-induced loads from north to west directions (240 - 30°), as can be seen from the less dense concentration of sea states in both polar plots.

Figure 5.10 indicates the differences between the JONSWAP and 2D-wave spectra against the wave directions.

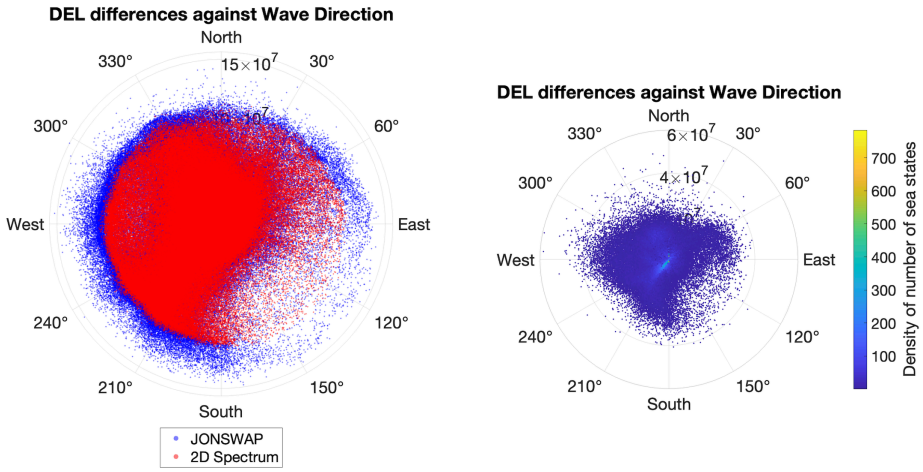

Figure 5.10: Dependence of DEL differences between JONSWAP and 2D-wave spectra on the wind-sea wave direction

From figure 5.10 it can be seen that DEL's calculated with the JONSWAP wave spectra (blue scatter points) seem to be overestimated across all directions compared to those calculated with the 2D-wave spectral data (red scatter points). Furthermore, from the right-side plot in figure 5.10 it can be seen that the largest differences of the DEL between both wave spectra occur mostly for wind-sea waves coming from the west.

Swell wave component

Figure 5.11 shows the distribution of DEL's for the JONSWAP and 2D-wave spectra over the swell wave directions.

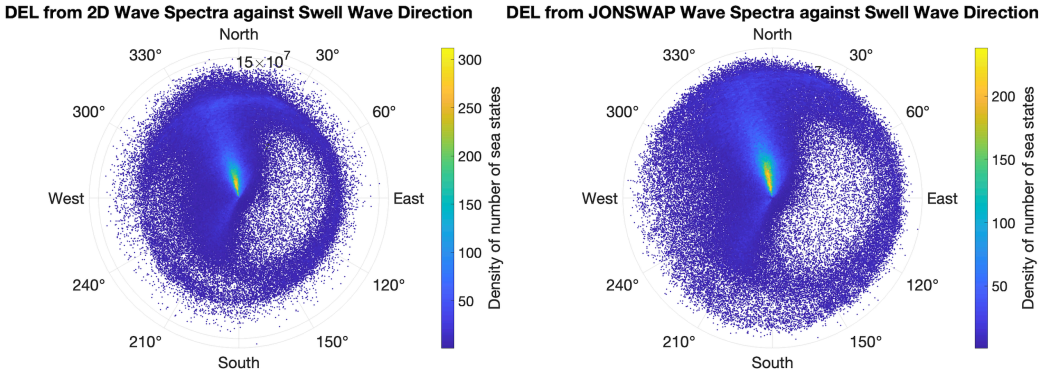

Figure 5.11: Dependence of the DEL from JONSWAP and 2D-wave spectra on the swell wave direction

It can be seen from figure 5.11, that most of the DEL, resulting from swell wave components is coming from northwest directions. The concentration of the DEL's resulting from 2D-wave spectra, seem exhibit a denser pattern with less variability in the data points, compared to the DEL's, obtained from the JONSWAP wave spectra.

Figure 5.12 indicates the distribution of the DEL differences between JONSWAP and 2D-wave spectra against the swell wave directions.

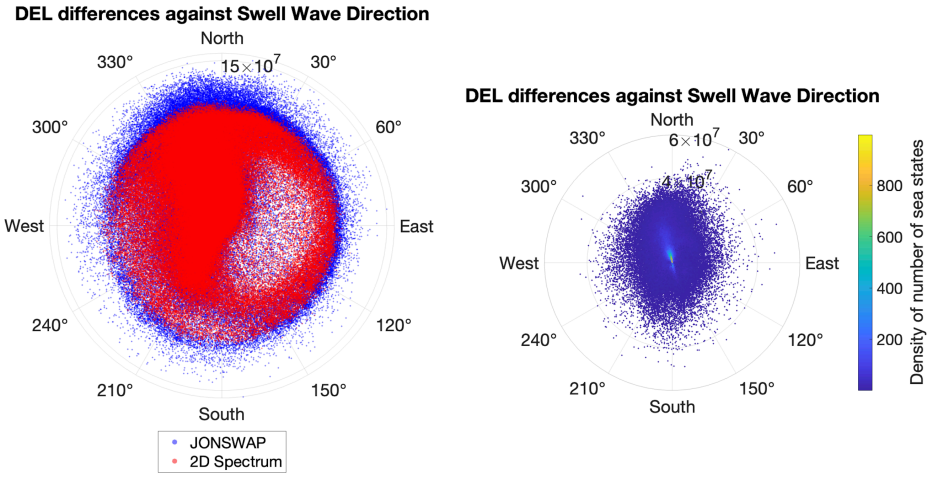

Figure 5.12: Dependence of DEL differences from JONSWAP and 2D-wave spectra on the swell wave direction

From the left-side plot in figure 5.12 the largest overestimation of the DEL, calculated with the JONSWAP wave spectra can be identified (blue scatter data) for swell waves coming from the north, compared to those calculated with the 2D-wave spectra (red scatter data). In the right-side plot a higher density of scatter points, corresponding to a higher number of sea states, is observed for swell waves coming from northwest direction.

5.2.4. Wind direction

Figure 5.13 shows how the DEL values from the 2D-wave spectra (left plot) and JONSWAP wave spectra (right plot) are distributed against the wind direction.

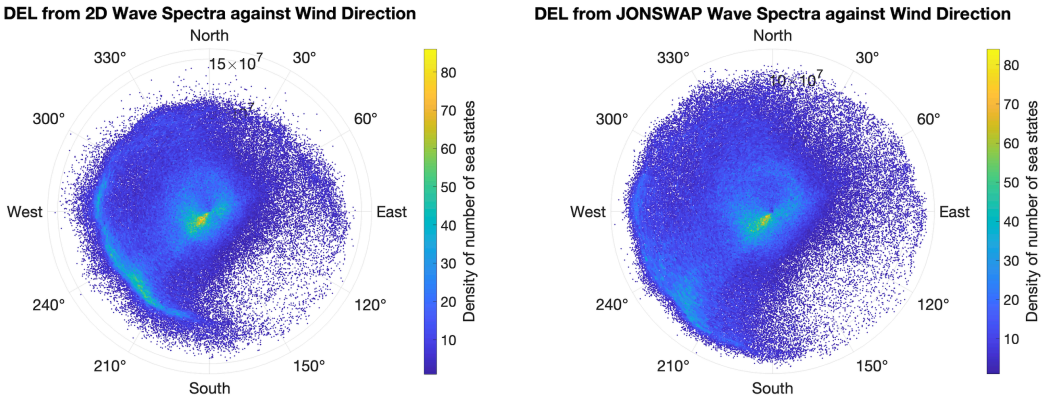

Figure 5.13: Comparison of the DEL from 2D and the JONSWAP wave spectra against the wind direction

The majority of sea states that contribute to the DEL values are concentrated between ∼ 180° and 300°, with the highest density around ∼ 210° to 240° wind direction which is identical to the observations from the DEL against the wave-sea directions.

The radial axis represents the DEL values. While most DEL values are distributed around the center, some extend outward for certain wind directions, suggesting higher DEL values for those directions. However, the concentration of higher DEL values remains in the 210° to 270° range, indicating that winds coming from these directions result in significant structural fatigue loads. The density of sea states is similar between the two spectra, although DEL's calculated with the JONSWAP wave spectra show slightly more spread across wind directions, while the 2D-wave spectrum concentrates more sea states in the 210° to 270° wind direction range.

Figure 5.14 shows the differences between both wave spectra types across different wind directions, visualized in a polar plot.

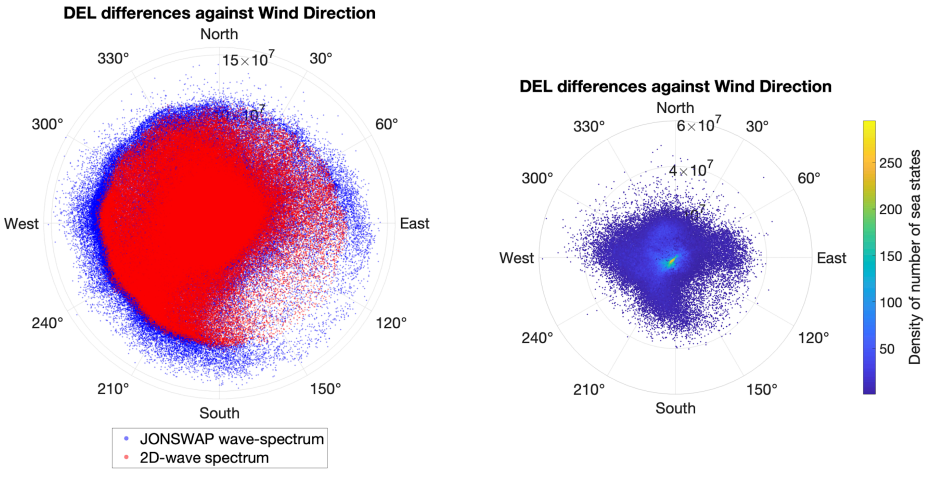

Figure 5.14: Dependence of DEL differences between JONSWAP and 2D-wave spectra on the wind direction

The majority of sea states in the left plot overlap heavily, particularly in the sector from 180° to 30°, where both wave spectra produce significant DEL values. Those DEL's, calculated with the 2D-wave spectral data (red points) are more clustered and concentrated in the center of the plot. The JONSWAP

wave spectrum affects a wider range of wave directions, resulting in more dispersed DEL values. The tendency of the highest density of the DEL differences in the right plot can be observed in the center but somewhat more concentrated to the west. Beyond these ranges, particularly from 30° to 90°, the DEL differences become a lot less pronounced which also results from fewer sea states contributing to the fatigue loads from East-South direction. It can be concluded that the DEL distribution between both spectra against the wind direction, show a similar pattern than the one of the wind-sea waves, as these are dependent on the locally generated wind.

5.2.5. Wind speed

The dependence of the DEL calculated from JONSWAP and 2D-wave spectra on the wind speed is shown in the figure 5.15.

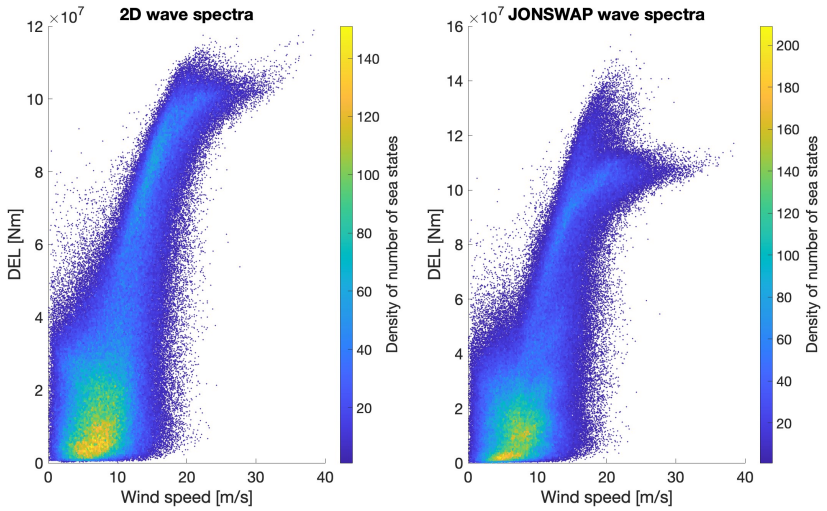

Figure 5.15: Dependence of DEL from JONSWAP and 2D-wave spectra on wind speed

For wind speeds below 10 m/s, both the JONSWAP and 2D-wave spectra produce relatively low DEL values. However, there is some indications of higher variability in DEL obtained with JONSWAP wave spectra, with occasional outliers showing slightly higher DEL values compared to those obtained from 2D-wave spectral data, though the overall predictions remain relatively consistent at these lower wind speeds.

The DEL values between a wind speed of 10 and 20 m/s, that were obtained with the 2D-wave spectral data, increase gradually, with most of the data being concentrated between 5 and 10 MNm. The distribution remains fairly smooth, with few outliers. This suggests a consistent estimate of the fatigue damage for this wind speed range. Higher DEL values are observed for the JONSWAP wave spectra, than in the 2D spectrum, with more data points scattered above 10 MNm. This indicates that the JONSWAP spectrum predicts higher fatigue damage for certain sea states compared to the 2D-wave spectrum in this wind speed range.

Above a wind speed of 20 m/s, the distribution of DEL from the 2D-wave spectral data values is still relatively contained, but the frequency of high DEL values decreases. There are fewer extreme values, which implies that the 2D-spectrum tends to smooth out the extreme fatigue damage predictions at higher wind speeds.

The DEL differences between the JONSWAP and 2D-wave spectra against the wind speed are shown in figure 5.16.

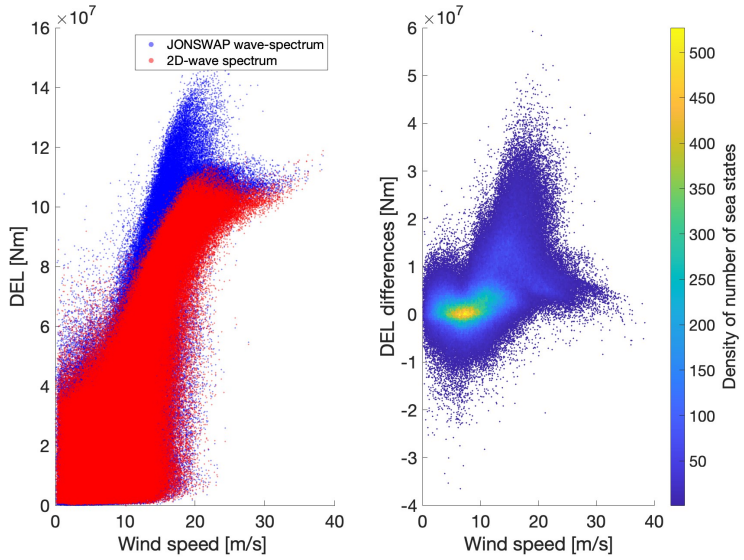

Figure 5.16: Dependence of the DEL differences between the JONSWAP and 2D-wave spectra against the wind speed

For wind speeds below 10 m/s the DEL differences are relatively small, as the red and blue data points (representing DEL values for the two spectra) overlap closely. This suggests that, at low wind speeds, both wave spectra yield mostly similar DEL values.

For wind speeds within the range from 10 to 20 m/s, the DEL values begin to show noticeable divergence, with the DEL differences becoming more pronounced. The DEL overestimation for this range can be quantified with $\sim$ 15 %, corresponding to $\sim$ 43 % of the data points. The maximum DEL values and DEL differences are reached at wind speeds between 15 and 20 m/s. The spread of the DEL differences is more substantial in this range, as depicted by the right-hand density plot. For wind speeds above 20 m/s which correspond to extreme sea states as they can be associated with the upper 5 % of the data points, the differences in the DEL values still remain slightly visible but decrease significantly since the JONSWAP and 2D-wave spectra tend to show more aligned DEL values.

To get a more extensive insight in the relation between the fatigue loads and the wind speed, the damage ratios and damage ratio differences need to be investigated for the analysis. Figure 5.17 shows the relative damage and damage difference ratios for the JONSWAP and 2D-wave spectra plotted against the wind speed.

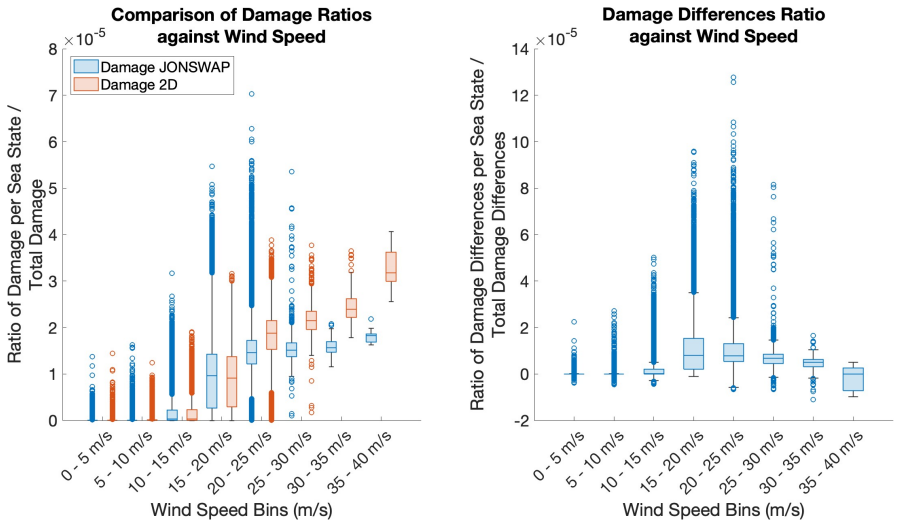

Figure 5.17: Damage and damage difference ratios against wind speed for JONSWAP and 2D wave spectra

Below wind speed ranges of 0–10 m/s both JONSWAP and 2D-wave spectra show very low damage ratios with only very small differences between the two spectra. Between 10–25 m/s wind speed range, the difference in damage ratios between JONSWAP and 2D-wave spectra become highly significant. The JONSWAP spectrum tends to predict pronounced higher damage and damage difference ratios with a larger spread and median values. Beyond wind speeds of 20 m/s, that correspond to the upper 5 % of the wind speed data which can thus be associated with extreme events, the damage difference ratios initially decrease between the JONSWAP and the 2D-wave spectra.

For further increasing wind speeds, those damage ratios, calculated with the JONSWAP spectral model continue to decrease whereas those calculated with 2D-wave spectral data are increasing. This leads to increasing damage difference ratios for the most extreme wind speeds. From that observation it can be concluded that the JONSWAP wave spectral model leads to underestimations of the fatigue loads for sea states resulting from extreme wind speeds compared to fatigue loads calculated with 2D-wave spectral data.

The defined ranges of the wind speed for which the highest DEL and DEL differences occur are summarized in table 5.3.

Range	Description
Below 10 m/s	Minimal DEL differences and strong overlap between both wave spectra.
10 to 20 m/s	The DEL values begin to increase and maximum DEL values are reached. Differences between the two spectra become the most crucial.
Above 20 m/s	DEL differences decrease but for the most extreme wind speeds JONSWAP wave spectra underestimated the fatigue loads compared to JONSWAP wave spectra.

Table 5.3: Defined wind speed ranges based on DEL difference

5.3. Dependence on wave spectral characteristics

Next to the investigation about the relation of the wave-induced fatigue loads and load differences against the wind and wave parameter, significant wave height, peak period as well as wind and wave direction, the wave spectral characteristics, directional width, frequency width and peakedness will be considered in this section.

5.3.1. Directional width parameter

Figure 5.18 visualizes the differences in the DEL from JONSWAP and 2D-wave spectra against the directional width values, calculated for the realistic 2D-wave spectra as shown in figure 4.5.

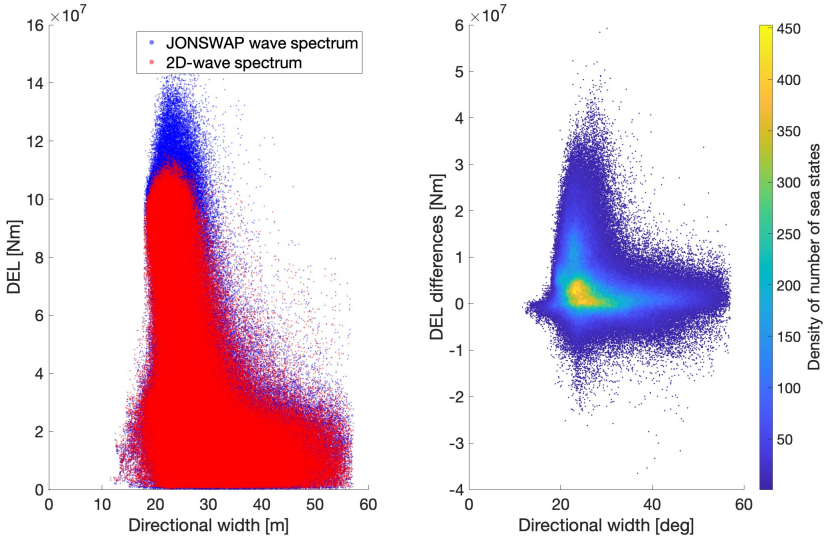

Figure 5.18: Dependence of DEL and DEL differences from JONSWAP and 2D-wave spectra on the directional width values

Below 20° of directional width the DEL values from the JONSWAP and 2D-wave spectra are relatively close, with minimal differences observed. This indicates that both spectra perform similarly in this range, and the directional width has a smaller impact on the predictions of the DEL differences.

The largest DEL differences are concentrated within the directional width range of 20° to 30°. Within this range $\sim$ 65 % of the sea states are located, leading to an DEL overestimation of $\sim$ 13.6 %. For directional widths larger than $\sim$ 30°, the DEL differences start to diminish again, with both spectra producing significantly lower DEL values.

Figure 5.19 shows the relation of the relative damage and damage difference ratios against the directional width, binned per 10° of width.

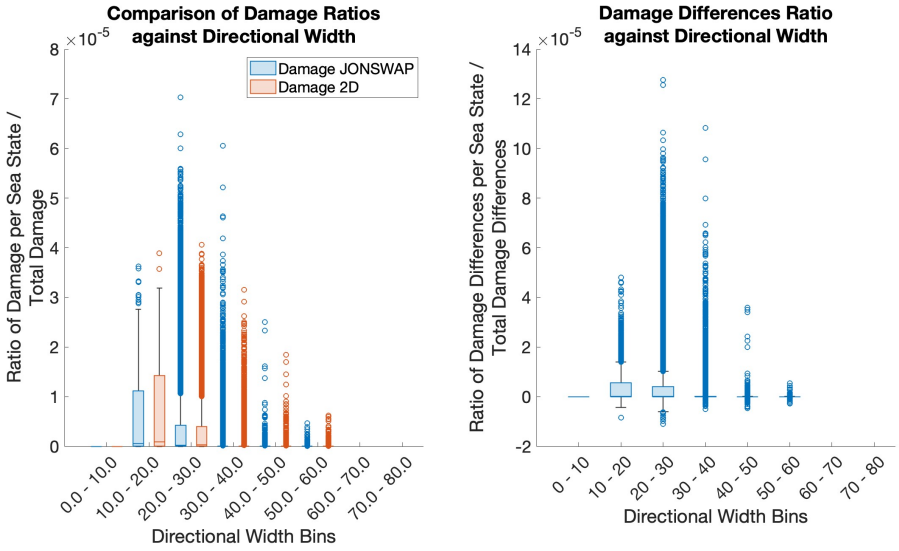

Figure 5.19: Damage and damage difference ratios against directional width for JONSWAP and 2D-wave spectra

As the directional width increases into the 20 - 30° and 30 - 40° bins, much higher damage ratios with greater variability are obtained from JONSWAP wave spectra, whereas damage ratios obtained with 2D-wave spectra are generally lower. This indicates that, as wave energy spreads over this range of directions, JONSWAP tends to predict more extreme damage compared to the 2D-wave spectra, resulting in an overestimation of the wave-induced fatigue loads within this range. This finding supports the previous made observations based on figure 5.18.

The presence of several high outliers indicates that, under specific sea states, the JONSWAP spectrum can produce extreme differences in damage predictions. For broader directional widths (> 40°), both spectra show lower damage ratios, and the differences between them diminish, suggesting that wave energy distributed over a wide range of directions leads to more consistent fatigue loading estimates across the spectra.

Table 5.4 summarizes the defined directional width ranges based on the fatigue load differences between JONSWAP and 2D-wave spectra.

Range	Description
Below 20°	Minimal DEL differences and strong agreement of DEL's between JONSWAP and 2D-wave spectra.
20° to 30°	Largest DEL differences are concentrated within this range. The JONSWAP spectrum overestimates the DEL values, with a significant spread in the DEL differences between the two spectra.
Beyond 30°	DEL differences diminish, with both spectra producing lower DEL values.

Table 5.4: Defined directional width ranges based on DEL differences

5.3.2. Frequency width parameter

Figure 5.20 visualizes the differences in the DEL from JONSWAP and 2D-wave-spectra against the frequency width values from the actual 2D-wave spectra, as shown in figure 4.7.

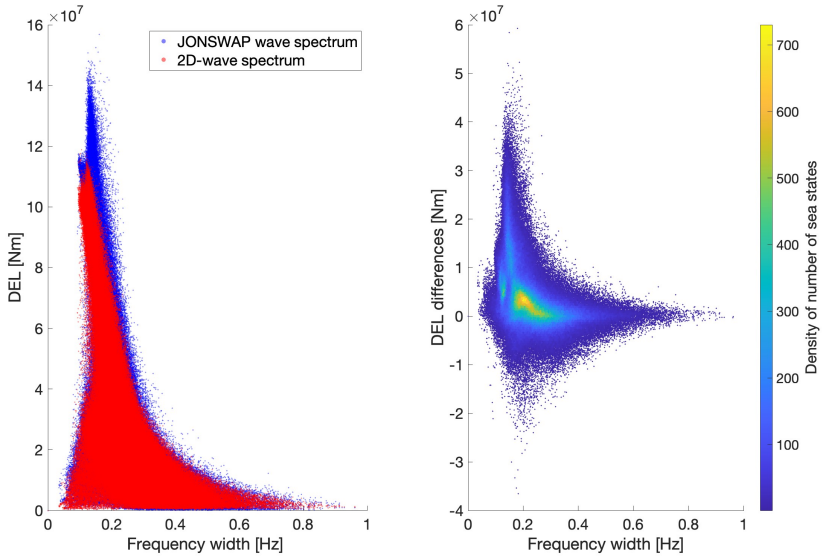

Figure 5.20: Dependence of the DEL and the DEL differences from JONSWAP and 2D-wave spectra on the frequency width parameter

At very low frequency widths, both the JONSWAP and 2D-wave spectra show similar DEL values, indicating that the spectra behave consistently in this range. The DEL differences are minimal, suggesting that both spectra yield similar fatigue damage estimates for low-frequency widths. Between 0.1 and 0.3 Hz frequency width, the highest DEL values are observed, with noticeable differences between the two spectra. With the JONSWAP wave spectra DEL values are $\sim$ 13 % overestimated, corresponding to $\sim$ 81 % of all data points. At a frequency width of 0.2 Hz the highest DEL values and differences between both spectra can be observed.

As the frequency width increases beyond 0.3 Hz, the DEL values for both spectra begin to converge. In this higher frequency range, both spectra produce more consistent results with fewer differences, suggesting a reduction in discrepancies and a more aligned prediction of fatigue damage.

Table 5.5 summarizes the defined ranges for which the highest DEL values and DEL differences with respect to the frequency width of the wave spectral data are visible.

Range	Description
Below 0.1 Hz	DEL values for both spectra are very much in agreement, with minimal differences observed.
0.1 to 0.3 Hz	Largest DEL and DEL differences are observed in this range. The JONSWAP-wave spectra tends to overestimate DEL compared to the 2D-wave spectra.
Beyond 0.3 Hz	DEL differences are diminishing significantly, with both spectra producing more comparable DEL values.

Table 5.5: Defined frequency width ranges based on DEL differences

In figure 5.21 the relative damage ratio and the relative damage difference ratios are shown against the frequency width for the JONSWAP and 2D-wave spectra.

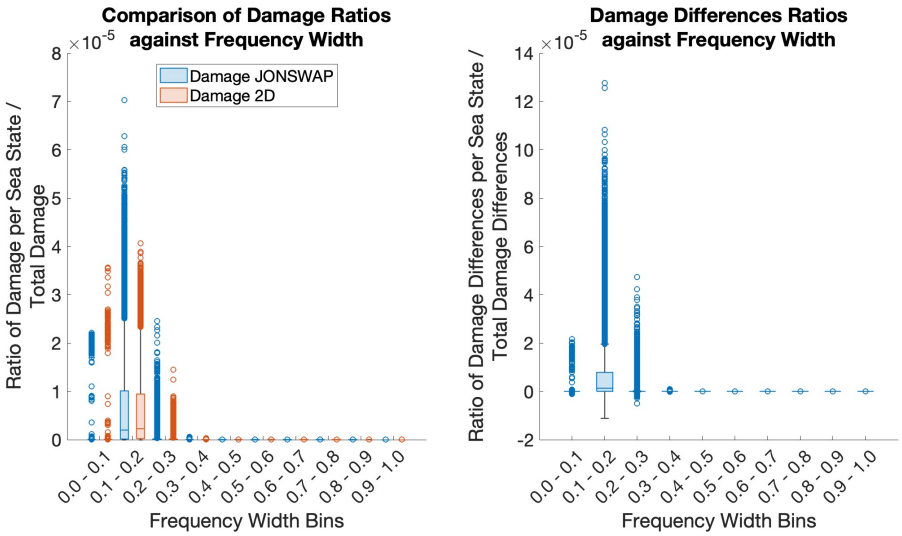

Figure 5.21: Damage and damage difference ratios against frequency width for JONSWAP and 2D wave spectra

For low frequency width values (below 0.1 Hz), both spectra show relatively low damage ratios, with the 2D-wave spectra exhibiting higher damage ratios with more outliers than the JONSWAP wave spectra. This suggests that for very narrow frequency widths below 0.1 Hz, where energy is concentrated within a small bandwidth, the 2D wave spectra slightly tend to predict higher fatigue damage. Outliers indicate variability, with some extending to higher damage ratios, implying larger discrepancies between the two spectra at these narrow frequencies.

Within the frequency range of 0.1 to 0.2 Hz the damage ratio increases significantly between both spectra, with JONSWAP wave spectra predicting higher damages, even if the variability and the median damage values for both spectra are nearly aligned. Within this range the highest number of outliers for the damage ratio as well as for the damage difference ratios are visible.

For frequency width between 0.2 and 0.3 Hz, the damage ratios and the damage difference ratios decrease again for both spectra. However, there are still some outliers, indicating variability in the predicted damage at this frequency range. The smaller box plots indicate a reduced difference in damage estimates between the two spectra.

For frequency widths greater than 0.3 Hz, the damage ratios drop to nearly zero for both spectra. This suggests that as frequency width broadens beyond a certain point, the predicted damage becomes minimal, implying more consistent or reduced fatigue loads at broader frequency distributions.

Damage difference ratios in this range approach zero, suggesting that both spectra predict very similar fatigue damage for broader frequency distributions.

5.3.3. Peakedness parameter

Figure 5.22 visualizes the differences in the DEL from JONSWAP and 2D-wave spectra against the peakedness values of the realistic 2D-wave spectra as they were shown in figure 4.9.

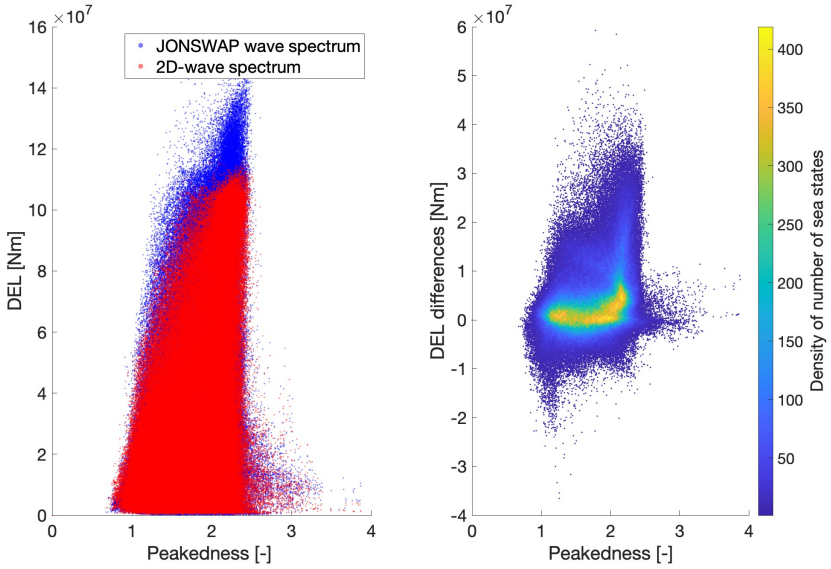

Figure 5.22: Dependence of the DEL and the DEL differences from JONSWAP and 2D-wave spectra on the peakedness parameter

For peakedness values below 1.0, the differences between the two spectra are minimal, indicating that the JONSWAP and 2D-wave spectra produce comparable DEL values in this range. As the peakedness increases beyond 1.0, the DEL values for both the JONSWAP and 2D-wave spectra begin to diverge, with the differences growing larger as the peakedness parameter increases. Notably, the JONSWAP spectrum consistently predicts higher DEL values compared to the 2D wave spectrum, particularly as the peakedness increases.

The largest differences in the DEL values start to be noticeable around a peakedness value of 1.5 and up to 2.5, where a density peak is also visible. There is a noticeable cluster of positive DEL differences around this peak, indicating that the JONSWAP wave spectrum tends to overestimate DEL relative to the 2D wave spectrum in this range. As the peakedness approaches 1.8, the gap between the DEL values from both spectra widens significantly. However, for peakedness values exceeding 2.5, the DEL values for both spectra decrease, with the differences between them also reducing.

Figure 5.23 shows the dependence of the damage ratio and the damage ratio differences against the peakedness parameter values.

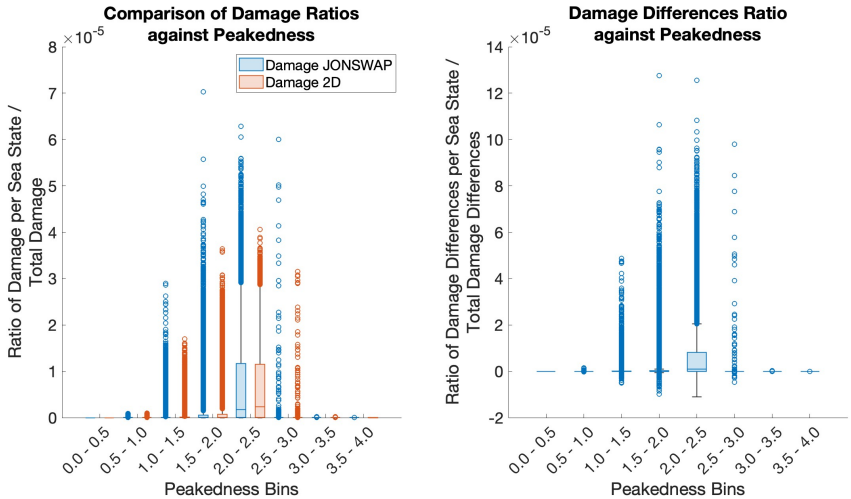

Figure 5.23: Damage and damage difference ratios against peakedness parameter for JONSWAP and 2D wave spectra

In the low peakedness parameter range (< 1.5) only very low damage ratios and damage ratio differences between both spectra are observed. The most significant differences between the spectra appear in the peakedness range between 1.5 and 2.5, with damage difference ratios reaching considerable high values. The DEL overestimation in this range can be quantified with $\sim$ 13 %, corresponding to $\sim$ 71 % of the observed data points. Outliers appear more frequently in the JONSWAP wave spectrum, especially above peakedness parameter values of 2.0, showing that JONSWAP wave spectra predicts more extreme damage events compared to the 2D-wave spectra. The wide spread of outliers, particularly in the JONSWAP-wave spectrum, reinforces the idea that the 2D spectrum provides more consistent damage estimates in this range. Damage difference ratios shrink again drastically for high peakedness values (> 2.5) and diminish nearly at all for peakedness values above 3.0.

Table 5.6 summarizes the defined ranges for the peakedness parameter for which the highest DEL and DEL differences were observed.

Range	**Description**
Below 1.0	Minimal DEL differences. Both spectra produce very similar DEL values.
1.5 to 2.5	Range with the most significant DEL differences. The two spectra behave differently, with the JONSWAP wave spectrum overestimating DEL values. The density peak is also located in this range, indicating a cluster of high DEL differences.
Beyond 2.5	Both spectra show a tendency for DEL values to decrease significantly.

Table 5.6: Defined peakedness parameter ranges based on DEL differences

5.4. Distance correlation analysis results

Figure 5.24 shows the results from the distance correlation calculation between the directional width, frequency width and the peakedness parameter based on the defined ranges of the significant wave height, peak period and wind speed for which the highest DEL differences between the JONSWAP and 2D-wave spectra were identified in the previous sections.

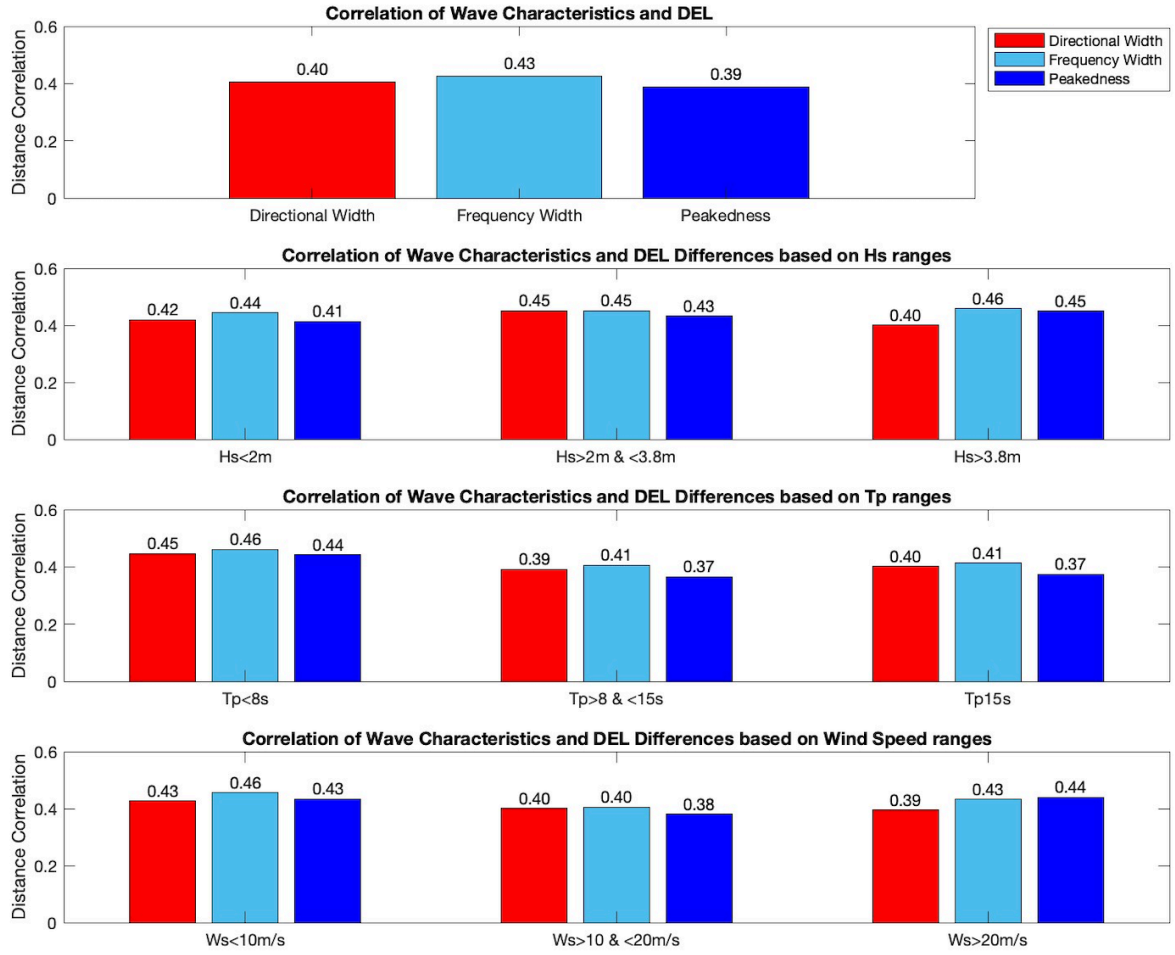

Figure 5.24: Results from distance correlation coefficients of wave characteristics

From the distance correlation analysis it can be concluded that even if small differences between the distance correlation coefficients are visible, the calculated values are occurring in a very narrow range, which can lead to the conclusion that with this method no significant higher dependencies for specific wave characteristics on the DEL differences can be identified .

Still, it looks like the frequency width seems to exhibit an overall larger influence on the DEL differences since it has the highest coefficient in relation to the total dataset of DEL differences, as can be seen in the top plot.

But this and the other calculated distance correlation coefficients can be interpreted to have a weak positive correlation based on the defined ranges of correlation coefficient values from table 3.4 which means that no significant relation and contribution to the research can be concluded from this analysis.

6. Discussion, limitations and recommendations

This research is based on specific assumptions, which lead to limitations of this research. This is reasonable since boundary conditions must be set for the scope of this research. To critical estimate the applicability of this research, the limitations and based on those research recommendations for future studies will be discussed in this section.

6.1. Limitations of the study

6.1.1. Site conditions

The results of this study are based on one investigated location in the Dutch North Sea, with a specific water depth and other environmental restraints. The JONSWAP spectral model is based on measurements and collected data in the Dutch North Sea and its performance is assumed to vary in other regions. This is why it would be especially interesting to investigate more locations to be able to give a more comprehensive interpretation of the research results and to make conclusions that would be more overall valid. For different locations with different environmental conditions, very deviating results could be expected for which it would be especially interesting to investigate the influence of the MetOcean characteristics on the wave-induced fatigue loads.

The Taiwan west coast and the US east coast were initially considered as additional locations for the analysis, and wave spectral data, along with bulk wave parameters, were provided by the DHI MetOcean database at no cost. However, due to time constraints, it was not feasible to include these regions in the scope of the current research. Therefore, it is recommended that future studies extend the investigation to these locations, which would provide valuable comparative insights into the performance of different spectral models in varying environmental conditions.

6.1.2. JONSWAP spectral parametrization

The JONSWAP wave spectra with which fatigue loads are calculated and compared to those based on the realistic 2D-wave spectral data, were calculated based on a gamma-value which was obtained with the Tp/Hs-ratio for each sea state. The investigations of the directional width, frequency width and peakedness parameter dependence, as shown in sections 4.2, 4.3, 4.4, revealed that JONSWAP wave spectra based on a gamma values of 1 or based on the Tp/Hs-ratio give a better representation of the wave characteristics of the realistic 2D-wave spectra. Differences between the DEL obtained from both spectra were observed, especially for narrow frequency and directional width. It can be assumed that the DEL differences between both spectra would be even larger, in case the JONSWAP wave spectra would not be calculated based on the Tp/Hs-ratio or with larger gamma values.

The obtained results are thus influenced by chosen parameters for the JONSWAP spectral parametrization, such as the assumption of the gamma value defining the peakedness of the wave spectrum.

6.1.3. Data model

For this research wave spectral data was obtained for specific spectral data models from the DHI MetOcean Database as stated in section 3.1. It is possible that different data models, which might be based on alternative assumptions or higher resolutions, could yield different fatigue load results. The 2D-wave spectra is based on the obtained wave spectral data, distributed over direction and frequency values and the JONSWAP wave spectra is calculated based on the bulk wave parameters that were obtained from the MetOcean database. In case different datasets for the wave spectral data and the bulk wave parameter would be used, also differences in the calculated fatigue loads could occur.

This points to a limitation in the applicability of the findings and suggests that further validation with real-world data or other models would strengthen the conclusions drawn from this research.

6.1.4. Wave fatigue loads

In this research, the focus was set on investigating wave-induced fatigue loads, which represent one of the critical limit states for the design of OWT. However, to gain a more comprehensive understanding of the structural performance under various conditions, it would be valuable to extend the analysis to include the ultimate limit state (ULS), which accounts for extreme, short-duration wave loads. By examining both fatigue and extreme loads, a more holistic perspective on the design challenges and risks could be achieved. This would allow for better optimization of turbine structures and ensure their resilience under both long-term operational conditions and rare but extreme events [59].

6.1.5. Wave fatigue load calculation method

For this research wave-induced fatigue loads were calculated with the frequency domain tool FUEL in the frequency-domain, which is a reasonable approach for the preliminary support structure design, to mostly decrease computational costs. Though, there are other methods to obtain wave-induced fatigue loads, such as the time-domain method which is an often used approach in the current engineering practice that could lead to more accurate results but which is also more time-extensive [60].

This research is thus based on the wave-induced fatigue loads, that were calculated within the frequency domain and it should be mentioned that slightly varying fatigue loads could have been obtained with time-domain calculations.

6.1.6. Extrapolation to other turbine design

The results of this study are based on the considered turbine design and location used in the analysis. Different offshore wind turbine designs, particularly those with different support structures or turbine sizes, may respond differently to wave-induced fatigue loads, limiting the applicability of the results.

6.2. Research recommendations

Based on the research limitations identified in this study, several recommendations can be proposed for future research. These suggestions aim to build upon the findings and addresses the constraints of this research, offering potential ideas for further investigation.

6.2.1. Expanding different locations

Expanding this study to cover different global locations would provide valuable insights, particularly given the diverse wave climates and environmental conditions in regions such as tropical and polar areas. For instance, tropical regions experience different swell patterns and hurricanes, which can lead to significantly different wave-induced fatigue loads. Similarly, polar regions face distinct challenges like sea ice and extreme cold, which also influence the performance and reliability of OWT's.

By investigating OWT's in locations with diverse environmental conditions, including variations in the wave and wind climate, a more comprehensive understanding of how MetOcean characteristics affect fatigue loads can be achieved. This would lead to more globally applicable design recommendations, enhancing the robustness and reliability of fatigue load predictions for OWT's deployed worldwide.

6.2.2. Investigating extreme loads

As the design of OWTs is influenced not only by fatigue loads but also by extreme loads, it would be valuable to investigate the ultimate limit state (ULS) in addition to the fatigue limit state (FLS) considered in this research. Including the ULS would provide a more comprehensive understanding of the structural performance under both long-term operational conditions and extreme events.

6.2.3. Investigating additional structural designs

Expanding this research by analyzing different substructure designs for OWT, such as tripod, jacket, or floating foundations, would increase the general applicability of these findings. By investigating how these alternative designs respond to wave-induced fatigue loads under similar MetOcean conditions, the study could provide a broader applicability across varying turbine sizes and structures. This would not only assess the resilience of different substructures but also offer insights into the optimal structural

designs for specific environmental settings, potentially leading to more cost-effective and sustainable engineering solutions.

6.2.4. Investigating additional design loading conditions

During production, OWT's experience different dynamic interactions with both wind and wave loads compared to the idling state. Investigating production conditions could provide a more comprehensive understanding of the loads that occur when the turbine is generating power, which is when it is most often operational. Considering both idling and production conditions would ensure a more robust and comprehensive design.

During production, OWT are subjected to different complex dynamic interactions, as opposed to the idling state. Investigating the turbine's response under production conditions can provide a more comprehensive understanding of the wave-induced loads that occur during regular operation, which is the turbine's primary operational state. By considering both idling and production conditions, the design process would capture a wider range of loading scenarios, leading to a more robust and reliable design. This dual consideration ensures that the turbine is structurally resilient across all operating modes, from downtime to peak production.

7. Conclusion

For the design of offshore wind turbines (OWT) and in the general engineering practice, using the simplified JONSWAP spectral parametrization is a common approach for the wave-induced fatigue load calculation. Indeed a lot more of the complexity of the sea surface can be captured by using actual frequency-directional wave spectra, which considers the distribution of the wave spectral density in its most representational form.

Within this research the influence of frequency-directional wave spectra on the wave-induced fatigue loads on OWT is investigated, as a comparison to the JONSWAP spectral parametrization. Realistic frequency-directional wave spectral data considers the wave spectral density distribution in its most authentic form across corresponding frequency and directional values, capturing the most naturalistic characteristics of the wave environment. Bi-modal frequency-dependent JONSWAP wave spectra was calculated based on bulk wave parameters for a wind-sea and swell component. No directional spreading function was applied, which leads to the orientation of the wind-sea and swell component in different directions. The wave spectral data was obtained from the DHI MetOcean database for a location in the Dutch North Sea. As part of the investigations it was aimed to find answers to three sub-questions.

1. **How do the bi-modal JONSWAP and the 2D-wave spectra influence the wave-induced fatigue load predictions on OWT?**

   To answer this research question, a fatigue load analysis was carried out within which the DEL and DEL differences as well as the damage ratios and the damage ratio differences against wave and wind parameter were investigated.

   It can be concluded that the JONSWAP spectral model leads to an overestimation in the range of $\sim$ 12 % to 15 % of the total wave-induced fatigue loads compared to those calculated with the 2D-wave spectra. For sea states corresponding to extreme events, which can be observed in the upper range (> 95 %) of the environmental parameters, with the JONSWAP wave spectra the wave-induced loads are underestimated compared to those calculated with the 2D-wave spectra. 2D-wave spectra appear to provide a more stable and consistent basis for fatigue load predictions due to their reduced variability and fewer extreme DEL values.

2. **What ranges of the investigated environmental parameters, significant wave height, peak period, wind speed as well as wind and wave direction, lead to the highest wave-induced fatigue loads and differences between the JONSWAP and 2D-wave spectra?**

   To find an answer to this research question, the relation between the fatigue loads, calculated with JONSWAP and 2D-wave spectra and the wave and wind parameters were investigated, as part of the fatigue load analysis in chapter 5.

   Especially large wave-induced fatigue loads and differences of those between the JONSWAP and 2D-wave spectra were found for specific ranges of the wave and wind parameters. These can be associated to significant wave heights between 2 and 3.8 m (14.70 % overestimation), to peak periods between 8 and 15 s (13.63 % overestimation) and wind speeds between 10 to 20 m/s (15.04 % overestimation). Furthermore, it was found that most of the fatigue damage can be associated with wind-sea components coming from the southwest and swell components from the northwest.

3. **Which wave characteristics, such as frequency width, directional width or peakedness, contribute most to the discrepancies between the JONSWAP and 2D-wave spectra in predicting fatigue damage?**

   It can be concluded that for the wave spectral density distribution of the 2D-wave spectrum over not only frequencies but also directions, the wave energy is expected to approach the structure more distributed over directions. Compared to that with the considered JONSWAP wave spectra the wave energy of the wave components was assumed to approach the structure from one

single direction, which could lead to higher fatigue-load estimations. Even if it can be said that this factor plays a role in the obtained wave-induced fatigue loads, it cannot be said whether this difference in the directional distribution between both spectra leads to the highest load differences since also the wave spectral density distributions over the frequencies differs for both types of wave spectra. For the 2D-wave spectra several peaks, corresponding to different wave components could be observed per sea state whereas for the bi-modal JONSWAP wave spectra two wave components, resulting consistently in only 2 peaks were considered. This difference in the frequency distribution will also contribute to the obtained fatigue load differences but it cannot be said whether it has a larger dependence on the loads than the directional width.

With the distance correlation analysis, shown in section 5.4, the dependence of the wave characteristics on the DEL differences was quantified, but from this analysis no clear difference between the relation of the wave spectral characteristics on the DEL differences was found, since the correlation coefficients were indicating very similar values. Furthermore, all gained correlation coefficients exhibited values which can be associated with only a weak dependence on the DEL differences. This results in the conclusion that with the chosen method for the distance correlation calculation, no answer on which could be relied on can be given to this question.

Still, ranges of the wave characteristics could be identified for which the highest wave-induced fatigue loads and the highest DEL differences based on the JONSWAP and 2D-wave spectra occur. These identified ranges correspond to wave spectra with a narrow frequency width (0.1 to 0.3 Hz) and directional width (20 to 30 deg). For wave spectra with broader frequency and directional width (> 30 deg and > 0.3 Hz) the wave load differences were decreasing between both wave spectra. It can thus not be said which wave characteristic has the largest influence on the wave-induced fatigue load differences between the JONSWAP and 2D-wave spectra but it can be said that those sea states that have a narrow directional and frequency width distribution contribute to higher DEL and DEL differences.

All in all, it can be concluded that the wave-induced fatigue load calculations might lead to overly conservative fatigue damage predictions compared to the realistic frequency-directional wave spectra which captures better the complexity of real sea states and thus provides a more comprehensive and more reliable basis for the fatigue load calculation on OWT's.

This research provides insights into the influence of realistic frequency-directional wave spectra on the wave-induced fatigue loads. Still this research comes with limitations as stated in section 6.1 and further research needs to be carried out to understand more in-depth authentic wave conditions and their influence on fatigue loads on OWT's.

For more physically representative fatigue load predictions obtained from authentic 2D-wave spectra, the design of OWT's could be improved in the future. This more efficient design, which would be based on more realistic fatigue loads, can lead to cost saving and ultimately can make OWT projects more sustainable.

References

[1] X. Sun, D. Huang, and G. Wu. “The current state of offshore wind energy technology development”. In: *Energy* 41.1 (2012), pp. 298–312.

[2] A. Bakun. “Climate change and ocean deoxygenation within intensified surface-driven upwelling circulations”. In: *Philosophical Transactions of the Royal Society A: Mathematical, Physical and Engineering Sciences* 375.2102 (2017), p. 20160327.

[3] G. Najafian and R. Burrows. “Probabilistic modelling of quasi-static response of offshore structures subject to nonlinear wave loading: Two approximate approaches”. In: *Applied ocean research* 16.4 (1994), pp. 205–221.

[4] M. Seidel. “Wave induced fatigue loads on monopiles-new approaches for lumping of scatter tables and site specific interpolation of fatigue loads”. In: *Conference Proceedings IWEC*. 2014.

[5] S. H. Sørum, J. R. Krokstad, and J. Amdahl. “Wind-wave directional effects on fatigue of bottom-fixed offshore wind turbine”. In: *Journal of Physics: Conference Series*. Vol. 1356. 1. 2019, p. 012011.

[6] M. Seidel. “Wave induced fatigue loads: Insights from frequency domain calculations”. In: *Stahlbau* 83 (8 2014), pp. 535–541. ISSN: 14371049. DOI: 10.1002/stab.201410184.

[7] J. H. Vugts. “Fatigue damage assessments and the influence of wave directionality”. In: *Applied Ocean Research* 27.3 (2005), pp. 173–185.

[8] V. Igwemezie, A. Mehmanparast, and A. Kolios. “Current trend in offshore wind energy sector and material requirements for fatigue resistance improvement in large wind turbine support structures–A review”. In: *Renewable and Sustainable Energy Reviews* 101 (2019), pp. 181–196.

[9] D. Kallehave et al. “Optimization of monopiles for offshore wind turbines”. In: *Philosophical Transactions of the Royal Society A: Mathematical, Physical and Engineering Sciences* 373.2035 (2015), p. 20140100.

[10] M. Seidel. “FEASIBILITY OF MONOPILES FOR LARGE OFFSHORE WIND TURBINES”. In: 2010.

[11] M. Kühn. “Dynamics and design optimisation of offshore wind energy conversion systems”. available at https://www.researchgate.net/publication/34768668. PHD thesis. Delft University of Technology, 2001.

[12] O. M. Mazzaretto, M. Menéndez, and H. Lobeto. “A global evaluation of the JONSWAP spectra suitability on coastal areas”. In: *Ocean Engineering* 266 (2022), p. 112756.

[13] J. Portilla-Yandún, L. Cavaleri, and G. van Vledder. “Wave spectra partitioning and long term statistical distribution”. In: *Ocean Modelling* 96 (2015), pp. 148–160.

[14] L. H. Holthuijsen. *Waves in oceanic and coastal waters*. Cambridge university press, 2007.

[15] International Electrotechnical Commission et al. “Wind energy generation systems-Part 3-1: Design requirements for fixed offshore wind turbines”. In: *International standard IEC* (2019), pp. 61400–3.

[16] S. Ahn, V. S. Neary, and T. Ha. “A practical method for modeling temporally-averaged ocean wave frequency-directional spectra for characterizing wave energy climates”. In: *Renewable Energy* 207 (2023), pp. 499–511.

[17] J. Sündermann and T. Pohlmann. “A brief analysis of North Sea physics”. In: *Oceanologia* 53.3 (2011), pp. 663–689.

[18] A. V. Boukhanovsky, L. J. Lopatoukhin, and C. G. Soares. “Spectral wave climate of the North Sea”. In: *Applied Ocean Research* 29.3 (2007), pp. 146–154.

[19] L. Björnsson. *Comparison of Idealized 1D and Forecast 2D Wave Spectra in Ship Response Predictions*. 2013.

[20] DET NORSKE VERITAS AS. *Offshore Standard - DNV-OS-J101 - Design of Offshore Wind Turbine Structures*. Jan. 2013. URL: http://www.dnv.com.

[21] W. Guachamin-Acero and J. Portilla-Yandún. "A study on vessel fatigue damage as a criterion for heading selection by application of 2D actual bimodal and JONSWAP wave spectra". In: *Ocean Engineering* 226 (2021), p. 108822.

[22] H. Rye and R. Svee. "Parametric representation of a wind-wave field". In: *Coastal Engineering 1976*. 1976, pp. 183–201.

[23] J. E. Stopa et al. "Comparison and validation of physical wave parameterizations in spectral wave models". In: *Ocean Modelling* 103 (2016), pp. 2–17.

[24] Deutsches Institut für Normung. *Beurteilung von mobilen Offshore Einheiten bezüglich ihres Einsatzgebietes*. DIN EN ISO 19905-1. DIN Norm. 2016.

[25] DNV GL AS. *DNVGL-RP-C205 Environmental conditions and environmental loads*. Sept. 2019.

[26] E. M. Bitner-Gregersen. "Joint probabilistic description for combined seas". In: *International Conference on Offshore Mechanics and Arctic Engineering*. Vol. 41960. 2005, pp. 169–180.

[27] J.-R. Bidlot. "Ocean wave model output parameters". In: *Reading: European Centre for Medium-RangeWeather Forecasts (ECMWF)* (2020).

[28] W.-T. Chao et al. "Analysis of Unidirectional Wave Spectral Characteristics in the Northeastern Waters of Taiwan". In: *Journal of Marine Science and Engineering* 11.12 (2023), p. 2285.

[29] C. G. Soares. "Representation of double-peaked sea wave spectra". In: *Ocean Engineering* 11.2 (1984), pp. 185–207.

[30] K. Hasselmann et al. "Measurements of wind-wave growth and swell decay during the Joint North Sea Wave Project (JONSWAP)." In: *Ergaenzungsheft zur Deutschen Hydrographischen Zeitschrift, Reihe A* (1973).

[31] V. Kudryavtsev, M. Yurovskaya, and B. Chapron. "2D parametric model for surface wave development under varying wind field in space and time". In: *Journal of Geophysical Research: Oceans* 126.4 (2021), e2020JC016915.

[32] H. Mitsuyasu et al. "Observations of the directional spectrum of ocean WavesUsing a cloverleaf buoy". In: *Journal of Physical Oceanography* 5.4 (1975), pp. 750–760.

[33] A. V. Babanin et al. "Numerical investigation of spectral evolution of wind waves. Part II: Dissipation term and evolution tests". In: *Journal of Physical Oceanography* 40.4 (2010), pp. 667–683.

[34] A. Toffoli et al. "Development of a bimodal structure in ocean wave spectra". In: *Journal of Geophysical Research: Oceans* 115.C3 (2010). DOI: https://doi.org/10.1029/2009JC005495. eprint: https://agupubs.onlinelibrary.wiley.com/doi/pdf/10.1029/2009JC005495. URL: https://agupubs.onlinelibrary.wiley.com/doi/abs/10.1029/2009JC005495.

[35] D. W. Wang and P. A. Hwang. "Evolution of the bimodal directional distribution of ocean waves". In: *Journal of physical oceanography* 31.5 (2001), pp. 1200–1221.

[36] T. H. C. Herbers, S. Elgar, and R. T. Guza. "Directional spreading of waves in the nearshore". In: *Journal of Geophysical Research: Oceans* 104.C4 (1999), pp. 7683–7693.

[37] R. B. Blackman and J. W. Tukey. "The measurement of power spectra from the point of view of communications engineering—Part I". In: *Bell System Technical Journal* 37.1 (1958), pp. 185–282.

[38] E. Le Merle et al. "Directional and frequency spread of surface ocean waves from SWIM measurements". In: *Journal of Geophysical Research: Oceans* 126.7 (2021), e2021JC017220.

[39] Y. Goda. "PROCEEDINGS OF THE FIRST INTERNATIONAL CONFERENCE - Behaviour of offshore structures, 'On Wave Groups'". In: *Boss'76*. Vol. 1. 1976.

[40] J.H. Vugts, J. van der Tempel, and E. A. Schrama. "Hydrodynamic loading on monotower support structures for preliminary design". In: *Proceedings of Special Topic Conference on Offshore Wind Energy*. 2001.

[41] J. Van Der Tempel. *Design of support structures for offshore wind turbines*. Published and distributed by the author, 2006.

[42] T. Dirlik. “Application of computers in fatigue analysis”. PhD thesis. University of Warwick, 1985.

[43] M. A. Miner. “Cumulative damage in fatigue”. In: (1945).

[44] A. Natarajan. “Damage equivalent load synthesis and stochastic extrapolation for fatigue life validation”. In: *Wind Energy Science* 7.3 (2022), pp. 1171–1181.

[45] DNV GL AS. *DNVGL-ST-0437 Loads and site conditions for wind turbines*. Nov. 2016. URL: http://www.dnvgl.com.

[46] DHI Group. *DHI Metocean Data Portal*. Accessed: (03-06-2024). 2024.

[47] Netherlands Enterprise Agency. *Metocean Assessment Modelling Report: IJmuiden Ver Wind Farm Zone*. Metocean Modelling. Dec. 2023.

[48] Netherlands Enterprse Agency. *Ijmuiden Ver - Wind & Water*. Accessed: (03-06-2024). 2024.

[49] M. Seidel, S. Voormeeren, and J.-B. van der Steen. “State-of-the-art design processes for offshore wind turbine support structures: Practical approaches and pitfalls during different stages in the design process”. In: *Stahlbau* 85.9 (2016), pp. 583–590.

[50] N. Barltrop and A. J. Adams. *Dynamics of fixed marine structures*. Vol. 91. Butterworth-Heinemann, 2013.

[51] C. Hübler, C. G. Gebhardt, and R. Rolfes. “Assessment of a standard ULS design procedure for offshore wind turbine sub-structures”. In: *Journal of Physics: Conference Series*. Vol. 1104. 1. IOP Publishing. 2018, p. 012013.

[52] P. Van der Valk and M. Ogno. “Identifying Structural Parameters of an Idling Offshore Wind Turbine Using Operational Modal Analysis”. In: Mar. 2014, pp. 271–281. ISBN: 978-3-319-04546-7. DOI: 10.1007/978-3-319-04546-7_31.

[53] L. Arany et al. “Simplified critical mudline bending moment spectra of offshore wind turbine support structures”. In: *Wind Energy* 18.12 (2015), pp. 2171–2197.

[54] L. Barj et al. “Wind/wave misalignment in the loads analysis of a floating offshore wind turbine”. In: *32nd ASME wind energy symposium*. 2014, p. 0363.

[55] C. Sun and V. Jahangiri. “Fatigue damage mitigation of offshore wind turbines under real wind and wave conditions”. In: *Engineering Structures* 178 (2019), pp. 472–483.

[56] M. Seidel. “6MW Turbines with 150m+ Rotor Diameter-What is the Impact on Substructures”. In: *Conference proceedings DEWEK*. 2012.

[57] D. Edelmann, T. F. Móri, and G. J. Székely. “On relationships between the Pearson and the distance correlation coefficients”. In: *Statistics & probability letters* 169 (2021), p. 108960.

[58] K. Al-Hameed. “Spearman’s correlation coefficient in statistical analysis”. In: *International Journal of Nonlinear Analysis and Applications* 13.1 (2022), pp. 3249–3255.

[59] Y. Xi et al. “Extreme load extrapolation and long-term fatigue assessment of offshore wind turbine tower based on monitoring data”. In: *Ocean Engineering* 300 (2024), p. 117180.

[60] L. Ziegler et al. “Sensitivity of wave fatigue loads on offshore wind turbines under varying site conditions”. In: *Energy Procedia* 80 (2015), pp. 193–200.